Hong Kong Journal of Radiology

# Hong Kong Journal of Radiology

# HKJR

## 香港放射科醫學雜誌

VOLUME 27 · NUMBER 2 · 2024

ISSN 2307-4620

**Highlights of this issue:**

- Analysis of Discordant Histologically Benign Breast Lesions and Predictive Factors Associated with True Discordance on Imaging
- Moderately Hypofractionated Versus Conventionally Fractionated Volumetric Modulated Arc Therapy for Definitive Treatment of Localised Prostate Cancer
- Application of Zero Echo Time Magnetic Resonance Angiography in Neuroimaging: A Pictorial Essay

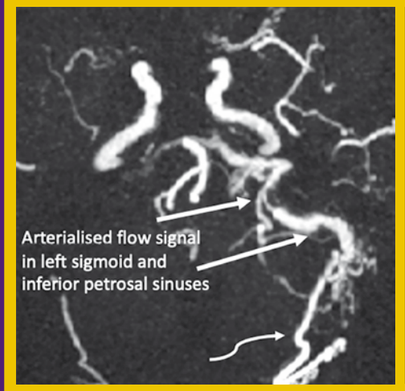


In the article "Application of Zero Echo Time Magnetic Resonance Angiography in Neuroimaging: A Pictorial Essay". The maximum intensity projection image of zero echo time magnetic resonance angiography depicts drainage into the left inferior petrosal sinus. Note the dilated left occipital arterial feeder (curved arrow).

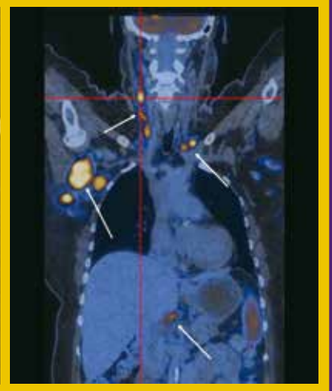

In the article "Radiologic-Pathologic Review of Non-Epithelial Malignancies and Metastases in the Breast: A Pictorial Essay". $^{18}$F-fluorodeoxyglucose positron emission tomography/computed tomography showed multiple hypermetabolic lymphadenopathies above and below the diaphragm (thin arrows), including both axillae. Histopathology of the right axillary lymph node confirmed classical Hodgkin lymphoma.

Official Publication of
Hong Kong College of Radiologists

HKAM PRESS

Vol. 27 No. 2, 2024 Pages e77-136

RADIOLOGY
HONG KONG 2024

# 32nd Annual Scientific Meeting of Hong Kong College of Radiologists

**23rd - 24th November 2024 (Sat & Sun)**

**Hong Kong Academy of Medicine**

**Jockey Club Building, Hong Kong SAR, China**

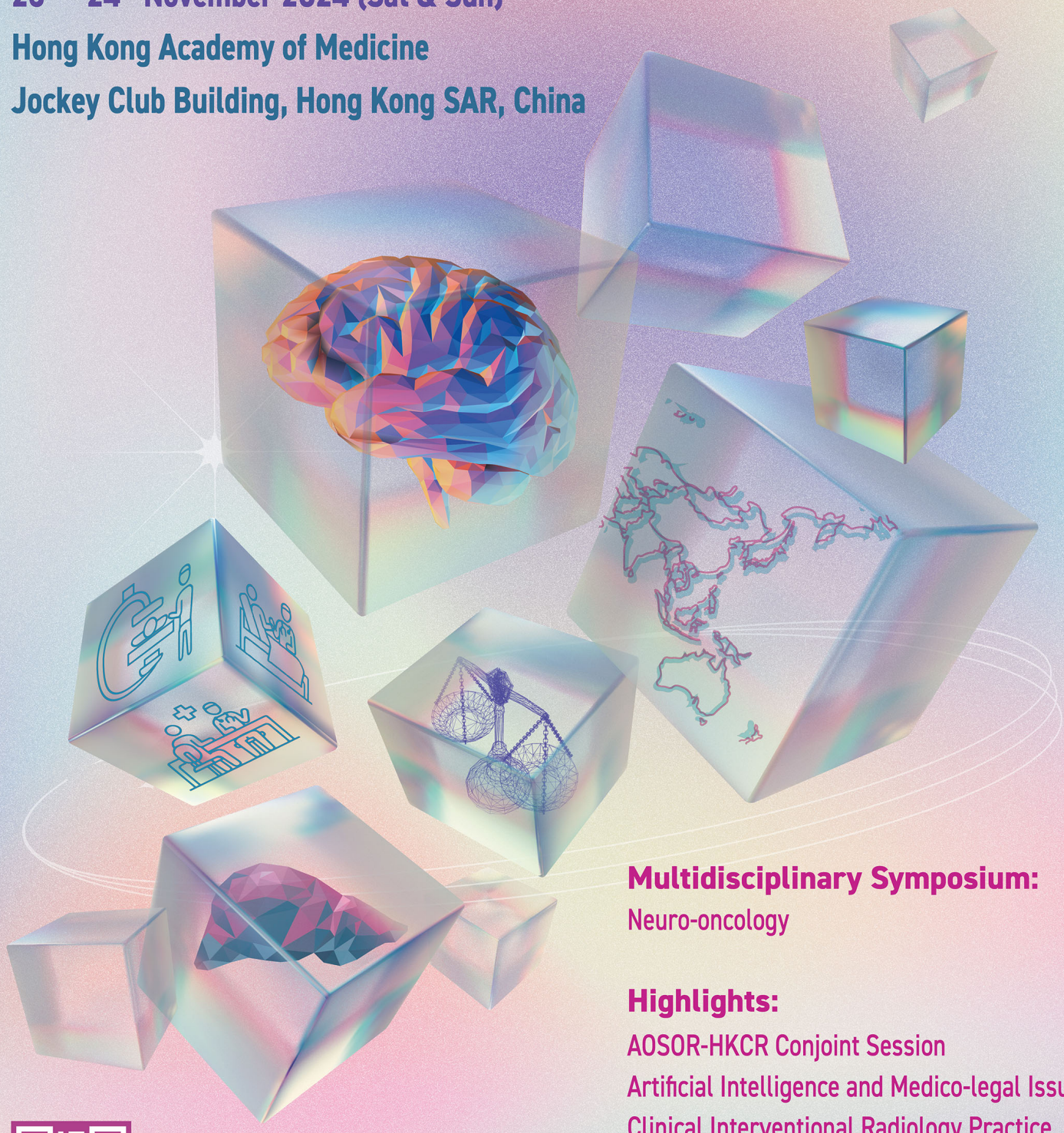

## Multidisciplinary Symposium:

Neuro-oncology

## Highlights:

AOSOR-HKCR Conjoint Session

Artificial Intelligence and Medico-legal Issues

Clinical Interventional Radiology Practice

Hepatobiliary Malignancies

For details

www.hkcr-asm.org

HKJR



COVER IMAGES

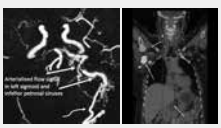

..... SEE PAGES e121 & e132

# Hong Kong Journal of Radiology

*Hong Kong Journal of Radiology* is a continuation of the *Journal of the Hong Kong College of Radiologists*. This journal is dedicated to publish all aspects of clinical oncology, diagnostic radiology, and nuclear medicine.

VOLUME 27 • NUMBER 2 • JUNE 2024

## Original Articles



## Case Reports



## Pictorial Essays



When citing this journal, abbreviate as ***Hong Kong J Radiol***.

Submit through **HKAMedTrack**, a secure online manuscript submission and review system, which facilitates communication and access to manuscripts for authors, reviewers, and editors

# www.hkamedtrack.org/hkjr


Complete author instructions can be found on the HKJR website <www.hkjr.org> and the **HKAMedTrack** website <www.hkamedtrack.org/hkjr>.

All submissions have to be made through **HKAMedTrack**.

# *Hong Kong Journal of Radiology*

**Aims and Editorial Policy**

*Hong Kong Journal of Radiology* **香港放射科醫學雜誌** is the official peer-reviewed academic journal of Hong Kong College of Radiologists, a founder College of the Hong Kong Academy of Medicine. The Journal is published online quarterly and is indexed in EMBASE/*Excerpta Medica*, SCOPUS, Emerging Sources Citation Index, and Index Copernicus. Papers are published on all aspects of diagnostic imaging, clinical oncology, and nuclear medicine, including original research, editorials, review articles, and case reports. Papers on radiological protection, quality assurance, audit in radiology, and matters related to radiological training or education are included.

All papers submitted are subject to peer review, and the Editorial Board reserves the right to edit papers in preparation for publication in the Journal. Authors are asked to refer to the *Information for Authors* published in each issue of the Journal, regarding the style and presentation of their articles. Failure to do so may result in rejection of their papers by the Editorial Board.

Manuscripts should be submitted online via the HKAMedTrack <www.hkamedtrack.org/hkjr>. Correspondence should be sent to:

Managing Editor, HKJR Editorial Office
c/o Hong Kong Academy of Medicine Press
10/F, Hong Kong Academy of Medicine Jockey Club Building
99 Wong Chuk Hang Road, Aberdeen, Hong Kong
Tel: (852) 2871 8809; Fax: (852) 2515 9061
Email: hkjr@hkam.org.hk

**Advertisements**

Correspondence concerning advertisements should be addressed to:

Executive Assistant
Hong Kong College of Radiologists
Room 909, 9/F Hong Kong Academy of Medicine Jockey Club Building
99 Wong Chuk Hang Road, Aberdeen, Hong Kong.
Tel: (852) 2871 8788; Fax: (852) 2554 0739
Email: hkjr@hkcr.org

**Reprints**

Reprints of individual articles are available to authors only. Reprints in large quantities (non-authors), for commercial or academic use, may be purchased from the publisher. For information and prices, please send an email to: hkjr@hkam.org.hk.

**Copyright**

On acceptance of an article by the Journal, the corresponding author will be asked to transfer copyright of the article to the College. The Copyright Transfer Assignment Form will be sent to the author at the time of acceptance.

**Disclaimer**

*Hong Kong Journal of Radiology* and the publisher do not guarantee, directly or indirectly, the quality or efficacy of any product or service described in the advertisements or other material which is commercial in nature in this issue. All articles published, including editorials and letters, represent the opinions of the authors and do not reflect the official policy of the Journal, Hong Kong College of Radiologists, the publisher, or the institution with which the author is affiliated, unless this is clearly specified.



*Hong Kong Journal of Radiology*
Online ISSN: 2307-4620

Hong Kong J Radiol. 2024;27(2):e80-8. Published 17 May 2024 | https://doi.org/10.12809/hkjr2317693

**ORIGINAL ARTICLE** **CME**

# Analysis of Discordant Histologically Benign Breast Lesions and Predictive Factors Associated with True Discordance on Imaging

**FFY Wan, KM Chu, TWY Chin, L Xu, WL Wong, JLF Chiu**

*Department of Radiology and Imaging, Queen Elizabeth Hospital, Hong Kong SAR, China*

## ABSTRACT

***Introduction:*** *Discordant benign breast lesions are suspicious for malignancy on imaging but show benign histology on initial biopsy. These lesions require further histological workup. This study sought to determine the frequency of discordant benign lesions and the rate of true discordance among them, and to identify predictive factors associated with true discordance.*

***Methods:*** *Clinical, radiological, and pathological data on all discordant benign breast lesions biopsied between 2012 and 2021 were retrieved from the departmental database of a Hong Kong hospital. Rate of discordant benign lesions, true and false discordance rates, and proportion of high-risk and benign lesions among false discordance were calculated. If the discordant benign lesion was found to be malignant in repeat percutaneous biopsy or excisional biopsy, it was true discordance. If a lesion's benignity was confirmed with excisional biopsy, it was false discordance. Univariate analysis was performed followed by multivariable logistic regression analysis to identify independent predictors associated with true discordance.*

***Results:*** *A total of 3080 breast biopsies were performed during the study period, of which 64 lesions (2.1%) were discordant benign lesions. Among 55 lesions with available additional workup results, 17 lesions (30.9%) were true discordant and 38 (69.1%) were false discordant. Nine (23.7%) of the false discordant lesions were high-risk lesions on final pathology. Older age (p = 0.019), presence of symptoms (p = 0.046), BI-RADS category 5 (p = 0.028), presence of microcalcifications with suspicious morphology (p = 0.047), and presence of architectural distortion (p = 0.04) were identified as independent predictors of true discordance.*

***Conclusion:*** *The high true discordance rate confirmed the importance of further histological workup in discordant benign breast lesions.*

***Key Words:*** *Biopsy; Breast; Histology; Neoplasms*

***Correspondence:*** *Dr FFY Wan, Department of Radiology and Imaging, Queen Elizabeth Hospital, Hong Kong SAR, China*
*Email: wfy471@ha.org.hk*

Submitted: 2 January 2023; Accepted: 21 June 2023.

Contributors: All authors designed the study and acquired and analysed the data. FFYW drafted the manuscript. All authors critically revised the manuscript for important intellectual content. All authors had full access to the data, contributed to the study, approved the final version for publication, and take responsibility for its accuracy and integrity.

Conflicts of Interest: All authors have disclosed no conflicts of interest.

Funding/Support: This research received no specific grant from any funding agency in the public, commercial, or not-for-profit sectors.

Data Availability: All data generated or analysed during the present study are available from the corresponding author on reasonable request.

Ethics Approval: This research was approved by the Kowloon Central Cluster Research Ethics Committee/ Kowloon East Cluster Research Ethics Committee of Hospital Authority, Hong Kong (Ref No.: KC/KE-22-0069/ER-1). The requirement for informed consent from the patients was waived by the Committee due to the retrospective nature of the research.

 

# 中文摘要

## 不一致組織學良性乳房病變及與影像學真正不一致相關的預測因子分析

尹芳盈、朱嘉敏、錢永恩、徐璐、黃慧琳、趙朗峰

**引言：**不一致良性乳房病變在影像學上疑似惡性腫瘤，但在初次活檢時顯示良性組織學，這些病變需要進一步組織學檢查。本研究旨在確定不一致良性病變的發病率以及它們真正不一致的比率，並確定與真正不一致相關的預測因子。

**方法：**我們從香港一家醫院的部門資料庫中檢索於2012至2021年間活檢的所有不一致良性乳房病變的臨床、放射學和病理數據，並計算不一致良性病變率、真假不一致率及假性不一致中的高風險病例和良性病變比例。如果重複經皮活檢或切除活檢發現不一致的良性病變為惡性，則為真正不一致；如果切除活檢證實病變為良性，則屬假性不一致。本研究先進行單變量分析，然後進行多變量邏輯迴歸分析，以確定與真正不一致相關的獨立預測因子。

**結果：**研究期間共進行了3080例乳房活檢，其中64例（2.1%）病灶為不一致良性乳房病變。在55例有額外檢查結果的病灶中，17例（30.9%）為真正不一致，38例（69.1%）為假性不一致。9例（23.7%）假性不一致病變在最終病理學上屬高風險病變。年齡較大（p = 0.019）、存在症狀（p = 0.046）、BI-RADS（乳房影像報告和數據系統）類別5（p = 0.028）、存在形態可疑的微鈣化（p = 0.047）以及存在結構扭曲（p = 0.04）為真正不一致的獨立預測因子。

**結論：**真正不一致比率高證實了對不一致良性乳房病變進行進一步組織學檢查的重要性。

## INTRODUCTION

Image-guided core needle biopsy is the current standard for initial workup and diagnosis of most BI-RADS (Breast Imaging Reporting and Data System) category 4 and 5 breast lesions detected on mammography. With technological advancements in both imaging techniques and core biopsy devices, the false-negative rates of image-guided core needle biopsy have been reported to be down to 2.5%,[1] with most cases identified because of radiological-pathological discordance. Such discordance happens when the pathology results do not match the imaging features, indicating that the lesion may not have been sampled adequately and creating the need for further histological workup.

Discordant benign lesions are lesions radiologically suspicious for malignancy (BI-RADS category 4 or 5) with a histological result that does not account for the radiological suspicion.[2] Up to 64% of discordant benign lesions from image-guided core needle biopsy turned out to be malignant in subsequent excisional biopsy.[3] If there is any concern regarding a discordant benign breast lesion, further investigation by repeating image-guided core needle biopsy or performing excisional biopsy is then be considered. If a true discordant benign lesion is recognised promptly, a missed malignancy can be identified, thus avoiding delay in diagnosis and treatment.

This retrospective analysis aimed to determine the frequency of discordant benign lesions and the proportion of true discordance among them. Potential predictive factors associated with true discordance were identified to assist radiologists in better evaluating for discordance.

## METHODS

### Data Collection

All cases with discordant benign breast lesions from 2012 to 2021 were retrieved from the departmental database of Department of Radiology and Imaging of Queen Elizabeth Hospital, Hong Kong. Data including patients' clinical details, radiological features, pathological findings, and imaging methods for biopsy guidance were described.

Discordant benign lesions were defined as lesions showing radiological findings suspicious for malignancy with no evidence of malignancy on initial pathological examination. In our institution, excisional biopsy was

the standard of care for patients with discordant benign pathological findings after two image-guided core needle biopsies. If a lesion was found to be malignant with repeat percutaneous biopsy or excisional biopsy, it was considered to represent true discordance. If a lesion's benignity was confirmed with final excisional biopsy, it was considered to represent false discordance (or concordance). The rates of discordant benign lesions, true discordance (Figure 1), and false discordance (Figure 2) were calculated.

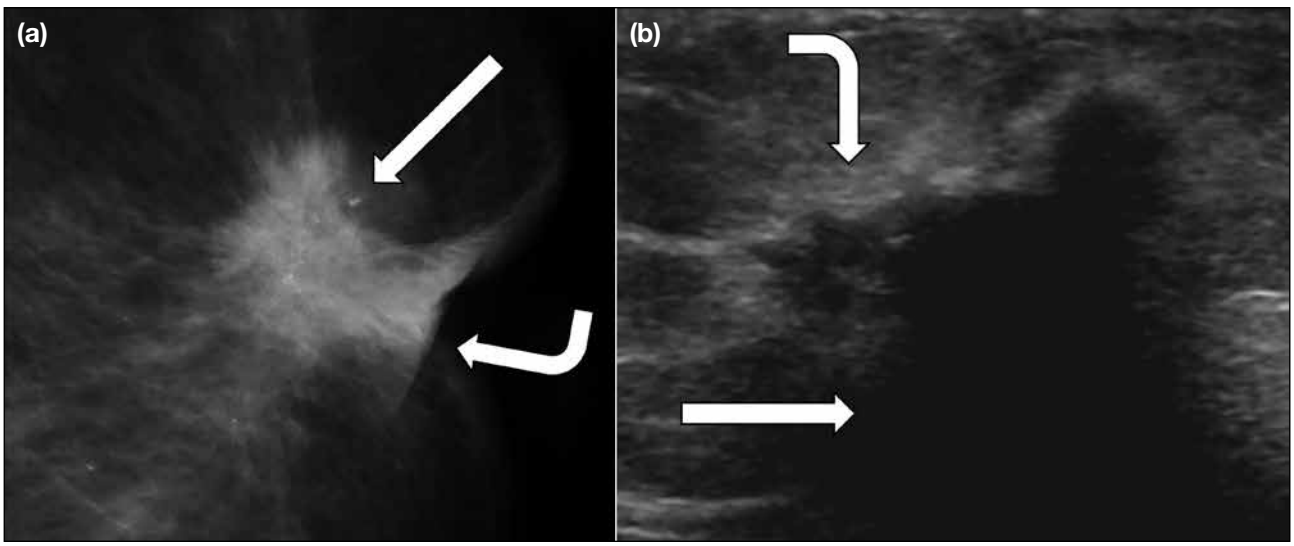


**Figure 1.** True discordance. An irregular high-density mass showing spiculated margins was noted to have fine pleomorphic calcifications (straight arrow) and architectural distortion in magnified craniocaudal view on mammogram (a). Associated skin and nipple retraction (curved arrow) was noted. Ultrasound of the mass (b) also showed suspicious features, including irregular shape, spiculated margin, significant posterior shadowing (straight arrow), and echogenic halo (curved arrow). The lesion was classified as Breast Imaging Reporting and Data System category 5 lesion. Ultrasound-guided biopsy of the mass was performed and the initial pathological diagnosis of fibrofatty tissue was considered discordant with the imaging findings. On repeat ultrasound-guided biopsy, the diagnosis of invasive ductal carcinoma was made.

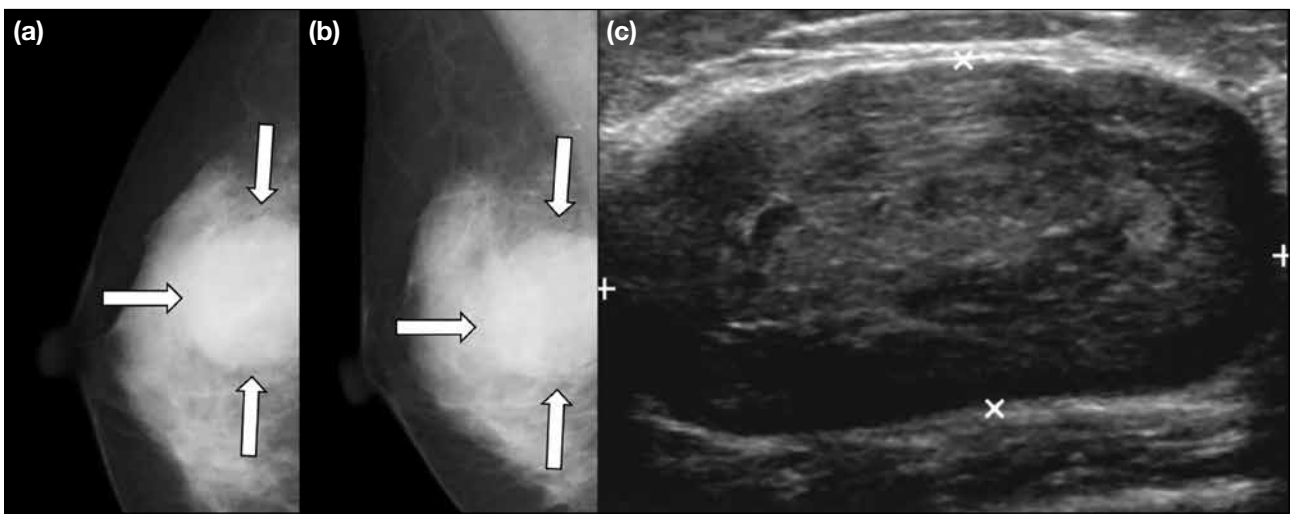


**Figure 2.** False discordance (concordance). (a) Craniocaudal view and (b) mediolateral oblique view of a large isodense mass with partially obscured margins (outlined by the arrows) was seen at the 9 o'clock position of the right breast on mammogram. No suspicious microcalcifications or architectural distortion was noted. Corresponding ultrasound of the mass (c) showing an oval circumscribed parallel hypoechoic mass with no definite posterior features. Ultrasound-guided biopsy was performed and the initial diagnosis of epidermal cyst was considered discordant, mainly due to the large lesion size. The same pathological diagnosis was noted on repeat ultrasound-guided biopsy. The patient subsequently underwent surgical excision of the breast mass and the final histological diagnosis was confirmed to be an epidermal cyst.

Patients' clinical details including age, presence of signs and symptoms (e.g., palpable breast mass or pathological nipple discharge), synchronous breast malignancy, past medical history or family history of breast cancer, and history of previous ipsilateral breast procedure were collected. Radiological features including lesion size (measured on ultrasound except for lesions only visualised on mammogram), BI-RADS category, presence of suspicious microcalcifications or architectural distortion on mammogram, presence of other radiologically suspicious lesions in the ipsilateral or contralateral breast, and presence of axillary lymphadenopathy on ultrasound or mammogram were reviewed. The imaging method for biopsy guidance was also noted, and all the above features were evaluated for their potential association with true or false discordance.

## Diagnostic Imaging Workup

All patients had had mammography and ultrasound of both breasts performed as the initial diagnostic workup, with interpretation and reporting performed by breast radiologists (years of experience: mean, 8.3 years; median, 7; range, 1-30). Assessment for any suspicious radiological features was made in accordance with the American College of Radiology BI-RADS Atlas.[4] The major findings to be evaluated included mass, microcalcifications, architectural distortion, and axillary lymphadenopathy. Suspicious features of masses include irregular shape, non-parallel orientation, non-circumscribed margins, and posterior shadowing on ultrasound. Morphology was useful in predicting the likelihood of malignancy for microcalcifications and other suspicious calcification morphologies including amorphous, coarse heterogeneous, fine pleomorphic, fine linear, and fine linear-branching microcalcifications. Linear or segmental distribution of the microcalcifications also elevated the suspicion for malignancy since they suggest deposits within the ductal system. Examples of other associated suspicious features were duct changes and skin changes. Suspicious lymph nodes usually displayed cortical thickening and hilar compression or displacement. The BI-RADS category indicates the likelihood of malignancy and guides the next step of management. Any lesions of BI-RADS category 4 or 5 require tissue diagnosis. BI-RADS category 4 lesions present with imaging findings that do not possess the classic appearance of malignancy but are sufficiently suspicious to indicate biopsy. BI-RADS category 5 lesions carry a very high probability of malignancy for which any non-malignant biopsy results are automatically considered discordant, leading to repeat percutaneous biopsy or excisional biopsy. Any radiologic-pathologic discordances were established in multidisciplinary meetings.

## Biopsy Technique

The choice of imaging modality for biopsy guidance was based on factors including lesion visibility, operator's and patient's preference, and availability of equipment. All sonographic-guided biopsies were performed with an automated biopsy gun (Bard; Magnum, Covington [GA], US) and a 14-gauge core needle with a 22-mm throw. A minimum of three core samples were obtained. All stereotactic-guided biopsies were performed with a directional vacuum-assisted device (Eviva Breast Biopsy System; Hologic, Marlborough [MA], US) and a 9-gauge core needle, and approximately 12 tissue samples were acquired. Biopsies were performed by breast radiologists. If microcalcifications or architectural distortion were deemed to be well-visualised and targeted on ultrasound, sonographic guidance was considered for biopsy. After biopsy of calcifications, specimen radiographs were acquired to verify sampling of the target calcifications. A marker clip was placed at the biopsy site, and its location on post-biopsy mammographic images was confirmed. Correlation with initial diagnostic imaging was performed to confirm biopsy of the targeted lesion.

## Statistical Analysis

The distribution of the numerical variables was first assessed for normality by using the Shapiro–Wilk test. If the data are not normally distributed, they are expressed as medians with interquartile ranges and analysed using Mann-Whitney *U* test.

Categorical variables were reported as counts and proportions. If there were <20% of cells with an expected frequency of <5 in a contingency table, the analysis of differences in characteristics between groups was performed using the Chi squared test. If there were ≥20% of cells with an expected frequency of ≤5 in a contingency table, the analysis between groups was assessed using Fisher's exact test for a 2 × 2 contingency table and Fisher-Freeman-Halton exact test for a contingency table larger than 2 × 2.

The variables with $p < 0.1$ in the univariate analysis were included in the multivariable logistic regression analysis to assess their abilities as independent predictors. The variables with $p < 0.05$ were considered statistically significant.

Statistical analyses were performed using SPSS (Windows version 28.0; IBM Corp, Armonk [NY], US).

## RESULTS

A total of 3080 breast biopsies were performed from 2012 to 2021, of which 64 lesions (2.1%) were discordant benign lesions. Among the 55 lesions with available additional workup results, 17 lesions (30.9%) were true discordant and 38 (69.1%) were false discordant (concordant). Overall, there were 14 lesions (25.5%) graded BI-RADS category 5, 13 lesions (23.6%) graded BI-RADS category 4C, and 28 lesions (50.9%) graded BI-RADS category 4B. There were no BI-RADS category 4A lesions. Repeat biopsy of the lesions was performed under either sonographic (n = 50, 90.9%) or stereotactic guidance (n = 5, 9.1%).

In univariate analysis, older age (p = 0.002), larger lesion size (p < 0.001), presence of symptoms (p = 0.076), BI-RADS category 5 (p < 0.001), presence of microcalcifications with suspicious morphology (p = 0.062), and presence of architectural distortion (p = 0.091) were predictors of true discordance. Synchronous breast malignancy (p = 0.149), past medical history (p = 1) or family history of breast cancer (p = 1), history of previous ipsilateral breast procedure (p = 0.309), presence of other radiologically suspicious lesions in the ipsilateral or contralateral breast (p = 0.36), presence of axillary lymphadenopathy (p = 0.435), and imaging guidance methods (p = 0.31) were non-significant variables (Tables 1 and 2).

In multivariable logistic regression analysis, older age (p = 0.019), presence of symptoms (p = 0.046), BI-RADS category 5 (p = 0.028), presence of microcalcifications with suspicious morphology (p = 0.047), and presence of architectural distortion (p = 0.04) were independent predictors of true discordance, while lesion size (p = 0.196) failed to remain a statistically significant independent predictor (Tables 1 and 2).

**Table 1.** Association of patient demographics with true and false discordance.*

| | Total (n = 55) | True discordance (n = 17) | False discordance (n = 38) | p Value from univariate analysis | p Value from multivariable analysis |
|---|---|---|---|---|---|
| Age, y | 59 (49-65) | 63 (59.5-72) | 54.5 (42.3-62.5) | 0.002 | 0.019 |
| Presence of symptoms | 31 (56.4%) | 13 (76.5%) | 18 (47.4%) | 0.076 | 0.046 |
| Synchronous breast malignancy | 10 (18.2%) | 5 (29.4%) | 5 (13.2%) | 0.149 | |
| Past medical history of breast cancer | 12 (21.8%) | 4 (23.5%) | 8 (21.1%) | 1 | |
| Family history of breast cancer | 3 (5.5%) | 1 (5.9%) | 2 (5.3%) | 1 | |
| History of previous ipsilateral breast procedure | 5 (9.1%) | 0 | 5 (13.2%) | 0.309 | |

* Data are shown as No. (%) or median (interquartile range).

**Table 2.** Association of radiological features with true and false discordance.*

| | Total (n = 55) | True discordance (n = 17) | False discordance (n = 38) | p Value from univariate analysis | p Value from multivariable analysis |
|---|---|---|---|---|---|
| Lesion size, cm | 1.6 (0.9-2.6) | 2.6 (1.7-5.4) | 1.15 (0.78-1.93) | < 0.001 | 0.196 |
| BI-RADS category | | | | < 0.001 | 0.028 |
| 4 | 41 (74.5%) | 7 (41.2%) | 34 (89.5%) | | |
| 5 | 14 (25.5%) | 10 (58.8%) | 4 (10.5%) | | |
| Presence of microcalcifications with suspicious morphology | 16 (29.1%) | 8 (47.1%) | 8 (21.1%) | 0.062 | 0.047 |
| Presence of architectural distortion | 8 (14.5%) | 5 (29.4%) | 3 (7.9%) | 0.091 | 0.04 |
| Presence of other radiologically suspicious lesions in the ipsilateral or contralateral breast | 19 (34.5%) | 4 (23.5%) | 15 (39.5%) | 0.36 | |
| Presence of axillary lymphadenopathy | 9 (16.4%) | 4 (23.5%) | 5 (13.2%) | 0.435 | |
| Imaging method for biopsy guidance | | | | 0.31 | |
| Ultrasound-guided | 50 (90.9%) | 17 (100%) | 33 (86.8%) | | |
| Stereotactic-guided | 5 (9.1%) | 0 | 5 (13.2%) | | |

Abbreviation: BI-RADS = Breast Imaging Reporting and Data System.
* Data are shown as No. (%) or median (interquartile range).

A total of 9 out of 38 (23.7%) false discordant lesions were high-risk on final pathology. The high-risk lesions included atypical ductal hyperplasia as the commonest pathology, followed by intraductal papilloma and lobular carcinoma in situ. The common final pathologies in concordant cases were sclerosing adenosis, fat necrosis, and fibroadenoma (Table 3).

## DISCUSSION

The reported percentages of imaging-pathology discordant lesions among biopsied breast lesions ranged from 2.2% to 5.8%.[5-7] The prevalence of discordant benign breast lesions in our institution was relatively low (2.1%). This might be explained by our quality control methods. During ultrasound-guided biopsy, satisfactory needle position was confirmed by obtaining post-fire images in orthogonal planes. For breast lesions with suspicious microcalcifications, specimen radiographs were performed to confirm the presence of target microcalcifications. Moreover, adequate sampling was achieved by obtaining at least three cores with minimal fragmentations.

In our institution, excisional biopsy is the standard of care for patients with discordant benign pathological findings after two image-guided core needle biopsies. Recently, vacuum-assisted breast biopsy has emerged as a potentially less invasive alternative to excisional biopsy for discordant benign lesions, with an upgrade rate ranging from 4.6% to 22.7%.[8] Because of the high sensitivity of contrast-enhanced magnetic resonance imaging (MRI) for detection of breast malignancies, it has been suggested to be of value in patients with discordant benign breast lesions to avoid further excisional biopsy. In a recent retrospective analysis, incorporating MRI into the algorithm for management of discordant benign breast lesions was shown to obviate the need for excisional biopsy in nearly 70% of patients with BI-RADS category 4 findings (excluding clusters of microcalcifications which are suspicious of underlying ductal carcinoma in situ).[9] A previous study also supported the use of MRI in determining the need for biopsy of BI-RADS category 4 lesions.[10] MRI is a potential tool for further workup of discordant benign breast lesions in the BI-RADS 4 category, especially in patients reluctant to undergo invasive excisional biopsy. However, using the criterion of non-enhancement to justify non-surgical management warrants further studies with larger populations since false-negative results could still occur with MRI.[10] Of note, the use of MRI in this setting has not been studied for BI-RADS category 5 lesions, likely due to the assumption that BI-RADS 5 category from mammography and ultrasound studies is unlikely to be overridden by the absence of suspicious malignant findings on MRI. Surgical resection still remains the gold standard for management of discordant benign lesions of BI-RADS category 5.

**Table 3.** Final pathologies of false discordant lesions (n = 38).

| High-risk lesions | Total No. | Benign lesions | Total No. |
|---|---|---|---|
| Atypical ductal hyperplasia | 3 | Sclerosing adenosis | 5 |
| Intraductal papilloma | 2 | Fat necrosis | 5 |
| Lobular carcinoma in situ | 2 | Fibroadenoma | 4 |
| Atypical lobular hyperplasia | 1 | Fibrocystic change | 3 |
| Complex sclerosing lesion | 1 | Usual ductal hyperplasia | 3 |
| | | Benign breast tissue | 2 |
| | | Lymphocytic mastopathy | 2 |
| | | Stromal fibrosis | 2 |
| | | Granulomatous mastitis | 1 |
| | | Granulation tissue | 1 |
| | | Epidermal cyst | 1 |

To our knowledge, this is the first study to evaluate for the potential predictive factors associated with true discordance. Although determining radiological-pathological concordance is crucial, no standard or guideline is currently available to assist in decision making. For this reason, evaluating for concordance still remains a subjective decision which could certainly vary among radiologists. Identification of predictors for true discordance may therefore be useful in decision making, especially in equivocal cases.

From our study, older age was a significant predictor of true discordance. The incidence of breast cancer is strongly related to older age, with the highest incidence rates in older women. For example, in Hong Kong from 2000 to 2020, more than half of the new cases of invasive breast cancers were in people aged ≥55 years.[11] The increase in incidence with age largely reflects cell DNA damage accumulating over time, which can be related to biological processes or exposure to risk factors. Hence, it is worth considering the age of the patient when assessing concordance of breast lesions. On the contrary, personal history and family history of breast cancers were not significant predictors for true discordance in this study. However, a definite conclusion could not be arrived at due to the small number of patients having a personal or family history of breast cancer in this study.

Imaging findings in patients with postprocedural

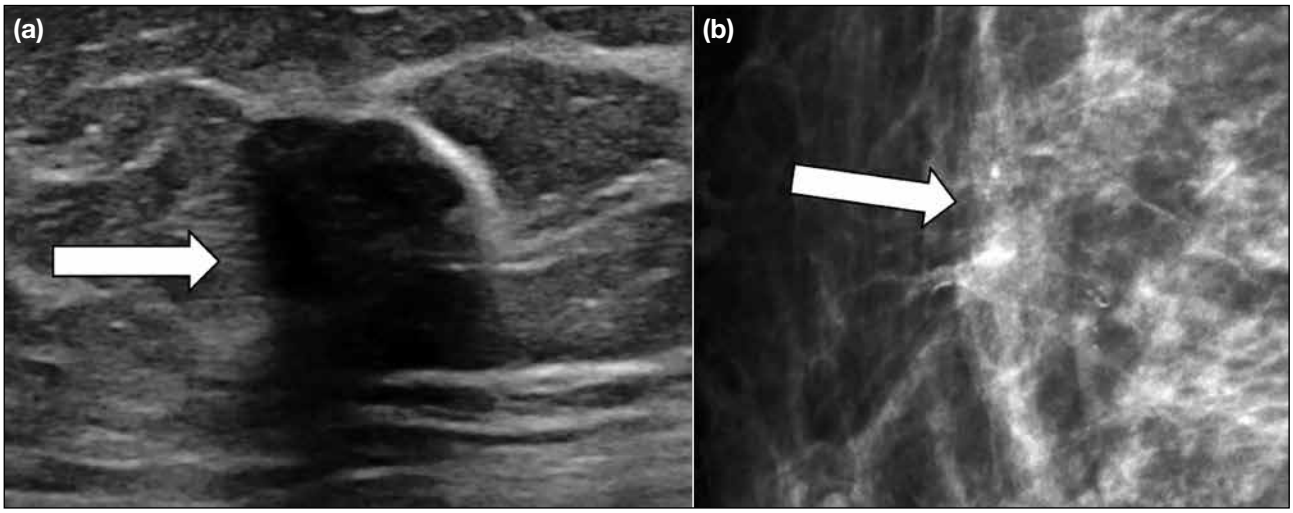


**Figure 3.** Examples of false discordance with final pathological diagnosis of fat necrosis. (a) A hypoechoic mass with significant posterior shadowing (arrow) on ultrasound was confirmed histologically to be fat necrosis. (b) Amorphous microcalcification (arrow) in magnified mediolateral oblique view on mammogram was considered suspicious and pathological workup also confirmed it to be fat necrosis.

changes may pose challenges in imaging interpretation and assessment of concordance, especially in view of the differential diagnosis of recurrent lesions.[1] Five discordant benign breast lesions in our study had a history of previous ipsilateral breast intervention. Subsequent histological workup confirmed all to be non-malignant with four of them being fat necrosis. Fat necrosis is an inflammatory condition commonly seen after breast surgery, radiation, infection or trauma. It is known to be a mimicker of malignancy both clinically and radiologically. Knowledge about the spectrum of suspicious radiological features of fat necrosis (Figure 3) as well as careful review of the biopsy technique and confirmation of biopsy adequacy are useful in the assessment for concordance in these patients.

BI-RADS is the internationally accepted standard for reporting breast imaging and BI-RADS category 5 lesions are highly suggestive of malignancy. With >95% probability of malignancy, BI-RADS category 5 was proven in our study to be a reliable factor in identifying true discordance. This also showed that our radiologists can successfully stratify lesions using BI-RADS risk assessment categories. In addition, microcalcifications of suspicious morphology and architectural distortion (Figure 4) are suspicious imaging findings included in the BI-RADS lexicon. Among the discordant benign breast lesions in this analysis, the presence of either finding was shown to be associated with a statistically significant higher malignancy rate.

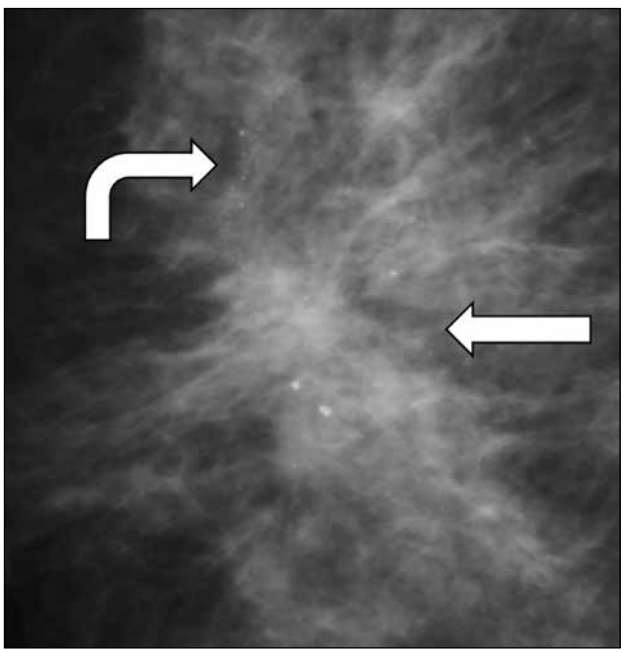

**Figure 4.** Fine pleomorphic microcalcifications (curved arrow) and architectural distortion (straight arrow) were seen with no definite associated mass in magnified mediolateral view on mammogram. Initial pathological diagnosis of atypical ductal hyperplasia was considered discordant with radiological findings. Repeat image-guided biopsy showed ductal carcinoma in situ, which was confirmed on subsequent surgical resection.

Lesion size was not a criterion for determination of the BI-RADS category and was confirmed in this study to be a non-significant predictor of true discordance. Although

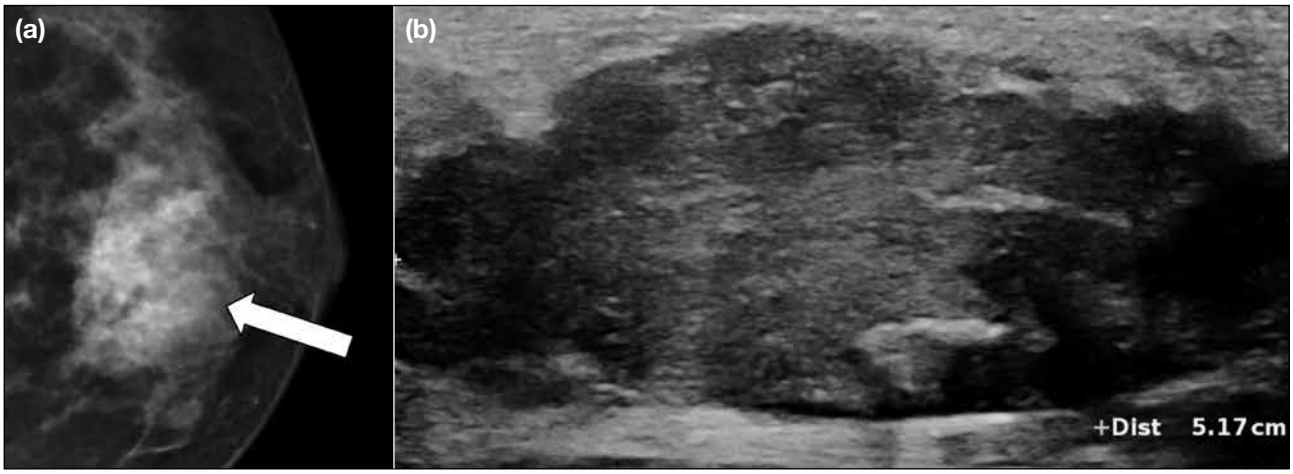


**Figure 5.** A large (>5 cm) oval high-density mass with partially obscured margins (arrow) was seen in craniocaudal projection on mammogram (a). No suspicious microcalcifications or architectural distortion were noted. Corresponding ultrasound of the mass (b) showing an oval circumscribed parallel hypoechoic mass with no definite posterior features. The pathological diagnosis of granulomatous mastitis was made on both initial and repeat ultrasound-guided biopsy. The result was considered discordant in view of the large lesion size. The patient underwent surgical excision of the mass and the final diagnosis was confirmed to be granulomatous mastitis. This was considered false discordance.

large breast masses (>5 cm) are understandably worrying for both patients and doctors, not all of them are malignant. Some benign breast lesions can present as large breast masses (Figure 5). According to the study by Sickles,[12] no statistically significant difference in the likelihood of cancer was found in relation to lesion size in non-palpable breast masses.

The imaging method for biopsy guidance was not found to be a significant factor in predicting true discordance. In our department, ultrasound-guided core needle biopsies were often performed with 14-gauge biopsy needles, while stereotactic-guided biopsies were usually done with 9-gauge vacuum-assisted biopsy devices. Since the size of the biopsy needles used between these two methods was also different, this acted as a potential confounder limiting proper comparison. However, it was worth noting that all five discordant benign lesions biopsied with stereotactic-guided vacuum-assisted biopsy were false discordant. This observation could possibly be explained by the higher biopsy adequacy obtained using a larger-bore biopsy needle with a vacuum-assisted device.

Among the false discordant lesions in our study, nearly one-fourth were high-risk lesions. This category refers to non-malignant lesions with increased lifetime risk of developing breast cancer, including atypical ductal hyperplasia, lobular neoplasia, papillary lesion, and radial scar.[13] Controversy exists regarding the appropriate management of these lesions, which is primarily related to the need for subsequent surgical excision. These patients should be managed by a multidisciplinary team with personalised management recommendations based on clinical, imaging, and pathological correlations.[14] For example, a pathological diagnosis of atypical ductal hyperplasia in a small lesion that was nearly entirely removed by vacuum-assisted biopsy may not require subsequent surgical resection.[15] On the other hand, if the same pathological diagnosis of atypical ductal hyperplasia was obtained with imaging showing extensive suspicious findings, there was a high possibility of co-existing higher-grade lesions and further surgical excision would be justified. Therefore, a single-standard approach does not exist for high-risk breast lesions and individualised management should be offered.

## Limitations

Our study was limited by its small sample size and retrospective approach. The strength of association between the independent predictors and true discordance (i.e., odds ratio) therefore cannot be reliably assessed and reported.

# CONCLUSION

The high true discordance rate of this study emphasised the importance of careful radiological-pathological correlation. Radiologists performing breast biopsy

should be aware of the possibility of false-negative diagnoses and be familiar with how to determine radiological-pathological concordance as well as the appropriate subsequent management. Future studies with larger populations are necessary to develop a predictive model for true discordance.

## REFERENCES


1. Park VY, Kim EK, Moon HJ, Yoon JH, Kim MJ. Evaluating imaging-pathology concordance and discordance after ultrasound-guided breast biopsy. Ultrasonography. 2018;37:107-20.
2. Youk JH, Kim EK, Kim MJ, Lee JY, Oh KK. Missed breast cancers at US-guided core needle biopsy: how to reduce them. Radiographics. 2007;27:79-94.
3. Liberman L. Percutaneous image-guided core breast biopsy. Radiol Clin North Am. 2002;40:483-500, vi.
4. American College of Radiology. Breast Imaging Reporting & Data System (BI-RADS®) Atlas 5th Edition. Available from: https://www.acr.org/Clinical-Resources/Reporting-and-Data-Systems/Bi-Rads. Accessed 26 Apr 2024.
5. Soyder A, Taşkin F, Ozbas S. Imaging-histological discordance after sonographically guided percutaneous breast core biopsy. Breast Care (Basel). 2015;10:33-7.
6. Sohn YM, Yoon JH, Kim EK, Moon HJ, Kim MJ. Percutaneous ultrasound-guided vacuum-assisted removal versus surgery for breast lesions showing imaging-histology discordance after ultrasound-guided core-needle biopsy. Korean J Radiol. 2014;15:697-703.
7. Son EJ, Kim EK, Youk JH, Kim MJ, Kwak JY, Choi SH. Imaging-histologic discordance after sonographically guided percutaneous breast biopsy: a prospective observational study. Ultrasound Med Biol. 2011;37:1771-8.
8. Jörg I, Wieler J, Elfgen C, Bolten K, Hutzli C, Talimi J, et al. Discrepancies between radiological and histological findings in preoperative core needle (CNB) and vacuum-assisted (VAB) breast biopsies. J Cancer Res Clin Oncol. 2021;147:749-54.
9. Sanders LM, El-Madany M, Persing A, Mehta A. Use of contrast-enhanced MRI in management of discordant core biopsy results. AJR Am J Roentgenol. 2019;212:1157-65.
10. Strobel K, Schrading S, Hansen NL, Barabasch A, Kuhl CK. Assessment of BI-RADS category 4 lesions detected with screening mammography and screening US: utility of MR imaging. Radiology. 2015;274:343-51.
11. Hong Kong Cancer Registry, Hospital Authority, Hong Kong. Hong Kong Cancer Statistics 2000-2020. Available from: https://www3.ha.org.hk/cancereg/. Accessed 1 Dec 2022.
12. Sickles EA. Nonpalpable, circumscribed, noncalcified solid breast masses: likelihood of malignancy based on lesion size and age of patient. Radiology. 1994;192:439-42.
13. Parikh J, Tickman R. Image-guided tissue sampling: where radiology meets pathology. Breast J. 2005;11:403-9.
14. Krishnamurthy S, Bevers T, Kuerer H, Yang WT. Multidisciplinary considerations in the management of high-risk breast lesions. AJR Am J Roentgenol. 2012;198:W132-40.
15. Krishnamurthy S, Bevers T, Kuerer HM, Smith B, Yang WT. Paradigm shifts in breast care delivery: impact of imaging in a multidisciplinary environment. AJR Am J Roentgenol. 2017;208:248-55.

Hong Kong J Radiol. 2024;27(2):e89-99. Published 20 May 2024 | https://doi.org/10.12809/hkjr2317749

**ORIGINAL ARTICLE** **CME**

# Moderately Hypofractionated Versus Conventionally Fractionated Volumetric Modulated Arc Therapy for Definitive Treatment of Localised Prostate Cancer

**TC Liu, PY Wu, KYC Zheng, HM Hung, K Chan**

*Department of Clinical Oncology, Pamela Youde Nethersole Eastern Hospital, Hong Kong SAR, China*

## ABSTRACT

***Introduction:*** *This retrospective study compares the treatment outcome of a reduced dose with moderate hypofractionation (60 Gray in 20 fractions [60 Gy/20 fr]) with conventionally fractionated (76 Gy/38 fr) volumetric modulated arc therapy for definitive treatment of localised prostate cancer in a public hospital in Hong Kong.*

***Methods:*** *All patients with low- or intermediate-risk prostate cancer (defined according to the National Comprehensive Cancer Network Guidelines) who received definitive radiotherapy from 1 January 2017 to 30 June 2022 were included.*

***Results:*** *A total of 105 patients were identified (58 receiving moderate hypofractionation and 47 receiving conventional fractionation). The median follow-up period was 38.3 months. Grade 2 acute gastrointestinal (GI) toxicity was more common with moderate hypofractionation than with conventional fractionation (15.5% vs. 2.1%, 95% confidence interval = 1.03-69.33; p = 0.02). In the moderate hypofractionation cohort, the planning target volume (PTV) in patients who experienced grade ≥2 acute genitourinary (GU) toxicity was significantly higher than those who did not (p = 0.03). None of the patients developed grade ≥3 acute GI toxicity. The incidence of grade 3 acute or late GU and late GI toxicities was rare with both fractionation schedules.*

***Conclusion:*** *This study shows that moderately hypofractionated radiotherapy is a safe, effective and feasible alternative to conventionally fractionated radiotherapy for low- and intermediate-risk prostate cancer in the Chinese community. Patients should be counselled on the potential increase in low-grade acute GI toxicity with moderate hypofractionation, which is usually self-limited and is not associated with increases in long-term toxicity. Close monitoring for acute GU toxicity in patients with larger PTVs is warranted.*

***Key Words:*** *Neoplasms; Prostate; Radiotherapy*

***Correspondence:*** *Dr TC Liu, Department of Clinical Oncology, Pamela Youde Nethersole Eastern Hospital, Hong Kong SAR, China*
*Email: ltc265@ha.org.hk*

Submitted: 18 July 2023; Accepted: 27 November 2023.

Contributors: TCL, PYW and KC designed the study. TCL and HMH acquired the data. TCL, PYW, KYCZ and KC analysed the data. TCL drafted the manuscript. TCL, PYW and KC critically revised the manuscript for important intellectual content. All authors had full access to the data, contributed to the study, approved the final version for publication, and take responsibility for its accuracy and integrity.

Conflicts of Interest: All authors have disclosed no conflicts of interest.

Funding/Support: This research received no specific grant from any funding agency in the public, commercial, or not-for-profit sectors.

Data Availability: All data generated or analysed during the present study are available from the corresponding author on reasonable request.

Ethics Approval: The research was approved by the Hong Kong East Cluster Research Ethics Committee of Hospital Authority, Hong Kong (Ref No.: HKECREC 2022-068). The requirement of patient consent was waived by the Committee due to the retrospective nature of the research.

Declaration: This research was presented orally at the 10th Joint Scientific Meeting of The Royal College of Radiologists and Hong Kong College of Radiologists (HKCR) and 31st Annual Scientific Meeting of HKCR (18-19 November 2023, Hong Kong).

Supplementary Material: The supplementary material was provided by the authors and some information may not have been peer reviewed. Any opinions or recommendations discussed are solely those of the author(s) and are not endorsed by the Hong Kong College of Radiologists. The Hong Kong College of Radiologists disclaims all liability and responsibility arising from any reliance placed on the content. To view the file, please visit the journal online (https://doi.org/10.12809/hkjr2317749).

 

# 中文摘要

## 中等強度大分割及傳統大分割體積調控弧型放射治療作為局部前列腺癌根治性治療方案的比較

廖芷霑、吳宇光、鄭裕誠、孔慶明、陳娟

**引言：**本回顧性研究旨在比較在香港一所公立醫院進行的已減劑量的中等強度大分割（60 Gy分20次）及傳統大分割（76 Gy分38次）體積調控弧型放射治療作為局部前列腺癌根治性治療方案。

**方法：**本研究納入在2017年1月1日至2022年6月30日期間接受根治性放射治療的所有低風險及中風險前列腺癌患者（根據美國國家綜合癌症網絡指引定義）。

**結果：**我們共找到105名患者（58名接受中等強度大分割，47名接受傳統大分割）。隨訪時間中位數為38.3個月。第2級急性腸胃道毒性於中等強度大分割中較常見，在傳統大分割則較少見（15.5%與2.1%，95%置信區間 = 1.03-69.33；p = 0.02）。在中等強度大分割隊列中，有第2級或以上急性泌尿生殖系統毒性的患者的治療計劃靶體積顯著高於沒有相關毒性的患者（p = 0.03）。沒有患者有第3級或以上急性腸胃道毒性。第3級急性或晚期泌尿生殖系統毒性及晚期腸胃道毒性在兩個分割治療計劃中均屬罕見。

**結論：**本研究顯示對於低風險及中風險前列腺癌華裔患者而言，中等強度大分割放射治療是傳統大分割放射治療的安全、有效且可行的替代方案。患者應獲告知中等強度大分割的低級急性腸胃道毒性有可能增加，而該增加通常具自限性，並與長期毒性增加無關。醫護人員應密切監察治療計劃靶體積較高的患者的急性泌尿生殖系統毒性。

## INTRODUCTION

Globally, prostate cancer ranks second in cancer incidence and fifth in cancer mortality among males; it has become the most frequently diagnosed cancer in >100 countries.[1] In Hong Kong, prostate cancer ranks fourth in cancer incidence.[2]

For low- or intermediate-risk prostate cancer, external beam radiotherapy (EBRT) and radical prostatectomy are associated with lower incidence of disease progression and metastasis compared to active surveillance. There is no difference in 10-year overall survival or disease-free survival between the two treatments.[3] Radiotherapy has the benefit of sparing patients from surgical and anaesthetic risks, which is especially relevant for patients of advanced age or with medical co-morbidities.

Dose escalation in definitive radiotherapy for prostate cancer increases tumour biological effective dose which leads to improvement in relapse-free survival.[4,5] On the other hand, the location of the prostate near organs at risk (OARs) such as the rectum and bladder leads to inevitably heightened gastrointestinal (GI) and genitourinary (GU) toxicities.[4-8] Recent advances in planning techniques and image guidance have led to improvement in treatment precision. Volumetric modulated arc therapy (VMAT) allows better dose conformation than traditional conformal EBRT, thus minimising dose to surrounding OARs. Image guidance strategies such as cone beam computed tomography (CT), in contrast to traditional two-dimensional kilovoltage imaging, allows more accurate definition and verification of targets and pelvic organs, thereby allowing tighter margins and smaller treatment volumes.

In the past decade, moderately hypofractionated EBRT (generally fractional doses of 2.4 Gray [Gy] to 3.4 Gy[9]) has been increasingly adopted to overcome the limitations of dose escalation in conventional radiotherapy by exploiting the low alpha/beta ratio of prostate cancer. The alpha/beta ratio is inversely correlated to the effect of change in fractional size in normal or malignant tissues. Most cancers have an alpha/beta ratio of approximately 10, whereas OARs typically have an alpha/beta ratio of about 3. Prostate cancer, in contrast to other cancers, has a lower alpha/beta ratio of approximately 1.5.[10,11]

Hypofractionation takes advantage of the low alpha/beta ratio of prostate cancer relative to surrounding OARs to enhance biologically equivalent tumour doses while minimising toxicity to normal tissues.[10,12-16]

Multiple studies have shown the comparable efficacy of moderate hypofractionation to conventional fractionation schedules.[17-22] The guidelines published by ASTRO/ASCO/AUA (the American Society for Radiation Oncology, the American Society of Clinical Oncology, and the American Urological Association) in 2018 recommended moderately hypofractionated EBRT over conventional schedules, especially when nodal irradiation was not required.[9] One of the most widely adopted regimens in clinical practice is 60 Gy in 20 daily fractions (60 Gy/20 fr).

The most relevant toxicities in prostate cancer radiotherapy include GU and GI toxicities as well as sexual dysfunction due to the target's proximity to the bladder, rectum, small bowel, and penile bulb. Most prospective clinical trials had demonstrated slightly increased acute GI toxicity in moderate hypofractionation compared to conventional schedules. Some trials had shown increases in late GU and GI side-effects (mostly of low grade), while others showed no significant differences. Overall, in all trials, there was no significant safety concern with moderately hypofractionated EBRT.[18-20,23-25]

The patient population of most large-scale prospective clinical trials has consisted mainly of Caucasians. So far, there are relatively scarce data reporting on the clinical utility, safety, and efficacy of moderately hypofractionated EBRT in Chinese populations.[26,27] Furthermore, most randomised trials did not necessitate the use of modern radiotherapy techniques such as VMAT,[17,18,22] nor the mode or intensity of image verification.[17-19,22]

Moderately hypofractionated VMAT for definitive treatment of low- and intermediate-risk prostate cancer was introduced in the Department of Clinical Oncology of Pamela Youde Nethersole Eastern Hospital in Hong Kong in January 2017. Since then, both moderate hypofractionation and conventional fractionation can be used for low- and intermediate-risk prostate cancer graded according to the National Comprehensive Cancer Network (NCCN) Guidelines at the clinician's discretion, although the former has been more commonly prescribed in recent years. In this study, we report our 6-year institutional experience in both treatment strategies, which provides real-world data on the toxicity and early treatment outcomes using modern EBRT technique in the local Chinese community under a public hospital setting. This is particularly relevant considering that moderate hypofractionation for prostate cancer has not been universally adopted in Hong Kong.

# METHODS

## Patients

This study included 105 consecutive patients with NCCN low- or intermediate-risk localised prostate cancer who received moderately hypofractionated or conventionally fractionated VMAT as definitive treatment from 1 January 2017 to 30 June 2022 at the Department of Clinical Oncology of Pamela Youde Nethersole Eastern Hospital. Patients had histologically confirmed prostate carcinoma, with clinical tumour (T) stage ≥2 disease by clinical and multiparametric magnetic resonance imaging staging, as well as a pretreatment prostate-specific antigen (PSA) level of ≤20 ng/mL and a Gleason score of ≤7. A bone scan or $^{68}$Gallium–prostate-specific membrane antigen–HBED-CC positron emission tomography–CT was used for staging when clinically indicated.

## Treatment Method

### *Moderate Hypofractionation*

For moderate hypofractionation, EBRT consisted of inversely planned VMAT of 60 Gy/20 fr, administering 5 fractions per week. Patients were simulated and treated in the supine position on a flat tabletop in a customised vacuum bag (or alpha cradle). They were instructed to maintain a comfortably full bladder and empty rectum (using micro-enema). Non-contrast CT images of the pelvis with slice thickness of 3 mm were acquired and fused with diagnostic multiparametric magnetic resonance imaging images for radiotherapy planning. Perirectal spacer was not employed in all cases.

The clinical target volume (CTV) was the whole prostate and proximal 1 cm of seminal vesicles for low- and favourable intermediate-risk disease, while the seminal vesicles were included in their entirety for unfavourable intermediate-risk disease. The planning target volume (PTV) was an 8-mm circumferential expansion from the CTV, except 5 mm posteriorly (towards the rectum). Online verification with cone beam CT was performed before each treatment fraction, complemented by the 6 degrees-of-freedom treatment couch for corrections. Typical dose distribution of moderately hypofractionated VMAT is illustrated in the Figure.

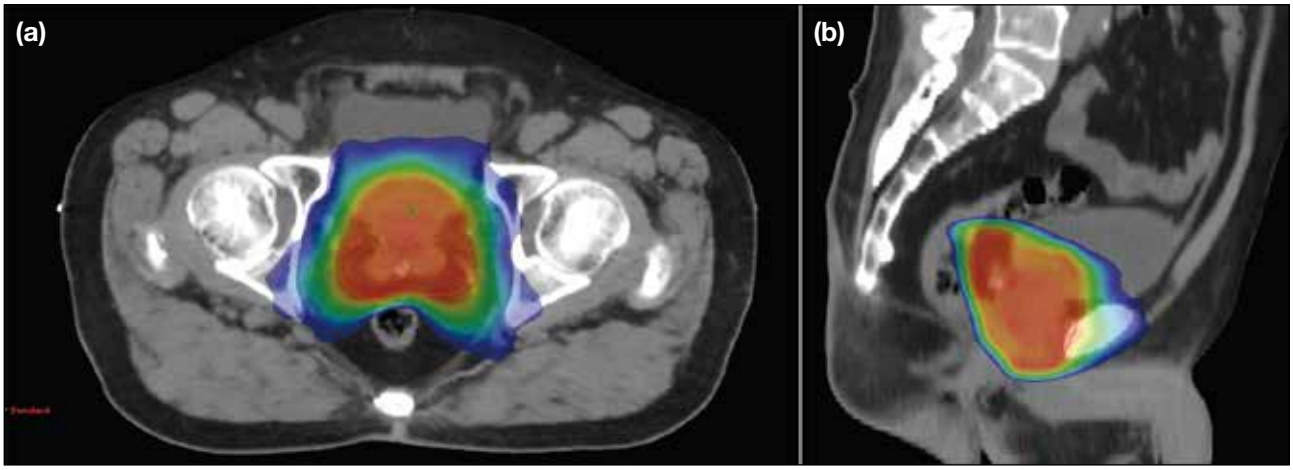


**Figure.** Typical dose distribution of moderately hypofractionated volumetric modulated arc therapy in axial (a) and sagittal (b) planes. Red colour maps the target volume receiving at least 100% dose.

### *Conventional Fractionation*

For conventional fractionation, EBRT consisted of inversely planned VMAT of 76 Gy/38 fr, administering 5 fractions per week. Patients were simulated and treated in the same setup as that used for moderate hypofractionation.

The CTV was the same as that of moderate hypofractionation, i.e., the whole prostate and proximal 1 cm of seminal vesicles for low- and favourable intermediate-risk disease, while the seminal vesicles were included in their entirety for unfavourable intermediate-risk disease. The PTV was a 10-mm circumferential expansion from the CTV, except 5 mm posteriorly (towards the rectum). Online verification consisted of daily on-board orthogonal kilovoltage imaging, and then with cone beam CT before the first three treatment fractions weekly. Planning objectives and dose constraints to OARs followed the standard institutional protocol (online supplementary Table). Normal organ and target dosimetric priorities were rectum and bladder and PTV coverage.

Neoadjuvant-concurrent luteinising hormone-releasing hormone analogue for 6 months was permitted for intermediate-risk patients in both treatment groups with adverse risk features. If given, this was initiated 3 months prior to radiotherapy.

## Follow-up

Clinical assessment was performed at least twice weekly during, at the end of, and 2 weeks after radiotherapy treatment, followed by every 3 to 6 months in the first 5 years, and annually thereafter. Post-treatment PSA level was checked at least half-yearly after radiotherapy.

## Assessment

The acute and late GI and GU toxicities arising from radiotherapy were scored according to the National Cancer Institute's CTCAE (Common Terminology Criteria for Adverse Events) version 5.0.[28] Acute treatment toxicities in this study were defined as events occurring within 18 weeks from the start of radiotherapy. Late toxicities were those appearing >18 weeks from the start of radiotherapy.

Biochemical failure was defined by the Phoenix criteria (rise of PSA level of ≥2 ng/mL above the nadir PSA level).[29] Clinical recurrence was defined by any clinical or radiological evidence of disease recurrence at local, regional, or distant sites.

## Endpoints and Statistical Analyses

The primary endpoint was the development of radiotherapy-related toxicity. Time-to-event was defined from the first fraction of radiotherapy to the appearance of treatment toxicity at follow-up. The data cut-off was 30 June 2023. Patients were censored at death or at data cut-off, whichever occurred first.

The influence of clinicopathological characteristics and radiotherapy-related parameters on radiotherapy-related toxicities were analysed. For acute toxicities, continuous variables were analysed by logistic regression;

categorical variables were analysed by Pearson's Chi squared test and Fisher's exact test. For late toxicities, continuous variables were analysed by univariate Cox regression; categorical variables were analysed by log-rank test.

A p value of $< 0.05$ was considered to indicate statistical significance. All statistical analyses were conducted using SPSS (Windows version 26.0; IBM Corp, Armonk [NY], United States).

The STROBE (Strengthening the Reporting of Observational Studies in Epidemiology) checklist was implemented in the preparation of the manuscript.

# RESULTS

## Patient Characteristics

Of the 105 patients identified, 58 had undergone moderate hypofractionation and 47 had undergone conventional fractionation. Table 1 shows the clinicopathological and treatment characteristics of both groups.

## Clinical Manifestations of Acute Genitourinary Toxicity

Among patients with any grade acute GU toxicities, the most frequently reported symptoms were urinary frequency (65.4% in the moderate hypofractionation group and 52.3% in the conventional fractionation group), followed by nocturia (13.5% in the moderate hypofractionation group and 25.0% in the conventional fractionation group) and dysuria (7.7% in the moderate hypofractionation group and 9.1% in the conventional fractionation group). Two patients in the moderate hypofractionation group had grade 3 acute GU toxicity, one presented as haematuria and another one as acute urinary retention. One patient in the conventional fractionation group had grade 3 acute GU toxicity, which presented as acute urinary retention (Table 2).

## Clinical Manifestations of Acute Gastrointestinal Toxicity

Among patients with any grade acute GI toxicities, the most reported symptoms were diarrhoea (75.0% in the

**Table 1.** Clinicopathological and treatment characteristics.*

| | Moderate hypofractionation (n = 58) | Conventional fractionation (n = 47) | p Value |
|---|---|---|---|
| Age, y | 71 (56-81) | 71 (59-83) | 0.16 |
| ECOG performance status score | | | |
| 0 | 16 (27.6%) | 7 (14.9%) | |
| 1 | 39 (67.2%) | 39 (83.0%) | |
| 2 | 3 (5.2%) | 1 (2.1%) | 0.22 |
| Charlson Comorbidity Index score | | | |
| 1 | 3 (5.2%) | 1 (2.1%) | |
| 2 | 19 (32.8%) | 7 (14.9%) | |
| 3 | 26 (44.8%) | 18 (38.3%) | |
| 4 | 7 (12.1%) | 12 (25.5%) | |
| ≥5 | 3 (5.2%) | 9 (19.1%) | 0.02 |
| Gleason score | | | |
| 3 + 3 | 22 (37.9%) | 14 (29.8%) | |
| 3 + 4 | 23 (39.7%) | 12 (25.5%) | |
| 4 + 3 | 13 (22.4%) | 21 (44.7%) | 0.05 |
| Baseline PSA, ng/mL | 8.5 (0.8-19.9) | 9.0 (0.8-19.1) | 0.46 |
| Tumour (T) stage | | | |
| T1 | 33 (56.9%) | 39 (83.0%) | |
| T2 | 25 (43.1%) | 8 (17.0%) | 0.004 |
| NCCN risk | | | |
| Low | 10 (17.2%) | 4 (8.5%) | |
| Favourable intermediate | 21 (36.2%) | 16 (34.0%) | |
| Unfavourable intermediate | 27 (46.6%) | 27 (57.4%) | 0.35 |
| Use of ADT | 46 (79.3%) | 43 (91.5%) | 0.08 |
| Prostate volume on planning CT, $cm^3$ | 45.0 (10.4-166.3) | 166.6 (81.9-408.3) | 0.89 |
| PTV, $cm^3$ | 125.4 (49.0-393.4) | 166.6 (81.9-408.3) | < 0.001 |
| Follow-up, mo | 28.3 (12.2-73.6) | 56.1 (14.8-77.6) | < 0.001 |

Abbreviations: ADT = androgen deprivation therapy; CT = computed tomography; ECOG = European Cooperative Oncology Group; NCCN = National Comprehensive Cancer Network; PSA = prostate-specific antigen; PTV = planning target volume.
* Data are shown as No. (%) or median (range).

**Table 2.** Incidence of toxicities in moderate hypofractionation versus conventional fractionation groups.* †

| | Acute GU toxicity | | Acute GI toxicity | |
|---|---|---|---|---|
| | Moderate hypofractionation (n = 58) | Conventional fractionation (n = 47) | Moderate hypofractionation (n = 58) | Conventional fractionation (n = 47) |
| Grade 1 | 35 (60.3%) | 29 (61.7%) | 6 (10.3%) | 9 (19.1%) |
| Grade 2 | 15 (25.9%) | 14 (29.8%) | 9 (15.5%) | 1 (2.1%) |
| Grade 3 | 2 (3.4%) | 1 (2.1%) | 0 | 0 |
| | Late GU toxicity | | Late GI toxicity | |
| | Moderate hypofractionation (n = 58) | Conventional fractionation (n = 47) | Moderate hypofractionation (n = 58) | Conventional fractionation (n = 47) |
| Grade 1 | 35 (60.3%) | 22 (46.8%) | 8 (13.8%) | 3 (6.4%) |
| Grade 2 | 4 (6.9%) | 8 (17.0%) | 9 (15.5%) | 7 (14.9%) |
| Grade 3 | 2 (3.4%) | 3 (6.4%) | 1 (1.7%) | 4 (8.5%) |

Abbreviations: GI = gastrointestinal; GU = genitourinary.
* Data are shown as No. (%).
† No grade 4 acute and late urinary or bowel toxicity were recorded.

moderate hypofractionation group and 80.0% in the conventional fractionation group), followed by rectal bleeding (16.7% in the moderate hypofractionation group and 10.0% in the conventional fractionation group).

## Clinical Manifestations of Late Genitourinary Toxicity

Among patients with any grade late GU toxicities, the most reported symptoms in the moderate hypofractionation group were nocturia (43.9%), followed by urinary frequency (29.3%) and incontinence (9.8%); the most reported symptoms in the conventional fractionation group were nocturia (51.5%), followed by urinary frequency (24.2%), haematuria (15.2%), and incontinence (3.0%). Two patients in the moderate hypofractionation group had grade 3 late GU toxicity, both present as haemorrhagic cystitis. Three patients in the conventional fractionation group had grade 3 late GU toxicity, two presented as haemorrhagic cystitis and one presented as urethral stricture (Table 2).

The median time to develop grade ≥2 late GU toxicity was 32.6 months for the moderate hypofractionation group and 26.4 months for the conventional fractionation group. There was no statistically significant difference between the two groups in time for occurrence of grade ≥2 late GU toxicity ($p = 0.48$).

## Clinical Manifestations of Late Gastrointestinal Toxicity

Among patients with any grade late GI toxicities, the most reported late GI toxicity was predominantly proctitis (88.9% in the moderate hypofractionation group and 100% in the conventional fractionation group). No faecal incontinence was reported. The incidence of grade ≥2 late GI toxicity was 17.2% in the hypofractionation group and 23.4% in the conventional fractionation group. One patient in the moderate hypofractionation group and four patients in the conventional fractionation group had grade 3 GI toxicity, all presented as proctitis (Table 2).

The median time to grade ≥2 late GI toxicity was 20.1 months for the moderate hypofractionation group and 22.4 months for the conventional fractionation group. There was no statistically significant difference between the two groups in time for occurrence of grade ≥2 late GI toxicity ($p = 0.48$).

## Erectile Dysfunction

The incidence of any grade erectile dysfunction was 6.9% in the moderate hypofractionation group and 10.6% in the conventional fractionation group. The median time to develop erectile dysfunction was 13.1 months in the moderate hypofractionation group and 6.5 months in the conventional fractionation group. There was no statistically significant difference between the two groups in the probability of developing erectile dysfunction ($p = 0.17$).

## Effect of Radiotherapy Parameters on Radiotherapy Toxicities

Table 3 shows the effect of radiotherapy parameters on radiotherapy toxicities. The PTV in patients who experienced grade ≥2 acute GU toxicity is significantly higher those who did not ($p = 0.03$). No significant clinical or treatment parameters were found to be predictive of other toxicity endpoints for the two fractionation schedules.

**Table 3.** Effect of radiotherapy parameters on treatment toxicities.*

| | Grade ≥2 acute GU toxicity | | Grade ≥2 acute GI toxicity | | Grade ≥2 late GU toxicity | | Grade ≥2 late GI toxicity | |
|---|---|---|---|---|---|---|---|---|
| | OR (95% CI) | p Value | OR (95% CI) | p Value | HR (95% CI) | p Value | HR (95% CI) | p Value |
| | | | | Moderate hypofractionation | | | | |
| Prostate volume | 1.02 (1.00-1.04) | 0.11 | 1.01 (0.99-1.04) | 0.30 | 1.02 (0.99-1.05) | 0.28 | 1.01 (0.98-1.03) | 0.54 |
| PTV | 1.01 (1.001-1.02) | 0.03 | 1.00 (0.98-1.01) | 0.53 | 1.02 (1.00-1.04) | 0.13 | 1.00 (0.98-1.01) | 0.76 |
| Rectum $V_{60}$ | | | 0.59 (0.21-1.68) | 0.33 | | | 0.62 (0.20-1.91) | 0.40 |
| Rectum $V_{58}$ | | | 0.91 (0.71-1.16) | 0.45 | | | 0.94 (0.77-1.16) | 0.57 |
| Bladder $V_{60}$ | 1.22 (0.86-1.73) | 0.27 | | | 0.83 (0.41-1.68) | 0.60 | | |
| Bladder $V_{50}$ | 1.05 (0.95-1.16) | 0.33 | | | 0.93 (0.80-1.09) | 0.37 | | |
| | | | | Conventional fractionation | | | | |
| Prostate volume | 0.99 (0.97-1.01) | 0.43 | 0.99 (0.92-1.06) | 0.80 | 1.00 (0.98-1.02) | 0.79 | 0.99 (0.97-1.01) | 0.43 |
| PTV | 1.00 (0.99-1.01) | 0.57 | 1.00 (0.97-1.03) | 0.82 | 1.00 (0.99-1.01) | 0.77 | 1.00 (0.99-1.01) | 0.35 |
| Rectum $V_{70}$ | | | 0.80 (0.45-1.43) | 0.45 | | | 0.96 (0.81-1.14) | 0.66 |
| Rectum $V_{50}$ | | | 0.87 (0.62-1.24) | 0.44 | | | 0.93 (0.85-1.03) | 0.16 |
| Bladder $V_{70}$ | 1.07 (0.96-1.20) | 0.22 | | | 1.07 (0.97-1.18) | 0.21 | | |
| Bladder $V_{55}$ | 1.04 (0.97-1.12) | 0.25 | | | 1.04 (0.98-1.11) | 0.20 | | |

Abbreviations: 95% CI = 95% confidence interval; GI = gastrointestinal; GU = genitourinary, HR = hazard ratio; OR = odds ratio; PTV = planning target volume.
* In the first column, $V_{60}$ means the volume of the organ-at-risk of interest receiving ≥60 Gy of the prescribed radiation dose, and so on.

**Table 4.** Comparison of characteristics and toxicity of moderate hypofractionation among landmark studies and the current study.

| | CHHiP[19] | HYPRO[22,24,25,30] | PROFIT[18] | RTOG 0415[17,23] | Current study |
|---|---|---|---|---|---|
| Fractionation and dose | 60 Gy/20 fr; 5 fr/week | 64.6 Gy/19 fr; 3 fr/week | 60 Gy/20 fr; 5 fr/week | 70 Gy/28 fr; 5 fr/week | 60 Gy/20 fr; 5 fr/week |
| NCCN low risk | 15% | Excluded | Excluded | 100% | 17.2% |
| NCCN intermediate risk | 73% | 26% | 100% | Excluded | 82.8% |
| NCCN high risk | 12% | 74% | Excluded | Excluded | Excluded |
| Use of concurrent ADT | 97% | 66% | Excluded | Excluded | 79.3% |
| Grade ≥2 acute GU toxicity | 49% | 60.5% | 30.9% | 27.0% | 29.3% |
| Grade ≥2 acute GI toxicity | 38% | 42% | 16.7% | 10.7% | 15.5% |
| Grade ≥2 late GU toxicity | 11.7%* | 41.3%* | 22.2%* | 29.7%* | 10.3% |
| Grade ≥2 late GU toxicity | 6%* | 19.0%* | 2.2%* | 3.5%* | 3.4% |
| Grade ≥2 late GI toxicity | 11.9%* | 21.9%* | 8.9%* | 22.4%* | 17.2% |
| Grade ≥3 late GI toxicity | 3%* | 3.3%* | 1.5%* | 4.1%* | 1.7% |
| Biochemical recurrence-free survival/DFS | 5-year biochemical or clinical failure-free rate: 90.6% (95% CI = 88.5%-92.3%) | 5-year relapse-free survival: 80.5% (95% CI = 75.7%-84.4%) | 5-year DFS: 85% (95% CI = 82%-88%) | 5-year DFS: 86.3% (95% CI = 83.1%-89.0%) | No biochemical failure/clinical recurrence in follow-up period |

Abbreviations: 95% CI = 95% confidence interval; ADT = androgen deprivation therapy; DFS = disease-free survival; GI = gastrointestinal; GU = genitourinary; NCCN = National Comprehensive Cancer Network.
* Till the end of study.

### Biochemical Failure and Clinical Recurrence

There was one biochemical failure with clinical recurrence in the conventional fractionation arm and none in the moderate hypofractionation arm.

## DISCUSSION

Landmark trials including CHHiP,[19] HYPRO (HYpofractionated irradiation for PROstate cancer),[22,24,25,30] PROFIT (Prostate Fractionated Irradiation Trial),[18] and RTOG 0415[17,23] have shown that moderately hypofractionated radiotherapy to prostate is as effective as conventional fractionation. However, the data on toxicities were less consistent (Table 4).

Our real-world data showed that the increased acute GI toxicity from moderately hypofractionated radiotherapy was limited to grade 2 and did not lead to increase in long-term toxicity. As recommended by the ASTRO/ASCO/AUA 2018 guideline, patients should be counselled on the small increased risk of acute GI

**Table 5.** Risk of genitourinary and gastrointestinal toxicities in moderate hypofractionation versus conventional fractionation groups.

| | OR (95% CI) | p Value |
|---|---|---|
| Grade ≥2 acute GU toxicity | 0.89 (0.38-2.04) | 0.77 |
| Grade ≥2 acute GI toxicity | 8.45 (1.03-69.33) | 0.02 |
| | HR (95% CI) | p Value |
| Grade ≥2 late GU toxicity | 0.77 (0.28-2.14) | 0.62 |
| Grade ≥2 late GI toxicity | 1.29 (0.54-3.12) | 0.57 |

Abbreviations: 95% CI = 95% confidence interval; GI = gastrointestinal; GU = genitourinary; HR = hazard ratio; OR = odds ratio.

toxicity with moderate hypofractionation.[9] Both the CHHiP[19] and PROFIT[18] trials showed lower rates of late GI toxicities with moderately hypofractionated EBRT. In contrast, the late GI toxicity rate was higher with moderate hypofractionation in the RTOG 0415 trial.[17] In our study, no difference was detected between the fractionation schedules for grade ≥2 late GI toxicity (p = 0.57) [Table 5]. For the incidence of grade 3 late GU and GI toxicities in the moderate hypofractionation cohorts, the rates were low in the current study (Table 2).

In general, the incidence of radiotherapy-related toxicities in the current study was lower than that reported in the landmark trials on moderate hypofractionation. There may be several reasons. First, the lower late toxicities may be attributed to shorter follow-up time. The landmark trials had a median follow-up of at least 60 months (62.4 months in CHHiP,[19] 60 months in HYPRO,[22] 72 months in PROFIT,[18] and 70 months in RTOG 0415[17,23]), while the median follow-up time in the current study was 38.3 months (range, 12.2-77.6). We expect more mature late toxicity data with longer follow-up. The long-term radiotherapy-related toxicities may not be fully reflected; nevertheless, it is worth noting that in the landmark prospective trials, the majority of grade ≥2 late toxicity occurred within the first 2 years of follow-up. Second, we adopted inversely planned VMAT with stringent planning aims and dose constraints for OARs, together with daily cone beam CT verification for moderate hypofractionation. Most of the landmark prospective trials did not mandate the use of intensity-modulated radiotherapy or VMAT,[17,18,22] nor did they require the technique or intensity of image verification.[17-19,22] In our study, modern dose planning with VMAT technique and intensive image guidance allowed tight PTV margins and more precise treatment delivery, which could be a contributing factor to the lower incidence of treatment-related toxicities. Third, due to the retrospective nature of this study that reflects on real-world clinical practice, meticulous and frequent documentation of toxicity was difficult. Our reporting on toxicities was limited by inter-clinician variation in toxicity charting (especially for low-grade events), and lack of formal reporting of patient-reported outcome. In addition, there may be cultural variations in toxicity reporting by patients, especially sexual dysfunction, which is often considered a sensitive topic and often underrepresented in the local Chinese population.

The PTV in patients who experienced grade ≥2 acute GU toxicity is significantly higher those who did not (p = 0.03). Interestingly, bladder $V_{60}$ and $V_{50}$, which reflect the bladder volume receiving high doses (≥60 Gy and ≥50 Gy, respectively), were not significant predictors of acute GU toxicity (Table 3). This may be due to interfractional variation in bladder filling during the course of radiotherapy, which may result in variation between planned and actual bladder doses. Nevertheless, in real life practice, it would be helpful to offer close monitoring of acute GU toxicities for patients with larger PTVs.

There was only one biochemical failure in the conventional fractionation arm and none in the moderate hypofractionation arm. The relatively lower incidence of biochemical or clinical failure in our local cohort compared to other landmark trials may be explained by shorter follow-up duration, differences in patient selection, and use of androgen deprivation therapy (ADT). As discussed above, the landmark trials had a median follow-up of at least 60 months, in contrast to 38.3 months in the current study, making it difficult to conclude on long-term disease control based on the current results. Furthermore, in this study, all patients were classified into low- or intermediate-risk categories according to the NCCN Guidelines. The presence of high-risk patients in CHHiP[19] and HYPRO[22] trials may be a reason for the higher biochemical or clinical failure rate in these trials. In PROFIT[18] and RTOG 0415 trials,[17] the use of ADT was not allowed. On the other hand, 79.3% patients in the hypofractionation cohort received ADT in the current study, which likely contributed to better biochemical control (Table 4).

We have observed a gradual but significant shift in practice from conventional fractionation to moderate hypofractionation over the years. Among patients treated between 2017 and 2019, adoption of moderate hypofractionation was 24.1%. The rate rose to 80.9% in 2020 to 2022. This reflects the evolution in treatment

paradigms with increasing clinical data and local experience to support moderate hypofractionation.

## Limitations

Other limitations of our current study include imbalance in baseline characteristics including Charlson Comorbidity Index score, tumour stage, PTV, and median follow-up time, which may be confounders on toxicity outcomes. This was due to the intrinsic nature of a retrospective study. The difference in follow-up duration between the two patient cohorts reflects real-world gradual adoption of moderate hypofractionation and growth in local experience in this technique. Despite the above limitations, it is worth noting that the study cohort represents local real-world data of all consecutive patients treated in the same institution over 5 years, using contemporary radiotherapy planning and intensive image guidance, for which similar reports in Chinese patients are scarce.

## Future Directions

Further dose escalation with an intraprostatic boost may improve disease control. The FLAME trial (Fluoxetine for motor recovery after acute ischaemic stroke) demonstrated superior biochemical disease-free survival with a focal 95-Gy boost to macroscopic tumour whilst toxicities and quality of life were not compromised.[31] The ongoing multicentre phase III PIVOTALboost trial may offer phase III data on dose escalation to the prostate (using brachytherapy or EBRT) on top of moderately hypofractionated EBRT in high-intermediate to high-risk patients.[32]

In recent years, there has been growing interest in ultra-hypofractionated EBRT for definitive treatment of prostate cancer (using ≥5 Gy per fraction) to further exploit the biological advantage of its low alpha/beta ratio. The HYPO trial showed comparable 5-year failure-free survival and late toxicities but increased acute GU and GI toxicities for ultra-hypofractionation compared to conventional schedules.[33] The 2-year toxicity data of the PACE-B trial[34,35] and early toxicity data of HEAT (The Helicobacter Eradication Aspirin Trial)[36] had not shown significant safety concerns with ultra-hypofractionated radiotherapy. The long-term data of these studies are eagerly awaited. Considering the encouraging results so far, the ASTRO/ASCO/AUA 2018 guidelines conditionally recommended that ultra-hypofractionated radiotherapy may be offered for low- and intermediate-risk prostate cancer but strongly encouraged treatment of intermediate-risk patients in a clinical trial or multi-institutional registry.[9] It is noteworthy that stereotactic ablative radiotherapy demands high precision in setup, planning, dosimetry, verification, and quality assurance.

The availability of biodegradable spacers placed between the rectum and prostate has been reported to reduce the volume of rectum irradiated and thus further mitigates GI toxicity. Both hydrogel and hyaluronic acid spacers have been demonstrated in phase III clinical trials to improve rectal sparing and reduce GI toxicity.[37,38] As moderately hypofractionated EBRT has been reported to result in more acute GI toxicity compared to conventional schedules, use of perirectal spacers may play a role in improving the therapeutic window in suitable patients.

The effect of high dose volumes (i.e., the volume receiving high dose) of rectum and bladder on radiotherapy-related toxicities was reported in this study. These OAR parameters were chosen due to the more established dose-response relationship with radiotherapy-related toxicities and reflected our local OAR constraints. Low dose volumes to OARs are potential predictors of low-grade toxicities, and it will be a meaningful future research direction to explore the dose-response relationship between low dose volumes to OARs (e.g., $V_{20}$) and radiotherapy-related toxicities.

# CONCLUSION

A major advantage of moderate hypofractionation is the reduction of ≥40% treatment visits, translating to improved patient convenience, alleviation of clinical manpower pressures, and demands on healthcare resources. With the demanding workload in the healthcare system, moderately hypofractionated radiotherapy is considered a cost-effective treatment strategy.[39]

Local institutional outcomes suggested that image-guided moderately hypofractionated radiotherapy using VMAT technique is a safe, effective, and feasible alternative to conventionally fractionated radiotherapy for low- and intermediate-risk prostate cancer in the Chinese community in a public hospital setting. Patients should be counselled on the potential increase in acute GI toxicity that is likely to be low-grade. It is encouraged to take note of the PTV during radiotherapy planning and to offer close monitoring for acute toxicities.

# REFERENCES

1. Sung H, Ferlay J, Siegel RL, Laversanne M, Soerjomataram I, Jemal A, et al. Global Cancer Statistics 2020: GLOBOCAN estimates of incidence and mortality worldwide for 36 cancers in

185 countries. CA Cancer J Clin. 2021;71:209-49.
2. Hospital Authority, Hong Kong SAR Government. Overview of Hong Kong Cancer Statistics of 2020. 2022. Available from: https://www3.ha.org.hk/cancereg/pdf/overview/Overview%20of%20HK%20Cancer%20Stat%202020.pdf. Accessed 1 Jun 2023.
3. Hamdy FC, Donovan JL, Lane JA, Mason M, Metcalfe C, Holding P, et al. 10-year outcomes after monitoring, surgery, or radiotherapy for localized prostate cancer. N Engl J Med. 2016;375:1415-24.
4. Michalski JM, Moughan J, Purdy J, Bosch W, Bruner DW, Bahary JP, et al. Effect of standard vs dose-escalated radiation therapy for patients with intermediate-risk prostate cancer: the NRG Oncology RTOG 0126 randomized clinical trial. JAMA Oncol. 2018;4:e180039.
5. Dearnaley DP, Jovic G, Syndikus I, Khoo V, Cowan RA, Graham JD, et al. Escalated-dose versus control-dose conformal radiotherapy for prostate cancer: long-term results from the MRC RT01 randomised controlled trial. Lancet Oncol. 2014;15:464-73.
6. Dearnaley DP, Sydes MR, Graham JD, Aird EG, Bottomley D, Cowan RA, et al. Escalated-dose versus standard-dose conformal radiotherapy in prostate cancer: first results from the MRC RT01 randomised controlled trial. Lancet Oncol. 2007;8:475-87.
7. Peeters ST, Heemsbergen WD, Koper PC, van Putten WL, Slot A, Dielwart MF, et al. Dose-response in radiotherapy for localized prostate cancer: results of the Dutch multicenter randomized phase III trial comparing 68 Gy of radiotherapy with 78 Gy. J Clin Oncol. 2006;24:1990-6.
8. Pollack A, Zagars GK, Starkschall G, Antolak JA, Lee JJ, Huang E, et al. Prostate cancer radiation dose response: results of the M. D. Anderson phase III randomized trial. Int J Radiat Oncol Biol Phys. 2002;53:1097-105.
9. Morgan SC, Hoffman K, Loblaw DA, Buyyounouski MK, Patton C, Barocas D, et al. Hypofractionated radiation therapy for localized prostate cancer: an ASTRO, ASCO, and AUA evidence-based guideline. J Clin Oncol. 2018;36:JCO1801097.
10. Fowler J, Chappell R, Ritter M. Is alpha/beta for prostate tumors really low? Int J Radiat Oncol Biol Phys. 2001;50:1021-31.
11. Brenner DJ, Hall EJ. Fractionation and protraction for radiotherapy of prostate carcinoma. Int J Radiat Oncol Biol Phys. 1999;43:1095-101.
12. Brenner DJ, Martinez AA, Edmundson GK, Mitchell C, Thames HD, Armour EP. Direct evidence that prostate tumors show high sensitivity to fractionation (low alpha/beta ratio), similar to late-responding normal tissue. Int J Radiat Oncol Biol Phys. 2002;52:6-13.
13. Khoo VS, Dearnaley DP. Question of dose, fractionation and technique: ingredients for testing hypofractionation in prostate cancer—the CHHiP trial. Clin Oncol (R Coll Radiol). 2008;20:12-4.
14. Proust-Lima C, Taylor JM, Sécher S, Sandler H, Kestin L, Pickles T, et al. Confirmation of a low $\alpha/\beta$ ratio for prostate cancer treated by external beam radiation therapy alone using a post-treatment repeated-measures model for PSA dynamics. Int J Radiat Oncol Biol Phys. 2011;79:195-201.
15. Vogelius IR, Bentzen SM. Meta-analysis of the alpha/beta ratio for prostate cancer in the presence of an overall time factor: bad news, good news, or no news? Int J Radiat Oncol Biol Phys. 2013;85:89-94.
16. Zaorsky NG, Palmer JD, Hurwitz MD, Keith SW, Dicker AP, Den RB. What is the ideal radiotherapy dose to treat prostate cancer? A meta-analysis of biologically equivalent dose escalation. Radiother Oncol. 2015;115:295-300.
17. Lee WR, Dignam JJ, Amin MB, Bruner DW, Low D, Swanson GP, et al. Randomized phase III noninferiority study comparing two radiotherapy fractionation schedules in patients with low-risk prostate cancer. J Clin Oncol. 2016;34:2325-32.
18. Catton CN, Lukka H, Gu CS, Martin JM, Supiot S, Chung PW, et al. Randomized trial of a hypofractionated radiation regimen for the treatment of localized prostate cancer. J Clin Oncol. 2017;35:1884-90.
19. Dearnaley D, Syndikus I, Mossop H, Khoo V, Birtle A, Bloomfield D, et al. Conventional versus hypofractionated high-dose intensity-modulated radiotherapy for prostate cancer: 5-year outcomes of the randomised, non-inferiority, phase 3 CHHiP trial. Lancet Oncol. 2016;17:1047-60.
20. Hickey BE, James ML, Daly T, Soh FY, Jeffery M. Hypofractionation for clinically localized prostate cancer. Cochrane Database Syst Rev. 2019;9:CD011462.
21. Avkshtol V, Ruth KJ, Ross EA, Hallman MA, Greenberg RE, Price RA Jr, et al. Ten-year update of a randomized, prospective trial of conventional fractionated versus moderate hypofractionated radiation therapy for localized prostate cancer. J Clin Oncol. 2020;38:1676-84.
22. Incrocci L, Wortel RC, Alemayehu WG, Aluwini S, Schimmel E, Krol S, et al. Hypofractionated versus conventionally fractionated radiotherapy for patients with localised prostate cancer (HYPRO): final efficacy results from a randomised, multicentre, open-label, phase 3 trial. Lancet Oncol. 2016;17:1061-9.
23. Bruner DW, Pugh SL, Lee WR, Hall WA, Dignam JJ, Low D, et al. Quality of life in patients with low-risk prostate cancer treated with hypofractionated vs conventional radiotherapy: a phase 3 randomized clinical trial. JAMA Oncol. 2019;5:664-70.
24. Aluwini S, Pos F, Schimmel E, Krol S, van der Toorn PP, de Jager H, et al. Hypofractionated versus conventionally fractionated radiotherapy for patients with prostate cancer (HYPRO): late toxicity results from a randomised, non-inferiority, phase 3 trial. Lancet Oncol. 2016;17:464-74.
25. Aluwini S, Pos F, Schimmel E, van Lin E, Krol S, van der Toorn PP, et al. Hypofractionated versus conventionally fractionated radiotherapy for patients with prostate cancer (HYPRO): acute toxicity results from a randomised non-inferiority phase 3 trial. Lancet Oncol. 2015;16:274-83.
26. Zhong QZ, Xia X, Gao H, Xu YG, Zhao T, Wu QH, et al. Hypofractionated versus conventionally fractionated image-guided volumetric-modulated arc radiotherapy for localized prostate cancer: a phase II randomized trial from China. Aging (Albany NY). 2021;13:6936-44.
27. Yao L, Shou J, Wang S, Song Y, Fang H, Lu N, et al. Long-term outcomes of moderately hypofractionated radiotherapy (67.5 Gy in 25 fractions) for prostate cancer confined to the pelvis: a single center retrospective analysis. Radiat Oncol. 2020;15:231.
28. United States Department of Health and Human Services. Common Terminology Criteria for Adverse Events (CTCAE) Version 5.0. 2017. Available from: http://ctep.cancer.gov/protocoldevelopment/electronic_applications/docs/ctcae_v5_quick_reference_5x7.pdf. Accessed 1 Jun 2023.
29. Roach M 3rd, Hanks G, Thames H Jr, Schellhammer P, Shipley WU, Sokol GH, et al. Defining biochemical failure following radiotherapy with or without hormonal therapy in men with clinically localized prostate cancer: recommendations of the RTOG-ASTRO Phoenix Consensus Conference. Int J Radiat Oncol Biol Phys. 2006;65:965-74.
30. Wortel RC, Pos FJ, Heemsbergen WD, Incrocci L. Sexual function after hypofractionated versus conventionally fractionated radiotherapy for prostate cancer: results from the randomized phase III HYPRO trial. J Sex Med. 2016;13:1695-703.
31. Kerkmeijer LG, Groen VH, Pos FJ, Haustermans K, Monninkhof

EM, Smeenk RJ, et al. Focal boost to the intraprostatic tumor in external beam radiotherapy for patients with localized prostate cancer: results from the FLAME randomized phase III trial. J Clin Oncol. 2021;39:787-96.
32. Syndikus I, Cruickshank C, Staffurth J, Tree A, Henry A, Naismith O, et al. PIVOTALboost: a phase III randomised controlled trial of prostate and pelvis versus prostate alone radiotherapy with or without prostate boost (CRUK/16/018). Clin Transl Radiat Oncol. 2020;25:22-8.
33. Widmark A, Gunnlaugsson A, Beckman L, Thellenberg-Karlsson C, Hoyer M, Lagerlund M, et al. Ultra-hypofractionated versus conventionally fractionated radiotherapy for prostate cancer: 5-year outcomes of the HYPO-RT-PC randomised, non-inferiority, phase 3 trial. Lancet. 2019;394:385-95.
34. Brand DH, Tree AC, Ostler P, van der Voet H, Loblaw A, Chu W, et al. Intensity-modulated fractionated radiotherapy versus stereotactic body radiotherapy for prostate cancer (PACE-B): acute toxicity findings from an international, randomised, open-label, phase 3, non-inferiority trial. Lancet Oncol. 2019;20:1531-43.
35. Tree AC, Ostler P, van der Voet H, Chu W, Loblaw A, Ford D, et al. Intensity-modulated radiotherapy versus stereotactic body radiotherapy for prostate cancer (PACE-B): 2-year toxicity results from an open-label, randomised, phase 3, non-inferiority trial. Lancet Oncol. 2022;23:1308-20.
36. Abramowitz MC, Kwon D, Freeman DE, Dogan N, Eade T, Punnen S, et al. Early toxicity and patient reported outcomes from a radiation hypofractionation randomized trial of extended vs accelerated therapy for prostate cancer (HEAT). Int J Radiat Oncol Biol Phys. 2018;102:e98-9.
37. Hamstra DA, Mariados N, Sylvester J, Shah D, Karsh L, Hudes R, et al. Continued benefit to rectal separation for prostate radiation therapy: final results of a phase III trial. Int J Radiat Oncol Biol Phys. 2017;97:976-85.
38. Mariados NF, Orio PF 3rd, Schiffman Z, Van TJ, Engelman A, Nurani R, et al. Hyaluronic acid spacer for hypofractionated prostate radiation therapy: a randomized clinical trial. JAMA Oncol. 2023;9:511-8.
39. Kraus RD, Weil CR, Abdel-Wahab M. Benefits of adopting hypofractionated radiotherapy as a standard of care in low-and middle-income countries. JCO Glob Oncol. 2022;8:e2200215.

Hong Kong J Radiol. 2024;27(2):e100-5. Published 21 May 2024 | https://doi.org/10.12809/hkjr2217670

## ORIGINAL ARTICLE

# Grouped Amorphous Microcalcifications on Mammography: A Single-Centre 8-Year Retrospective Cohort Study on an Asian Population

**JK Fung, AYT Lai, AHC Wong, CKM Mo, KH Chin, WWC Wong**

*Department of Radiology, Pamela Youde Nethersole Eastern Hospital, Hong Kong SAR, China*

## ABSTRACT

***Introduction:*** *Grouped amorphous microcalcifications on mammography are classified as BI-RADS (Breast Imaging Reporting and Data System) category 4B. While recent international studies support a lower subcategory (4A), we sought to measure the malignancy rate of grouped amorphous microcalcifications classified as BI-RADS category 4A or above in the Asian population.*

***Methods:*** *All cases at our hospital with any kind of suspicious microcalcifications underwent either stereotactic-guided vacuum-assisted biopsy or excisional biopsy with stereotactic localisation from 2013 to 2020 were retrieved. Cases with grouped amorphous microcalcifications as the most suspicious morphology on magnified views were selected. Only cases with at least 2 years of follow-up were included. Final histological diagnosis was based on the highest grade of tissue diagnosis at biopsy or excision.*

***Results:*** *Among 333 biopsied cases, 121 were grouped amorphous microcalcifications. The majority of patients (92.5%) were ethnic Chinese while the rest (7.5%) were Pacific Islanders. A total of 4.1% (n = 5) had malignant final pathology, with four ductal carcinomas in situ (DCIS) and one invasive ductal carcinoma. A total of 9.1% (n = 11) had high-risk pathology (all atypical ductal hyperplasia). In two cases, the microcalcifications were located adjacent to surgical scars, with one diagnosed as DCIS.*

***Conclusion:*** *The malignancy rate of grouped amorphous microcalcifications in our study is in line with recent studies, providing support for classifying a BI-RADS category 4A for these calcifications. The majority of the malignant lesions came back as DCIS, which carries promising post-treatment survival rates. Histological diagnosis remains indicated for grouped amorphous microcalcifications, yet more nuanced management plans may be employed in the future.*

***Key Words:*** *Breast; Calcinosis; Neoplasms*

***Correspondence:*** *Dr JK Fung, Department of Radiology, Pamela Youde Nethersole Eastern Hospital, Hong Kong SAR, China*
*Email: fk100@ha.org.hk*

Submitted: 14 November 2022; Accepted: 29 September 2023.

Contributors: All authors designed the study, acquired and analysed the data. JKF, AYTL, AHCW, CKMM and KHC drafted the manuscript. All authors critically revised the manuscript for important intellectual content. All authors had full access to the data, contributed to the study, approved the final version for publication, and take responsibility for its accuracy and integrity.

Conflicts of Interest: All authors have disclosed no conflicts of interest.

Funding/Support: This research received no specific grant from any funding agency in the public, commercial, or not-for-profit sectors.

Data Availability: All data generated or analysed during the present study are available from the corresponding author on reasonable request.

Ethics Approval: The research was approved by the Hong Kong East Cluster Research Ethics Committee of Hospital Authority, Hong Kong (Ref No.: HKECREC-2022-062). Informed patient consent was waived by the Committee due to the retrospective nature of the research.

# 中文摘要

## 乳房X光檢查中的聚集無定形微鈣化：亞洲人群的單中心8年回顧性隊列研究

馮喬政、黎爾德、黃可澄、巫冠文、錢凱、黃慧中

**引言：**乳房X光檢查中的聚集無定形微鈣化歸類為 BI-RADS（乳房影像報告和數據系統）類別 4B。雖然最近的國際研究支持更低的子類別（4A），但我們嘗試評估亞洲人群中分類為BI-RADS 4A類或以上的聚集無定形微鈣化的惡性率。

**方法：**我們檢索於2013至2020年期間在本院接受立體定位真空輔助活檢或立體定位切除活檢的所有疑似微鈣化病例，並選擇放大視圖中最可疑的形態學為聚集無定形微鈣化的病例。我們僅納入至少追蹤兩年的病例。最終的組織學診斷是基於活檢或切除時組織學診斷的最高等級。

**結果：**333例活檢中，121例為無定形微鈣化。大多數患者（92.5%）是華裔，其餘患者（7.5%）是太平洋島民。總共4.1%（n = 5）最終病理為惡性，其中4例為導管原位癌，1例為浸潤性乳管癌。總共9.1%（n = 11）有高風險病理（皆為非典型導管增生）。2例的微鈣化位於手術疤痕附近，其中1例被診斷為導管原位癌。

**結論：**本研究中分組的無定形微鈣化的惡性率與最近的研究一致，為這些鈣化的BI-RADS 4A 類分類提供了支持。大多數惡性病變以導管原位癌的形式復發，治療後的存活率良好。組織學診斷仍適用於聚集無定形微鈣化，但未來可能會採用更細緻的處理計劃。

## INTRODUCTION

Amorphous morphology is categorised as 4B in the fifth edition of BI-RADS (Breast Imaging Reporting and Data System) of the American College of Radiology (ACR), with a positive predictive value of malignancy of approximately 20% based on older case series.[1] Recent retrospective studies, including mostly Western populations, have reported a malignancy rate of ≤10% for grouped distribution, which may suggest a more nuanced treatment approach.[2,3]

Studies targeting grouped microcalcifications in the Asian population are lacking. A relatively representative study including 216 subjects by Iwase et al[4] reported a malignancy rate of 2.8% in the Japanese population. The objective of our study was to report the malignancy rate of grouped amorphous microcalcifications in the Asian population.

## METHODS

Mammographically detected microcalcifications classified as BI-RADS category ≥4A are routinely scheduled for biopsy in our centre at Pamela Youde Nethersole Eastern Hospital in Hong Kong. We retrieved all such cases that underwent either stereotactic-guided vacuum-assisted biopsy or excisional biopsy with stereotactic-guided localisation from 2013 to 2020 in our centre from the electronic patient record.

Preprocedural mammograms were reviewed independently by two breast radiologists (with 5 and ≥10 years of experience, respectively) on dedicated 5-megapixel breast imaging displays (MDMG-5221; Barco NV, Kortrijk, Belgium). The radiologists were blinded to the histological results.

All cases without dedicated magnification views were excluded. Cases with grouped amorphous microcalcifications, defined according to the fifth edition of BI-RADS as the most suspicious morphology (i.e., either mammographically or sonographically having a higher BI-RADS score, with category 4C being the most suspicious), were documented by the radiologists. Associated features, including proximity to previous surgical scars, history of or concurrent malignancy, and presence of multiple (≥3) groups of amorphous calcifications in the same quadrant, were also recorded. In the event of any discrepancies, a final decision was

made by a third experienced breast radiologist (with ≥10 years of experience).

Only cases with ≥2 years' follow-up in our institution were included. Final histological diagnosis was obtained from the electronic patient record and based on the highest-grade tissue diagnosis at biopsy or excision. Final statistical database was analysed with SPSS (Windows version 29.0; IBM Corp, Armonk [NY], United States).

## RESULTS

A total of 333 cases of mammographically-detected suspicious microcalcifications underwent biopsy in our centre across the 8-year span. Twenty-two cases without dedicated magnification views were excluded. A total of 130 clusters of amorphous microcalcifications in 130 cases were identified. Eight cases with <2 years of follow-up in our institution were excluded (seven benign and one high-risk pathology). One case of invasive ductal carcinoma with architectural distortion as the more suspicious feature was excluded from statistical analysis.

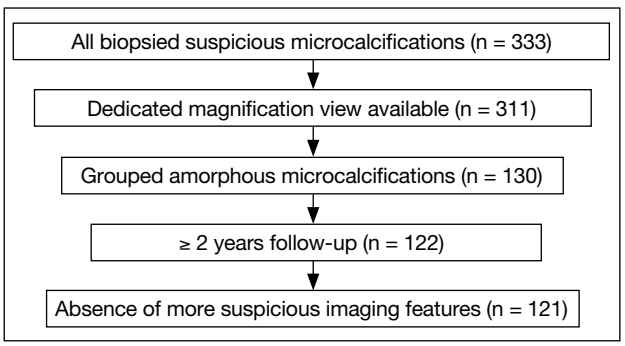


**Figure 1.** Summary of the cases.

The final study included 121 groups of amorphous microcalcifications in 120 patients (Figure 1). One patient underwent two biopsies 6 years apart, for one group of amorphous microcalcifications in each breast. Both were proven benign. The majority of patients (92.5%) were Chinese and the rest (7.5%) were Pacific Islanders (Table).

**Table.** Patient demographics, results, and associated features.*

| | |
|---|---|
| Ethnicity (n = 120) | |
| Chinese | 111 (92.5%) |
| Pacific Islanders | 9 (7.5%) |
| Age range, y (n = 120) | |
| ≤40 | 2 (1.7%) |
| 41-50 | 46 (38.3%) |
| 51-60 | 47 (39.2%) |
| ≥61 | 25 (20.8%) |
| Pathology (n = 121)† | |
| Benign | 105 (86.7%) |
| No evidence of malignancy | 30 (24.8%) |
| Fibrocystic change | 73 (60.3%) |
| Foreign body granulomatous reaction | 1 (0.8%) |
| Focal ductal hyperplasia | 1 (0.8%) |
| High risk‡ | 11 (9.1%) |
| Malignancy | 5 (4.1%) |
| DCIS | 4 (3.3%) |
| Invasive | 1 (0.8%) |
| Associated features | |
| Adjacent to surgical scars | 2 |
| History of/concurrent malignancy | 29 |
| Multiple groups of amorphous microcalcifications in the same quadrant | 13 |

Abbreviation: DCIS = ductal carcinoma in situ.
* Data are shown as No. or No. (%), unless otherwise specified.
† Cases of grouped amorphous microcalcifications included in final study.
‡ All are atypical ductal hyperplasia.

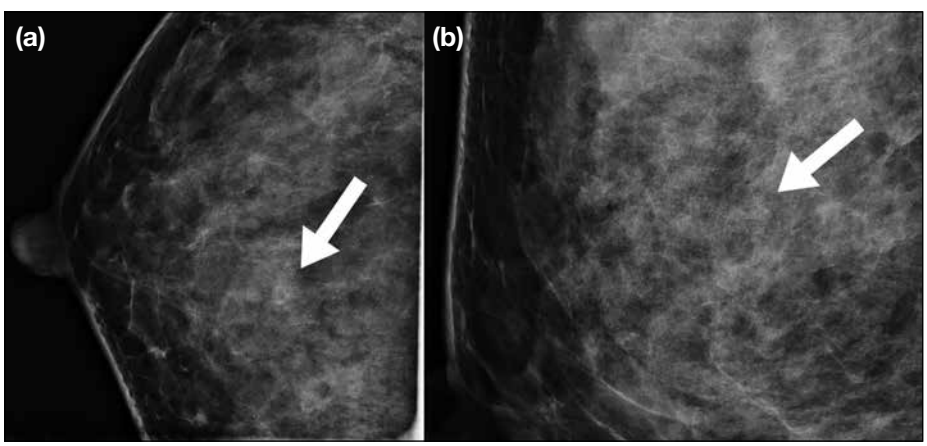


**Figure 2.** A 41-year-old female's follow-up of bilateral probably benign lesions. (a) Magnified craniocaudal view of the right breast. A group of amorphous microcalcifications (arrow) is faintly observed at middle-to-posterior depth in the central portion. (b) Magnified mediolateral oblique view of the right breast showing corresponding grouped microcalcifications (arrow) at middle-to-posterior depth in the upper portion. Pathology of stereotactic-guided vacuum-assisted biopsy and subsequent mastectomy confirmed ductal carcinoma in situ.

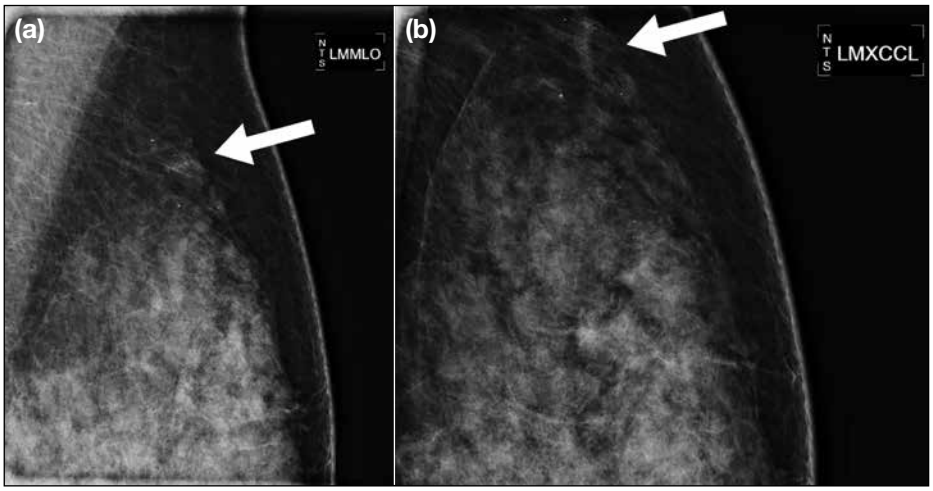


**Figure 3.** A 52-year-old female's follow-up of bilateral probably benign lesions. (a) Magnified mediolateral oblique view of the left breast. Grouped amorphous microcalcifications newly observed in the upper portion of the breast (arrow). (b) Exaggerated magnified craniocaudal view of the left breast showing corresponding grouped amorphous microcalcifications in the upper outer quadrant (arrow). No sonographic correlate. Pathology of vacuum-assisted biopsy specimen was ductal carcinoma in situ and subsequent excision specimen was upgraded to invasive ductal carcinoma.

Malignancy was found on pathology in 4.1% (n = 5) of the cases. The majority of these cases (80%) came back as ductal carcinoma in situ (DCIS) [Figure 2]. Two cases underwent surgical excision, and two cases underwent simple mastectomy. The remaining case was shown to be invasive ductal carcinoma on the surgical specimen of breast conservation treatment, which was upgraded from DCIS on vacuum-assisted biopsy (Figure 3). It was positive for oestrogen and progesterone receptors and negative for human epidermal growth factor receptor 2.

In all, 9.1% (n = 11) had high-risk pathology and all yielded atypical ductal hyperplasia (ADH) [Table]. Eight cases underwent local excision and two underwent wide local excision. There was no upgrade in the final pathology of any of the 10 cases who underwent surgical excision. One was concluded to have been completely removed by vacuum-assisted excision in a joint clinico-radiological-pathological meeting involving pathologists, radiologists, and breast surgeons. Two cases had the microcalcifications located adjacent to the surgical scars for previous DCIS and invasive tubular carcinoma and came back as benign foreign body granulomatous reaction (Figure 4) and DCIS (Figure 5), respectively.

Within the 2-year follow-up period, there was no recurrence in the malignant and high-risk groups. The grouped macrocalcifications in the benign groups all remained stable. As for the 13 cases with multiple groups of amorphous microcalcifications, the other groups also showed no substantial change, and thus were not rebiopsied.

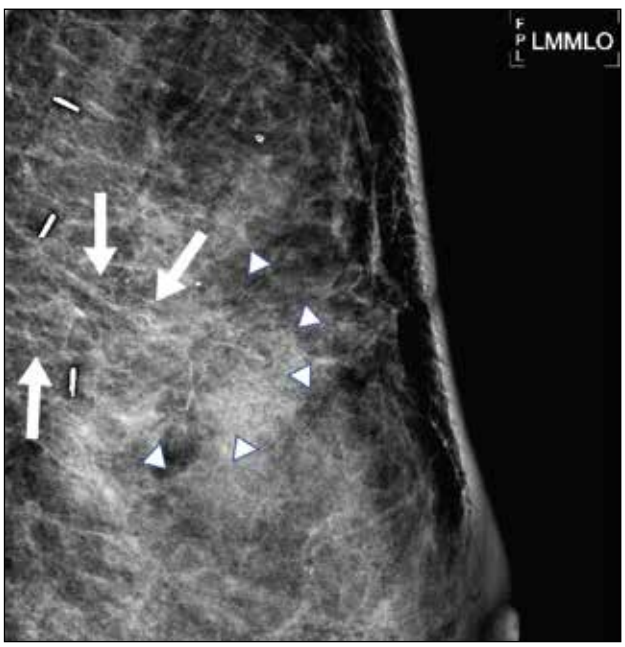


**Figure 4.** Magnified mediolateral oblique view of the upper left breast in a 55-year-old female patient 1 year after local excision of tubular carcinoma. A new group of amorphous and punctate microcalcifications (arrows) at middle-to-posterior depth adjacent to the surgical scar (arrowheads) was detected. Pathology of the microcalcifications showed benign pathology with a foreign body granulomatous reaction. Follow-up mammograms over 2 years showed no substantial change.

## DISCUSSION

Amorphous microcalcifications with grouped distribution are the most common type of suspicious microcalcifications. Studies examining the malignancy rate of grouped amorphous microcalcifications are

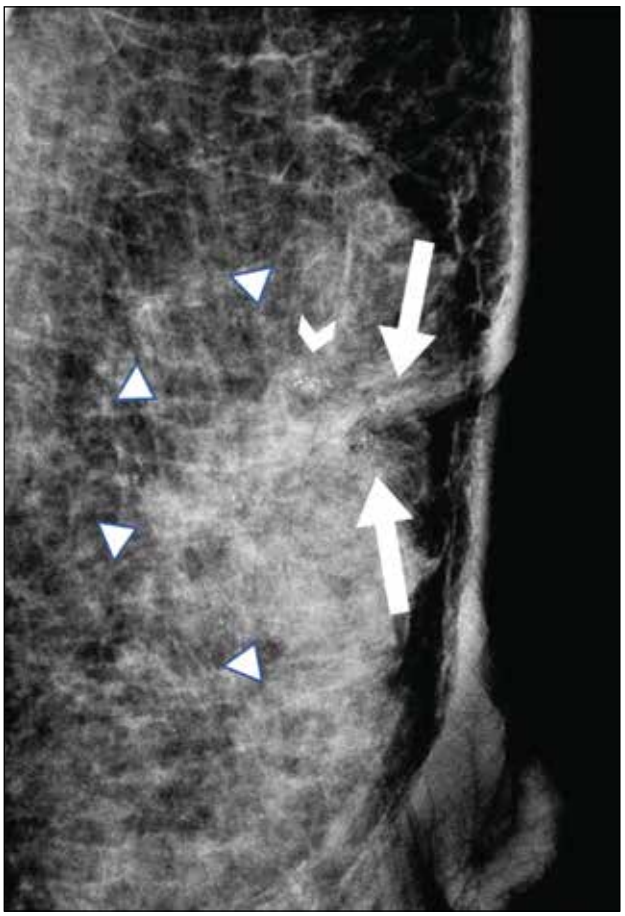

**Figure 5.** A 46-year-old female with history of left breast conservative treatment for ductal carcinoma in situ (DCIS). Magnified mediolateral oblique view of the upper portion of the left breast 2 years after breast conservation treatment demonstrated a new group of amorphous microcalcifications (arrows) anterior to the surgical site (arrowheads), later confirmed as DCIS on stereotactic-guided vacuum-assisted biopsy. Another group of punctate microcalcifications (notched arrowhead) showed no substantial interval change. A mastectomy was subsequently performed and confirmed no residual malignancy.

limited. The single-institutional retrospective study performed by Iwase et al[4] is by far the relatively more representative one covering the Asian population. Our study sought to reveal the malignancy rate from an 8-year database, with vast majority of Chinese ethnicity, and to compare it with the reported rates of current international studies.

The BI-RADS lexicon was developed by the ACR to standardise the description and management of mammographically detected findings. Various combinations of microcalcification morphology and distribution are subcategorised by their respective malignancy risks, aligned with positive predictive values generated from ACR's national mammography database. BI-RADS category 4A and 4B lesions carry malignancy risks of 2% to 10% and 10% to 50%, respectively.[1] While biopsy is recommended for both subcategories, BI-RADS category 4B lesions commonly require a more comprehensive and meticulous management plan, including rebiopsies in cases of benign pathological findings, or even prophylactic surgical excision subject to multiple factors and patient preference. Other studies[2,4,5] have revealed malignancy rates ranging from 2.8% to 7.6%, which fall within the BI-RADS 4A category. This is in line with the 4.1% malignancy rate (95% confidence interval = 1.4%-9.4%) in our study, comprised of ethnic Chinese and Pacific Islanders.

In recent years, screening programmes advocate a high call-back biopsy rate, arousing controversies on the acceptable malignancy risk and critics on unnecessary biopsies and misallocated healthcare resources.[2,3,6] Apart from recent evidence supporting a lower BI-RADS subcategory as discussed above, the majority of the malignancies come back as DCIS, which is known to carry a high survival rate after surgical and optional adjuvant treatments.[2,3] This is also coherent with our results, with 80% (n = 4) of malignant cases being DCIS. Ongoing prospective trials such as the LORIS trial (LOw RISk DCIS) and the COMET initiative (Core Outcome Measures in Effectiveness Trials) are exploring alternative treatment options including observation.[3] Taking the latest evidence into consideration, a more nuanced management plan may be employed in the future.

Oligane et al[2] showed a higher risk of malignancy when multiple amorphous groups are present in the same quadrant. This feature was absent in the malignant cases from our dataset. There is currently no agreed standard management of the rest of the unbiopsied groups. In our institution, when multiple groups of low-suspicion microcalcifications are present in the same quadrant, the largest group of the most suspicious morphology/distribution combination is targeted for biopsy, as in the previous example in Figure 5. Majewski et al[7] demonstrated a low malignancy rate in secondary biopsy of other morphologically similar group(s) after initial histopathology showing a high-risk lesion, meaning an initial negative biopsy of one group is already useful to predict negative outcome in the others. Hence, we also advocate short follow-up intervals for the other groups

and biopsy only if any increase in extent or suspicion are observed.

### Limitations

There are a few limitations to this study. First, as with other published studies, it retrospectively included cases of suspicious microcalcifications from histopathological results. There could be under-called suspicious microcalcifications on initial mammograms not subjected to biopsy. This also raises the issue of inter-reader disagreement, particularly on calcification descriptors such as morphology, as suggested by Lee et al.[8] It is routine practice in our institution to perform a preprocedural joint-specialty review for selected ambiguous cases and for all external referrals to ensure appropriate diagnosis and management.

Second, eight cases were excluded from the final study due to lost or insufficient (<2 years) follow-up after biopsy, with seven benign and one ADH on biopsy. Oligane et al[2] reported a low (2.9%; all to DCIS) surgical upgrade rate for high-risk lesions. In the very unlikely situation that all eight cases turned out malignant 2 years after the biopsy, the overall malignancy rate would be 10% (13/130), falling between the BI-RADS 4A and 4B categories.

Third, our centre does not offer screening services. All screening-detected cases in this study were referrals from outside institutions. Of particular note, our centre has a large volume of surveillance cases with a personal history of breast malignancy or high-risk lesions, and these have been a proven independent predictor of higher malignancy risk by Oligane et al.[2] In our study, 29 cases (24%) of known or concurrent malignancy were included (Table), where two of which were DCIS cases, four of which were ADH, and the rest benign.

Finally, the single-centre setting may limit the external validity of the study.

## CONCLUSION

The findings of this study are in line with recent studies and support the BI-RADS category 4A for grouped amorphous microcalcifications. The majority of the malignant lesions also come back as DCIS, which carries a promising post-treatment survival rate. Histological diagnosis remains indicated, yet more nuanced management plans may be implicated in future practice. Further meta-analyses could be directed to exploring differences in malignancy rates across ethnicities, age, and breast density in order to tailor management.

## REFERENCES

1. American College of Radiology. Breast Imaging Reporting and Data System, 5th edition. Reston, VA: American College of Radiology; 2013.
2. Oligane HC, Berg WA, Bandos AI, Chen SS, Sohrabi S, Anello M, et al. Grouped amorphous calcifications at mammography: frequently atypical but rarely associated with aggressive malignancy. Radiology. 2018;288:671-9.
3. Moy L. Should we continue to biopsy all amorphous calcifications? Radiology. 2018;288:680-1.
4. Iwase M, Tsunoda H, Nakayama K, Morishita E, Hayashi N, Suzuki K, et al. Overcalling low-risk findings: grouped amorphous calcifications found at screening mammography associated with minimal cancer risk. Breast Cancer. 2017;24:579-84.
5. Kim SY, Kim HY, Kim EK, Kim MJ, Moon HJ, Yoon JH. Evaluation of malignancy risk stratification of microcalcifications detected on mammography: a study based on the 5th edition of BI-RADS. Ann Surg Oncol. 2015;22:2895-901.
6. Shen L, Ma X, Jiang T, Shen X, Yang W, You C, et al. Malignancy risk stratification prediction of amorphous calcifications based on clinical and mammographic features. Cancer Manag Res. 2021;13:235-45.
7. Majewski SA, Zuley ML, Pinnamaneni N, Ganott MA. Frequency of carcinoma at secondary imaging-guided percutaneous breast biopsy performed after a high-risk pathologic result at primary biopsy. AJR Am J Roentgenol. 2013;201:439-47.
8. Lee AY, Wisner DJ, Aminololama-Shakeri S, Arasu VA, Feig SA, Hargreaves J, et al. Inter-reader variability in the use of BI-RADS descriptors for suspicious findings on diagnostic mammography: a multi-institution study of 10 academic radiologists. Acad Radiol. 2017;24:60-6.

Hong Kong J Radiol. 2024;27(2):e106-11. Published 24 May 2024 | https://doi.org/10.12809/hkjr2317751

CASE REPORT

# Isolated Unilateral Facet Tuberculosis of the Lumbar Spine: A Case Report

**HL Chan[1], YH Sin[2], KF Tam[1]**

*[1]Department of Radiology, North District Hospital, Hong Kong SAR, China*
*[2]Department of Orthopaedics and Traumatology, North District Hospital, Hong Kong SAR, China*

## INTRODUCTION

Spinal tuberculosis without vertebral body involvement is rare and can be challenging to diagnose given its non-specific clinical symptoms and atypical radiological features. We present a case of isolated unilateral facet tuberculosis of the lumbar spine in a 70-year-old man who presented with right lower limb radiating pain, weight loss and dry cough. Subsequent radiological and histopathological examination confirmed spinal tuberculosis involving isolated unilateral facet.

## CASE PRESENTATION

A 70-year-old man presented with a 3-month history of back pain and radiating pain as well as impaired sensation over the right buttock and lateral side of the right lower limb since January 2023. He had no history of trauma or injury but had lost 10 pounds in the last 6 months and had a chronic dry cough with occasional shortness of breath at rest. Medical history was otherwise unremarkable with no history of primary neoplasm or family history of malignancy. He was admitted to the orthopaedic ward after presenting to the emergency department due to unbearable pain.

Physical examination revealed fair general condition, blood pressure 164/85 mm Hg, pulse rate 102 bpm, and no fever. There was localised paraspinal muscle spasm and tenderness at the right L4-L5 level. There was mild reduced sensation over the right L3 to L5 dermatome and right big toe dorsiflexion power reduced to grade 4/5 of the Medical Research Council Scale for Muscle Strength (corresponding to L5 myotome). Both lower limbs had preserved power and limb reflexes were unremarkable.

### Laboratory Investigation

Laboratory investigations revealed a microcytic hypochromic anaemia with haemoglobin level 12.6 g/dL, mean corpuscular volume 78.6 fL, mean corpuscular haemoglobin level 25.4 pg, white blood cell count $8.4 \times 10^9$/L, and platelet count $266 \times 10^9$/L. Erythrocyte sedimentation rate was increased at 42 mm/h, and C-reactive protein level was elevated at 20.1 mg/L.

***Correspondence:*** *Dr HL Chan, Department of Radiology, North District Hospital, Hong Kong SAR, China*
*Email: chl284@ha.org.hk*

Submitted: 19 July 2023; Accepted: 5 October 2023.

Contributors: All authors designed the study. HLC and YHS acquired the data. All authors analysed the data. HLC and YHS drafted the manuscript. KFT critically revised the manuscript for important intellectual content. All authors had full access to the data, contributed to the study, approved the final version for publication, and take responsibility for its accuracy and integrity.

Conflicts of Interest: All authors have disclosed no conflicts of interest.

Funding/Support: This study received no specific grant from any funding agency in the public, commercial, or not-for-profit sectors.

Data Availability: All data generated or analysed during the present study are available from the corresponding author on reasonable request.

Ethics Approval: The patient was treated in accordance with the Declaration of Helsinki. Patient's informed consent for the study and publication was obtained.

Liver and renal function tests were unremarkable. Blood tests for tumour markers including carcinoembryonic antigen, carbohydrate antigen 19-9, alpha-fetoprotein, and prostate-specific antigen were all normal.

## Radiological Investigations

Lumbar spine radiograph showed mild disc narrowing at L4-L5 level with no lytic changes or endplate erosion (Figure 1). No significant erosion or arthrosis at the facet joints of the lumbar spine were noted.

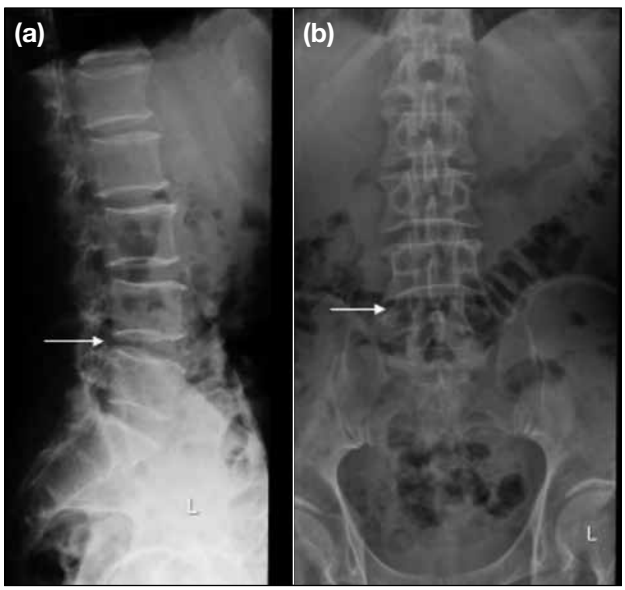


**Figure 1.** (a) Lateral and (b) frontal projection of the lumbar spine radiograph of the patient showed mild disc narrowing at L4-L5 level (arrows), without lytic changes or endplate erosion.

In view of the history of back pain and radiating right lower limb pain, magnetic resonance imaging (MRI) of the lumbar spine was performed and revealed abnormal bone marrow oedema in the right L4 inferior articular process and the right L5 superior articular process adjacent to the right L4/5 facet joint. No significant joint effusion in the right facet joint was seen. Bony erosion of the right L5 superior articular process was also noted. There was a T2-weighted slightly hyperintense epidural lesion in the right lateral recess and the right subarticular region of the spinal canal at level L4-L5, compressing the thecal sac and the right L5 descending nerve (Figure 2). The rest of the spine in T2-weighted sagittal screening was unremarkable.

A contrast MRI (intravenous gadolinium injection) was performed 10 days later (Figure 3), which confirmed the epidural lesion at the right lateral recess with rim enhancement, suggestive of an epidural abscess. There was also interval development of a 1-cm small peripheral rim-enhancing nodular T1-weighted intermediate soft tissue lesion posterior to the right L4/5 facet, next to the right L5 lamina.

Dual-energy computed tomography (DECT) of the

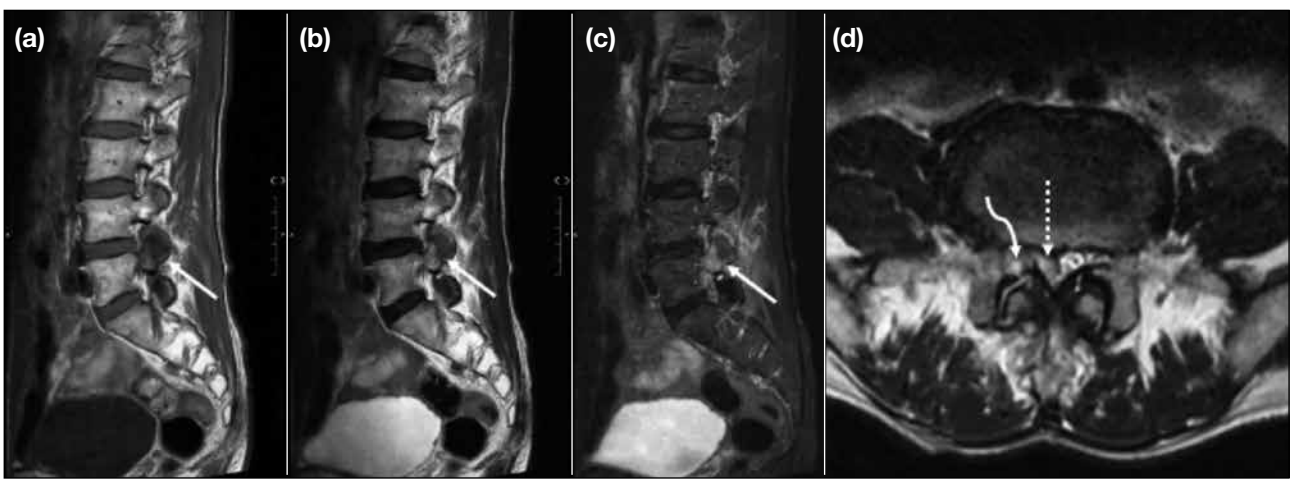


**Figure 2.** Magnetic resonance imaging of the lumbosacral spine of the patient. (a) T1-weighted sagittal image, (b) T2-weighted sagittal image, (c) T2-weighted short tau inversion recovery sagittal image, and (d) T2-weighted axial image at L4-L5 level. Abnormal bone marrow oedema in the right L4 inferior articular process and the right L5 superior articular process adjacent to the right L4/5 facet joint was shown (arrows in [a] to [c]). There was no significant joint effusion in the right facet joint. (d) Bony erosion of the right L5 superior articular process was noted (curved arrow). T2-weighted slightly hyperintense epidural lesion in the right lateral recess and the right subarticular region of the spinal canal at L4-L5 level was noted (dashed arrow), with compression on the thecal sac and the right L5 descending nerve.

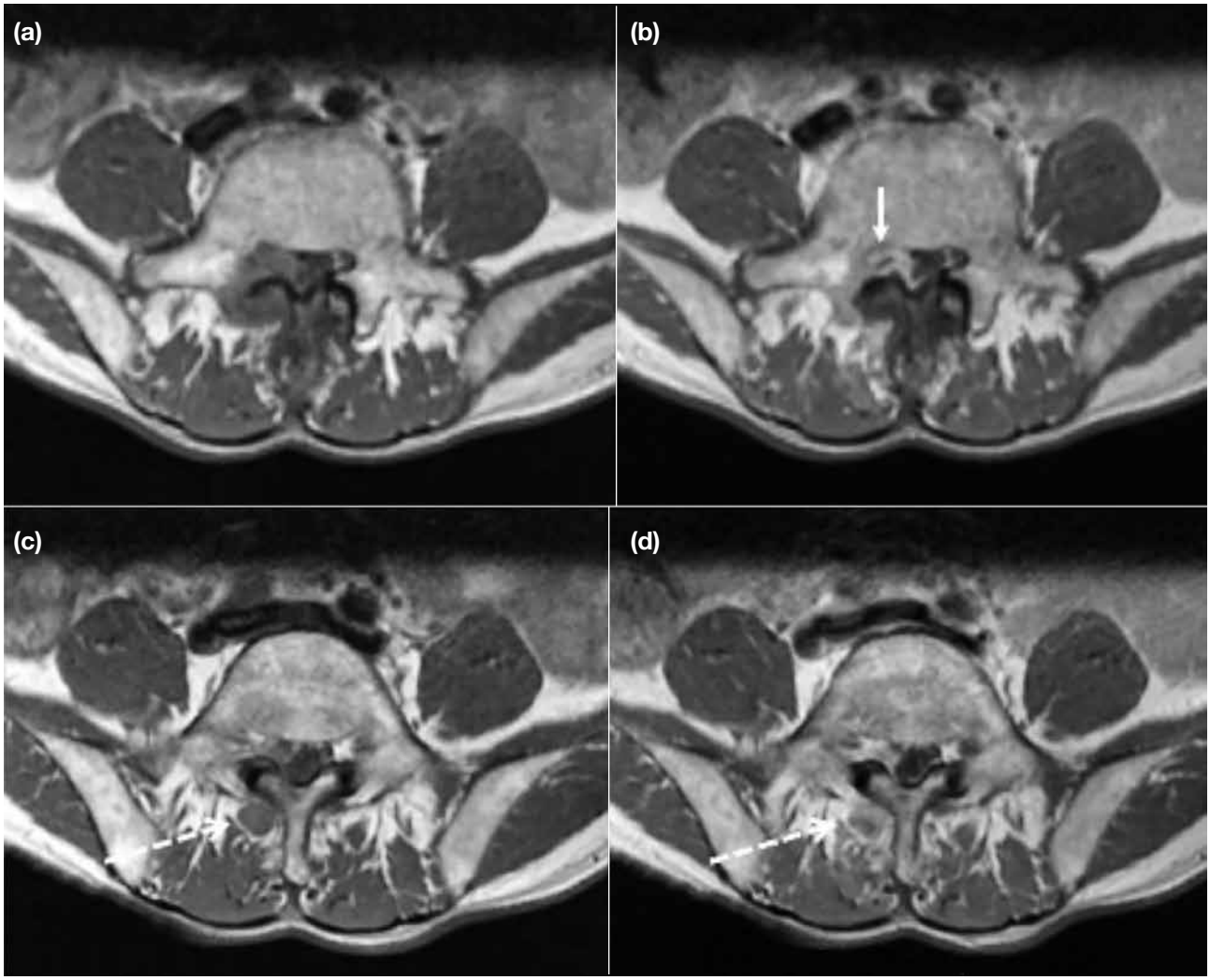


**Figure 3.** Contrast magnetic resonance imaging of the lumbar spine of the patient at L4-L5 level. (a, c) T1-weighted axial scan and (b, d) T1-weighted post-contrast scan showing the epidural lesion at the right lateral recess with rim enhancement, suggestive of epidural abscess (arrow in [b]). There was also interval development of a 1-cm small peripheral rim enhancing nodular T1-weighted intermediate soft tissue lesion (dashed arrows in [c] and [d]) posterior to the right L4/5 facet and next to the right L5 lamina.

lumbar spine showed no internal calcification or significant monosodium urate on colour-coded DECT. Computed tomography (CT) showed focal bone erosion at the superior articular process of L5 and small nodular soft tissue posterior to the right L4/5 facet next to the right L5 lamina (Figure 4), corresponding to the MRI findings.

Chest radiograph revealed progression of left upper zone opacification compared with an X-ray 6 years previously (Figure 5). Sputum acid-fast bacillus smear test was negative, but sputum culture 6 weeks later grew *Mycobacterium tuberculosis*. At this stage the top differential diagnosis was infective facet arthritis (particularly tuberculosis) but other possible differential diagnoses included gouty arthritis (unlikely because of negative urate deposition on DECT and no prior history of gouty arthritis) and malignancy (but no personal or family history of neoplasm and normal tumour markers). Radiologically, the imaging features were more suggestive of a joint disease with involvement of both articular sides of the right L4/5 facet. Malignancy or metastasis would be considered unlikely to cross the facet joint. The interval development of a small peripheral rim-enhancing nodular soft tissue lesion posterior to the right L4/5 facet after 10 days (on contrast MRI) also pointed to infection and made other differential diagnoses unlikely.


**Figure 4.** Axial computed tomography showing (a) focal bone erosion at the superior articular process of L5 (arrow) and (b) a small nodular soft tissue lesion posterior to the right L4/5 facet next to the right L5 lamina (dashed arrow).

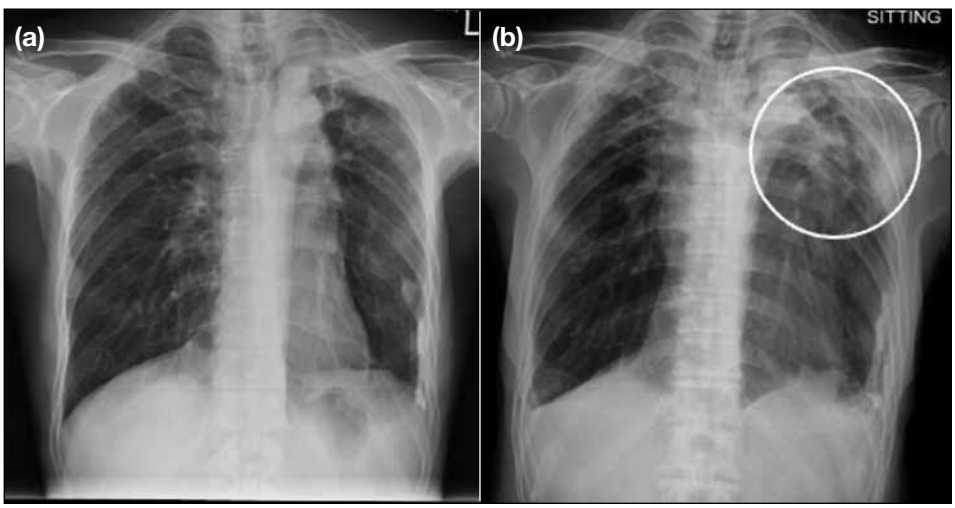


**Figure 5.** (a) Chest radiograph of the patient 6 years previously. (b) Current chest radiograph showing progression of left upper zone opacification (circle) compared with that 6 years ago.

CT-guided biopsy of the enhancing soft tissue lesion posterior to the right L4/5 facet was performed (Figure 6) using a co-axial system with a 17-gauge coaxial introducer (Merit Medical, South Jordan [UT], United States) and an 18-gauge Temno needle (Merit Medical, South Jordan [UT], United States). A total of four passes of biopsy were performed. Pathology results showed focal epithelioid granuloma formation. Scant acid-fast bacilli were highlighted by Ziehl-Neelsen stain but no fungal organisms were detected by periodic acid–Schiff or Grocott's methenamine silver stains. There was no evidence of malignancy. Overall features suggested mycobacterial infection.

Microbiology consultation suggested pulmonary tuberculosis with bone and joint involvement. The patient was commenced on antitubercular therapy of isoniazid, rifampicin, pyrazinamide, and ethambutol. A course of at least 9 to 12 months was planned in view of bone involvement.

The patient's neurological symptoms improved after 1 month of treatment. Laboratory tests also showed erythrocyte sedimentation rate reduced to 35 mm/h and C-reactive protein level reduced to 6.2 mg/L. CT of the lumbosacral spine after 2 months showed no further destruction or erosion of the right L4/5 facet joint and

interval reduction in size of the granulomatous soft tissue nodule posterior to the right L4/5 facet (Figure 7).

## DISCUSSION

*Mycobacterium tuberculosis* is a slow-growing fastidious, aerobic bacillus. The primary site of infection is usually the lungs with spinal infection always secondary and occurring by hematogenous dissemination.[1] Spinal tuberculosis accounts for approximately 10% of extrapulmonary tuberculosis.[2] It is disseminated through the intercostal arteries, lumbar arteries and the vertebral venous plexus (Batson's plexus).[3]

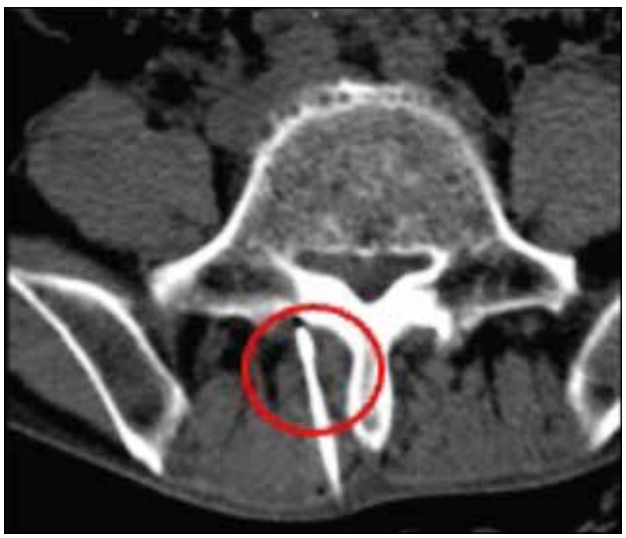

**Figure 6.** Computed tomography–guided biopsy of the enhancing soft tissue (circle) posterior lesion at the right L4/5 facet.

Tuberculosis causes the development of granulomatous inflammation that is characterised by the infiltration of lymphocytes and epithelioid cells. These cells may combine to form large Langhans-type giant cells and ultimately lead to caseating necrosis of the affected tissue, resulting in cold abscess formation.[1] Typical histopathological features of spinal tuberculosis include presence of tubercles, caseous necrosis, and tuberculous granuloma, while occasional atypical features may be encountered due to complex osteoclast development via dysregulation of cytokines and chemokines.[4,5] In our case, pathology revealed granuloma formation, one of the typical features, together with acid-fast bacilli highlighted by Ziehl-Neelsen stain, confirming the diagnosis of spinal tuberculosis.

Spinal tuberculosis most commonly manifests with vertebral body involvement (anterior element) and is seen in 90% to 95% of cases.[6] Posterior element involvement is relatively rare and occurs by spread of infection via the posterior vertebral venous plexus.[6] According to a study by Narlawar et al[7] of patients with spinal tuberculosis, only 3.06% (33/1076) showed isolated involvement of posterior elements in the absence of any associated involvement of anterior elements. Even more rare, only 1.3% (14/1076) showed isolated unilateral articular process involvement.[7]

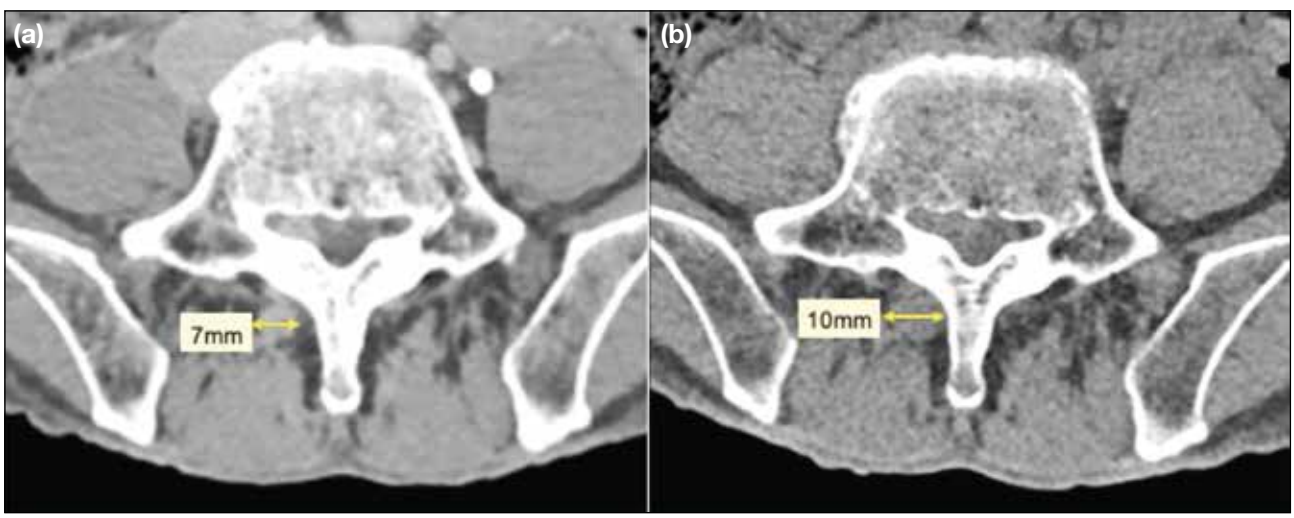


**Figure 7.** (a) Computed tomography (CT) of the lumbosacral spine of the patient after 2 months showing no further destruction or erosion of the right L4/5 facet joint and interval reduction in size of the granulomatous soft tissue nodule posterior to the facet, measuring 7 mm in transverse dimension, compared with 10 mm on CT 2 months previously (b) [double arrows].

Posterior spinal tuberculosis is usually associated with extradural granuloma and granulation tissue that form near the dural sac with intraspinal extension of tubercular granulation tissue or epidural abscess, causing spinal canal stenosis.[8] The diagnosis of posterior spinal tuberculosis can be challenging. The presenting symptoms include localised back pain, radiating pain or varying grades of paraplegia, along with other symptoms related to primary tuberculosis such as weight loss and chronic cough.[8] In our case, the patient presented with right sciatica that is rather non-specific and can mimic other musculoskeletal disorders (e.g., prolapsed intervertebral disc). Nonetheless the history of weight loss, chronic dry cough, and elevated inflammatory markers prompted further investigation.

Imaging studies including MRI and DECT revealed abnormal bone marrow oedema at the articular processes, focal bony erosion, rim-enhancing epidural tissue and a rim-enhancing nodular soft tissue lesion posterior to the right L4/5 facet. These findings supported a diagnosis of spinal tuberculosis,[9] later confirmed by histopathological examination of the biopsy specimen.

The differential diagnoses of isolated unilateral facet arthritis may include pyogenic arthritis, but no bacteria were detected in the culture of the facet biopsy. Gouty arthritis was also possible, but biopsy showed no gouty deposit and DECT detected no urate deposit.

The treatment of spinal tuberculosis depends on the severity of the disease and the presence of any neurological deficits or spinal instability. In general, antitubercular therapy is the mainstay of treatment. Surgery may be required in cases where there is neurological deficit, paravertebral abscess, spine instability or resistance to antitubercular medications.[10]

The American Thoracic Society, the Centers for Disease Control and Prevention, and the Infectious Diseases Society of America recommend antitubercular therapy for spinal tuberculosis comprised of an intensive phase of 2 months of isoniazid, rifampicin, pyrazinamide, and ethambutol, followed by a continuation phase for 7 to 10 months of isoniazid and rifampicin, with a total treatment duration of 9 to 12 months.[11] This is longer than the usual 6-month regimen for pulmonary tuberculosis. The decision to use longer treatment for spinal tuberculosis is because it is often associated with a higher risk of relapse and treatment failure compared with other forms of tuberculosis. The prolonged therapy is thought to reduce the risk of relapse and improve treatment outcomes.[12]

## CONCLUSION

Isolated unilateral facet tuberculosis of the lumbar spine is a rare form of spinal tuberculosis that poses diagnostic challenges. Clinical and radiological features are atypical. Diagnosis is usually based on a combination of clinical, laboratory, and imaging findings, along with a high index of suspicion. A multidisciplinary approach involving orthopaedic surgeons, radiologists, and microbiologists is necessary for optimal management of spinal tuberculosis. Antitubercular therapy is the mainstay of treatment, with surgery reserved for cases with neurological deficits or spinal instability.

## REFERENCES


1. Rajasekaran S, Soundararajan DC, Shetty AP, Kanna RM. Spinal tuberculosis: current concepts. Global Spine J. 2018;8(4 Suppl):96S-108S.
2. Batirel A. Tuberculous Spondylodiscitis. In: Sener A, Erdem H, editors. Extrapulmonary Tuberculosis. Cham: Springer International Publishing; 2019. p 83-99.
3. Shim HK, Cho HL, Lee SH. Spinal tuberculosis at the posterior element of spinal column: case report. Clin Neurol Neurosurg. 2014;124:146-50.
4. Hoshino A, Hanada S, Yamada H, Mii S, Takahashi M, Mitarai S, et al. *Mycobacterium tuberculosis* escapes from the phagosomes of infected human osteoclasts reprograms osteoclast development via dysregulation of cytokines and chemokines. Pathog Dis. 2014;70:28-39.
5. Li Y, Wang Y, Ding H, Zhang N, Ma A, Shi J, et al. Pathologic characteristics of spinal tuberculosis: analysis of 181 cases. Int J Clin Exp Pathol. 2020;13:1253-61.
6. Kumar K. Spinal tuberculosis, natural history of disease, classifications and principles of management with historical perspective. Eur J Orthop Surg Traumatol. 2016;26:551-8.
7. Narlawar RS, Shah JR, Pimple MK, Patkar DP, Patankar T, Castillo M. Isolated tuberculosis of posterior elements of spine: magnetic resonance imaging findings in 33 patients. Spine (Phila Pa 1976). 2002;27:275-81.
8. Kumar K. Posterior spinal tuberculosis: a review. Mycobact Dis. 2017;7:1000243.
9. Boruah DK, Gogoi BB, Prakash A, Lal NR, Hazarika K, Borah KK. Magnetic resonance imaging evaluation of posterior spinal tuberculosis: a cross-sectional study. Acta Radiol. 2021;62:1035-44.
10. Rasouli MR, Mirkoohi M, Vaccaro AR, Yarandi KK, Rahimi-Movaghar V. Spinal tuberculosis: diagnosis and management. Asian Spine J. 2012;6:294-308.
11. Nahid P, Dorman SE, Alipanah N, Barry PM, Brozek JL, Cattamanchi A, et al. Official American Thoracic Society/Centers for Disease Control and Prevention/Infectious Diseases Society of America Clinical Practice Guidelines: treatment of drug-susceptible tuberculosis. Clin Infect Dis. 2016;63:e147-95.
12. Pandita A, Madhuripan N, Pandita S, Hurtado RM. Challenges and controversies in the treatment of spinal tuberculosis. J Clin Tuberc Other Mycobact Dis. 2020;19:100151.

Hong Kong J Radiol. 2024;27(2):e112-6. Published 28 May 2024 | https://doi.org/10.12809/hkjr2317740

CASE REPORT

# Dendriform Pulmonary Ossification in a Young Man: A Case Report

**PL Lam[1], KK Cheng[2], KH Lee[1], JCH Tsang[3], ACL Chan[3], DHY Cho[1]**

*[1]Department of Diagnostic and Interventional Radiology, Kwong Wah Hospital, Hong Kong SAR, China*
*[2]Radiology Department, Hong Kong Baptist Hospital, Hong Kong SAR, China*
*[3]Department of Pathology, Queen Elizabeth Hospital, Hong Kong SAR, China*

## INTRODUCTION

Diffuse pulmonary ossification is characterised by metaplastic mature bone formation in the lungs. There are two distinct morphologies, namely, nodular and dendriform. The more common nodular pulmonary ossification occurs within alveolar spaces due to organisation of intra-alveolar exudates. The underlying culprits include chronic pulmonary congestion, such as in mitral valve stenosis, as well as previous insults causing haemosiderin accumulation.[1] On the contrary, dendriform pulmonary ossification (DPO) describes bony depositions in the alveolar interstitium that produce a branching 'dendriform' pattern.[2] It is sparsely reported with <100 cases recorded in the literature. In addition, DPO is often diagnosed only during autopsy. It is generally seen in older individuals aged >60 years.[3]

## CASE PRESENTATION

A 23-year-old Chinese man with good past health presented to the accident and emergency department (AED) in June 2017 with acute abdominal pain, vomiting and diarrhoea for 1 day. Apart from obesity (body mass index 32.5 kg/m$^2$), his physical examination and vital signs were normal. Chest radiograph incidentally revealed reticulonodular shadows over both lungs with basal predominance (Figure 1a). He was discharged 4 days later after recovering from acute gastroenteritis. Computed tomography (CT) of the thorax and medical specialist outpatient clinic consultation were arranged but the patient defaulted from follow-up.

Four years later, at the age of 27 years, the patient again presented to the AED with a 5-day history of mild right ankle pain. His physical examination was normal other than mild right ankle tenderness that quickly resolved with analgesics. Nonetheless chest radiograph revealed mild interval progression of bilateral pulmonary reticulonodular shadows (Figure 1b). The patient agreed to further workup of his abnormal radiographic findings.

Early CT of the thorax was performed 4 days later (Figure 2). There were numerous small (<3 mm)

***Correspondence:*** *Dr PL Lam, Department of Diagnostic and Interventional Radiology, Kwong Wah Hospital, Hong Kong SAR, China*
*Email: lpl404@ha.org.hk*

Submitted: 21 June 2023; Accepted: 29 September 2023.

Contributors: All authors designed the study, acquired, and analysed the data. PLL drafted the manuscript. All authors critically revised the manuscript for important intellectual content. All authors had full access to the data, contributed to the study, approved the final version for publication, and take responsibility for its accuracy and integrity.

Conflicts of Interest: All authors have disclosed no conflicts of interest.

Funding/Support: This study received no specific grant from any funding agency in the public, commercial, or not-for-profit sectors.

Data Availability: All data generated or analysed during the present study are available from the corresponding author on reasonable request.

Ethics Approval: The patient was treated in accordance with the tenets of the Declaration of Helsinki. The patient provided informed consent for all treatments and procedures, and consent for publication of this case report.

hyperdense nodules in the bronchovascular, interlobular septal, perifissural and subpleural spaces of both lungs with basal and peripheral predominance. These interstitial nodules appeared to form contiguous branching lines producing a 'dendriform' pattern. Lung volumes were preserved with no honeycombing or traction bronchiectasis. There were no focal consolidations, ground-glass opacities, pleural effusion or pleural plaque. Mediastinal and hilar lymph nodes were not enlarged or calcified. Trachea and main bronchi

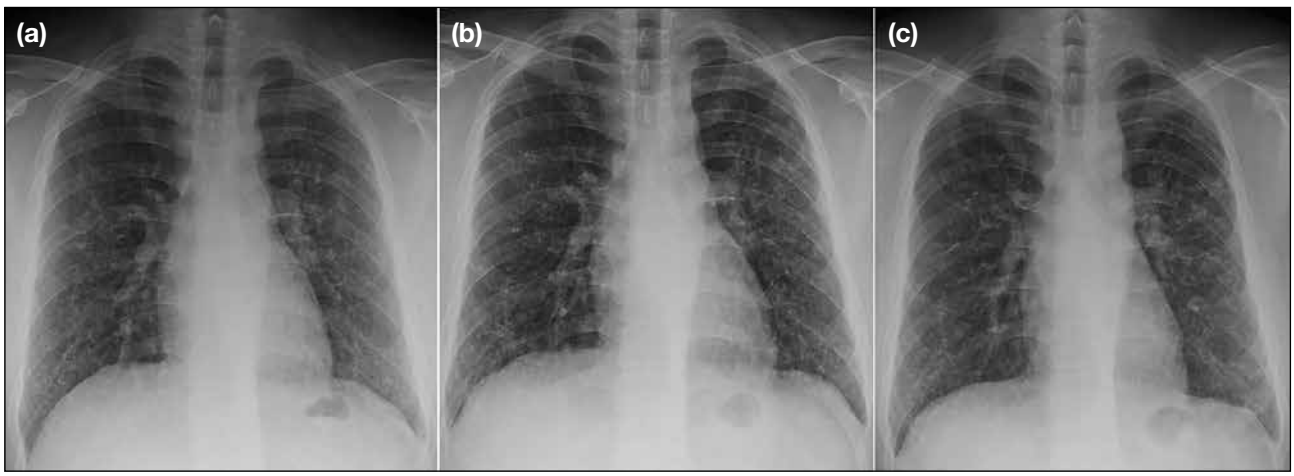


**Figure 1.** Chest radiographs in frontal projection. (a) Scan performed when the patient first presented to the Accident and Emergency department (AED) at the age of 23 years showing reticulonodular shadows over both lungs with basal predominance. (b) Scan performed when the patient presented to the AED at the age of 27 years showing mild interval progression of bilateral pulmonary reticulonodular shadows. (c) Scan performed at the age of 28 years, 1 year after pathological confirmation of dendriform pulmonary ossification, showing no significant interval progression.

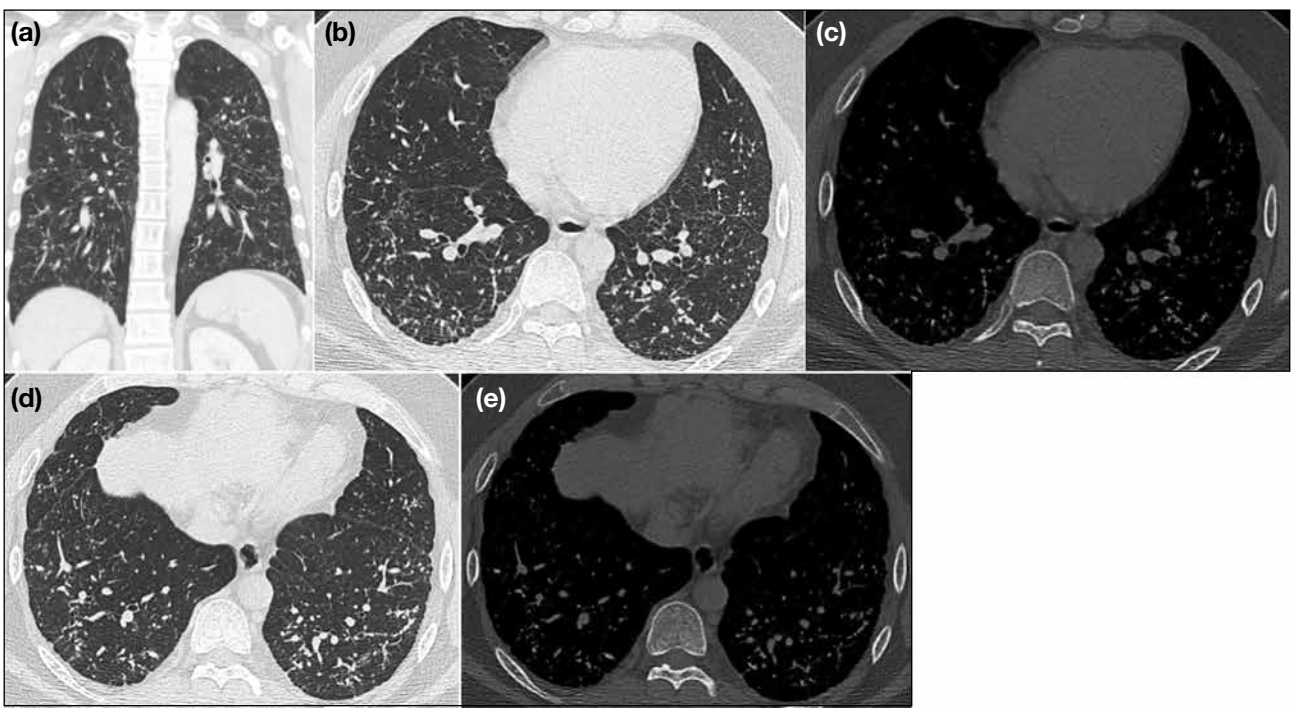


**Figure 2.** Computed tomography of the thorax with coronal reformatted image in the lung window (a). Axial images at T8 level in the lung (b) and bone windows (c), respectively. Axial images at T9 level in the lung (d) and bone windows (e), respectively. They show numerous small (<3 mm) pulmonary nodules with basal and peripheral predominance in the interstitial spaces, producing a branching 'dendriform' appearance. The calcific density of these nodules is more easily appreciated in the bone window.

were patent without focal stenosis or wall calcifications. Heart size was normal and pulmonary vasculature was not dilated. DPO was considered as one of the primary differential diagnoses but the young age at presentation and scarcity of prior case reports hindered a definitive radiological diagnosis.

Upon further inquiry, the patient recalled a 1-minute episode of heavy fume exposure after lighting firecrackers during Chinese New Year at the age of 8 years. Otherwise, he could recollect no other occasion of potential hazardous inhalation. He worked indoors as an accountant and considered occupational risks unlikely. He was also a non-smoker. Barring occasional snoring, he experienced no breathing difficulties and had normal exercise tolerance.

Lung function tests were normal but polysomnography revealed mild-to-moderate obstructive sleep apnoea (OSA) [sleep efficiency = 69%, respiratory disturbance index = 9.1, and oxygen desaturation index = 13.3].

Blood tests, including complete blood count, coagulation profile, immunoglobulin patterns, liver, renal, and endocrine functions were all within the normal reference range. Biological markers for rheumatic diseases, such as rheumatoid factor, anti-nuclear antibodies, anti-neutrophil cytoplasmic antibody, C3, and C4, were negative.

Microbiological examination showed past varicella zoster virus infection with positive anti–varicella zoster virus immunoglobulin G antibody. Sputum, serum and urine cultures were negative. Bronchoalveolar lavage was negative for acid-fast bacilli, fungi, ova, and cysts. Reverse transcription polymerase chain reaction of throat saliva for coronavirus disease 2019 was negative. Antibodies to human immunodeficiency virus were also negative.

No malignant cells were detected on sputum cytology or bronchoalveolar lavage. Transbronchial biopsy of the right lower lobe was unable to establish a pathological diagnosis.

The patient was referred to the cardiothoracic team for lung biopsy. Video-assisted thoracoscopic wedge resections of the left upper and left lower lobes were performed 6 months after the initial CT study. Gross examination of the biopsied specimens showed lung tissue with calcific gritty cut surfaces. Microscopic sections revealed interstitial foci of ossification with mature bony trabeculae and bone marrow tissue (Figure 3), consistent with DPO. There was no evidence of alveolar microlithiasis. Congo red stain showed no amyloid deposition. Ziehl-Neelsen stain for acid-fast bacilli and Grocott methenamine silver stain for fungi were negative.

Since the patient was asymptomatic for DPO, he opted for observation. He was also put on continuous positive airway pressure machine for his OSA. Regular consultation at medical specialist outpatient clinic and follow-up chest radiograph at 6-month intervals were arranged. He had no new complaints. The latest chest radiograph performed over 1 year after the lung biopsy showed no significant interval disease progression (Figure 1c).

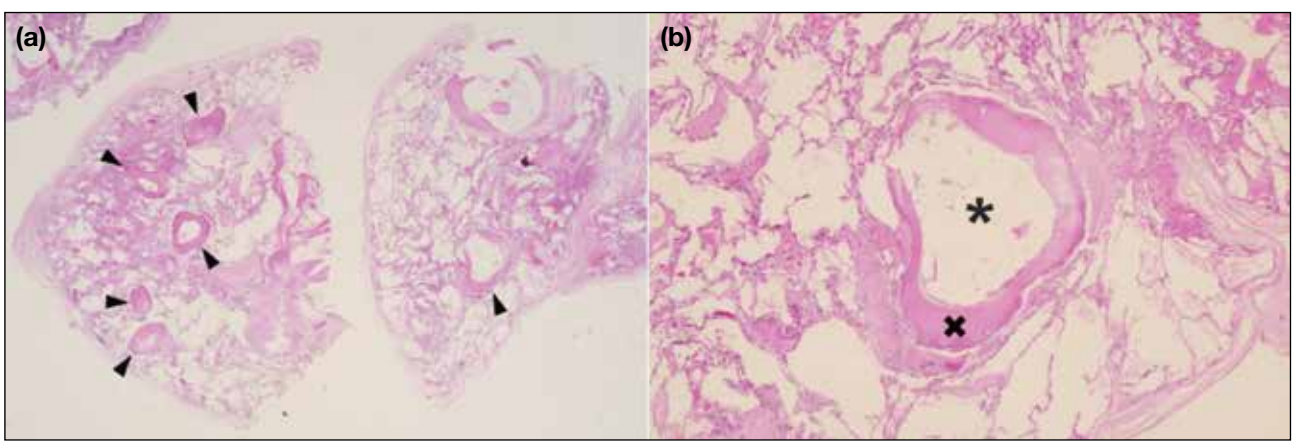


**Figure 3.** Micrographs of the specimen from wedge resection of left lung tissue with haematoxylin and eosin stain showing (a) foci of ossification (arrowheads) in lung interstitium (×100) and (b) an ossified focus showing mature bony trabeculae (cross) and bone marrow tissue (asterisk) [×400].

## DISCUSSION

To the best of our knowledge, this is the youngest reported case of DPO in the literature. On chest radiograph, there are reticulonodular shadows in both lungs, usually with basal predominance.[4] There may be slow interval disease progression.[5] The underlying pathological bony deposition in the alveolar interstitium can be better delineated by CT. Numerous small (usually <3 mm) pulmonary nodules, typically with basal and peripheral predominance, are seen in the interstitial spaces and create the unique tree branch–like morphology of DPO. The calcific density of these nodules can be more easily appreciated in the bone window.[6]

One major diagnostic challenge to recognising DPO lies in distinguishing it from concurrent pulmonary disease. In several case reports, patients had concurrent interstitial lung disease (ILD), especially usual interstitial pneumonia.[1,3] Although the pathophysiology of DPO remains to be elucidated, pulmonary ossifications are often found in areas with more extensive fibrosis.[6] It has been hypothesised that in injured lung tissue, pulmonary fibroblasts and macrophages will undergo metaplasia into osteoblasts and osteoclasts. This may give rise to ectopic ossification.[7] ILD shares some common radiological features with DPO, such as involvement of the alveolar interstitium with basal and peripheral predominance.[8] Reviewing the lung fields after adjusting to the bone window is helpful to reveal the dendriform ossifications amongst the labyrinthine reticulations in ILD.

Another challenge in reaching an unequivocal radiological diagnosis of DPO is related to the long list of differentials for diffuse hyperdense pulmonary nodules. They include, but are not limited to, pulmonary alveolar microlithiasis, previous infections (such as healed varicella pneumonia, tuberculosis, and fungal infections), pneumoconiosis, metastasis, hypercalcaemia, sarcoidosis, and amyloidosis.[9] Although the branching interstitial involvement in DPO is a key distinguishing radiological feature,[10] it may not always be convincingly identified. Other radiological features, e.g., the fine sand–like microcalcifications in pulmonary alveolar microlithiasis,[11] the random scatter and coalescence of nodules in healed varicella pneumonia,[12] the presence of mediastinal lymphadenopathy or calcified lymph nodes in tuberculosis, histoplasmosis and sarcoidosis, can provide clues to the correct diagnosis.[9] In addition, the patient's demographics, occupational risks, inhalation exposure and medical history are often helpful to reduce the possible differentials.

The biggest hurdle to a conclusive radiological diagnosis for this patient was his young age of onset. In a retrospective study by Gruden et al,[13] the mean age of 52 patients with DPO was 78 years (range, 58-96). The authors also proposed some potential risk factors, two of which were present in our patient—OSA and gender. OSA was found in 15 patients (28.8%) in this study.[13] It was hypothesised that aspiration could be the underlying pathogenic pathway for DPO, since other possible risks factors included gastroesophageal reflux disease and debilitating neurological conditions. As for gender, DPO has a strong male predilection. In past studies, the proportion of males ranged from >85%[3] to 100%[13]. Nonetheless while OSA is not uncommon in young men, DPO is rare, if not unprecedented. A case series by Baddini Martinez and Ramos[14] of three patients diagnosed with DPO >20 years after transitory inhalation of hydrocarbon combustion products may offer some insight into our case. Our patient recounted a brief episode of heavy fume exposure after lighting firecrackers during his formative years. Baddini Martinez and Ramos[14] hypothesised that these combustion products could initiate an inflammatory process in lung tissue, causing deposition of collagen and dystrophic calcification, and subsequently inducing bone and marrow precursor cells.

There is no specific management guideline for DPO. Some patients are asymptomatic while others require symptomatic relief of respiratory complaints. Follow-up monitoring by interval imaging may be helpful.[3,10]

## REFERENCES


1. Lara JF, Catroppo JF, Kim DU, da Costa D. Dendriform pulmonary ossification, a form of diffuse pulmonary ossification: report of a 26-year autopsy experience. Arch Pathol Lab Med. 2005;129:348-53.
2. Müller KM, Friemann J, Stichnoth E. Dendriform pulmonary ossification. Pathol Res Pract. 1980;168:163-72.
3. Fernández-Bussy S, Labarca G, Pires Y, Díaz JC, Caviedes I. Dendriform pulmonary ossification. Respir Care. 2015;60:e64-7.
4. Reddy TL, von der Thüsen J, Walsh SL. Idiopathic dendriform pulmonary ossification. J Thorac Imaging. 2012;27:W108-10.
5. Felson B, Schwarz J, Lukin RR, Hawkins HH. Idiopathic pulmonary ossification. Radiology. 1984;153:303-10.
6. Kim TS, Han J, Chung MP, Chung MJ, Choi YS. Disseminated dendriform pulmonary ossification associated with usual interstitial pneumonia: incidence and thin-section CT-pathologic correlation. Eur Radiol. 2005;15:1581-5.
7. Tseung J, Duflou J. Diffuse pulmonary ossification: an uncommon incidental autopsy finding. Pathology. 2006;38:45-8.
8. Lynch DA, Sverzellati N, Travis WD, Brown KK, Colby TV, Galvin JR, et al. Diagnostic criteria for idiopathic pulmonary fibrosis: a Fleischner Society White Paper. Lancet Respir Med. 2018;6:138-53.
9. Marchiori E, Souza AS Jr, Franquet T, Müller NL. Diffuse

high-attenuation pulmonary abnormalities: a pattern-oriented diagnostic approach on high-resolution CT. AJR Am J Roentgenol. 2005;184:273-82.
10. Jamjoom L, Meziane M, Renapurkar RD. Dendriform pulmonary ossification: report of two cases. Indian J Radiol Imaging. 2013;23:15-8.
11. Korn MA, Schurawitzki H, Klepetko W, Burghuber OC. Pulmonary alveolar microlithiasis: findings on high-resolution CT. AJR Am J Roentgenol. 1992;158:981-2.
12. Kim JS, Ryu CW, Lee SI, Sung DW, Park CK. High-resolution CT findings of varicella-zoster pneumonia. AJR Am J Roentgenol. 1999;172:113-6.
13. Gruden JF, Green DB, Legasto AC, Jensen EA, Panse PM. Dendriform pulmonary ossification in the absence of usual interstitial pneumonia: CT features and possible association with recurrent acid aspiration. AJR Am J Roentgenol. 2017;209:1209-15.
14. Baddini Martinez JA, Ramos SG. Inhalation of hydrocarbon combustion products as a cause of dendriform pulmonary ossification. Med Hypotheses. 2008;71:981-2.

Hong Kong J Radiol. 2024;27(2):e117-24. Published 22 May 2024 | https://doi.org/10.12809/hkjr2317713

PICTORIAL ESSAY

# Application of Zero Echo Time Magnetic Resonance Angiography in Neuroimaging: A Pictorial Essay

**WC Law[1], BMH Lai[1], CY Cheung[2], KT Wong[1], JM Abrigo[1]**

*[1]Department of Imaging and Interventional Radiology, The Chinese University of Hong Kong, Prince of Wales Hospital, Hong Kong SAR, China*
*[2]Department of Radiology, North District Hospital, Hong Kong SAR, China*

## INTRODUCTION

Cerebrovascular malformations are characterised by abnormal communications between high–velocity-flow arteries and low–velocity-flow veins and venous sinuses in the brain. Such gradient differences put cerebrovascular malformations at risk for intracranial haemorrhage, which is often associated with significant morbidity and mortality. Digital subtraction angiography (DSA) is the gold standard for imaging assessment because of its high spatial resolution and dynamic information. However, it is an invasive procedure and uses a high radiation dose, making it less than ideal for screening and surveillance purposes.

Magnetic resonance angiography (MRA) with time-of-flight (TOF) technique is widely used as a non-invasive investigation to diagnose or follow up patients with cerebrovascular malformations. It does not require contrast medium and utilises the inflow effect for generation of images of vessels.[1] However, there are some limitations of this technique. It is influenced by haemodynamics; for instance, in areas with complex vessel direction, such as the internal carotid artery (ICA) siphon, the images may be suboptimal with heterogeneous flow signal. It may also depict artefactual flow signal in the cavernous sinus in patients without carotid cavernous fistula (CCF)[2] or in the dural venous sinuses in patients without dural arteriovenous fistula (AVF).[1] Magnetic susceptibility artefacts and radiofrequency shielding often lead to difficulty in evaluation of patients who have undergone previous interventions such as coil embolisation and stenting.

In clinical practice, contrast-enhanced MRA may be

***Correspondence:*** *Dr WC Law, Department of Imaging and Interventional Radiology, Prince of Wales Hospital, The Chinese University of Hong Kong, Hong Kong SAR, China*
*Email: lwc926@ha.org.hk*

Submitted: 21 March 2023; Accepted: 29 September 2023.

Contributors: WCL and JMA designed the study. WCL acquired data. All authors analysed the data. WCL and JMA drafted the manuscript. All authors critically revised the manuscript for important intellectual content. All authors had full access to the data, contributed to the study, approved the final version for publication, and take responsibility for its accuracy and integrity.

Conflicts of Interest: All authors have disclosed no conflicts of interest.

Funding/Support: This study received no specific grant from any funding agency in the public, commercial, or not-for-profit sectors.

Data Availability: All data generated or analysed during the present study are available from the corresponding author on reasonable request.

Ethics Approval: This study was approved by the Joint Chinese University of Hong Kong–New Territories East Cluster Clinical Research Ethics Committee, Hong Kong (Ref No.: 2022.396). Informed patient consent was waived by the Committee due to the retrospective nature of the study.

Acknowledgement: The authors thank Mr William Kin-ming Kwong, Senior Radiographer in the Department of Imaging and Interventional Radiology in Prince of Wales Hospital, for his technical support on magnetic resonance imaging protocols.

additionally performed for clarification. The multiphase acquisition slightly increases the complexity of interpretation but allows dynamic visualisation of early venous drainage, confirming arteriovenous shunting. It does require intravenous administration of gadolinium contrast, which is contraindicated in patients with renal impairment, and also makes it less than ideal for surveillance screening purposes. In addition, the spatial resolution of contrast-enhanced MRA is usually inferior to that of TOF MRA.

Zero echo time (ZTE) MRA, also called silent MRA, is a relatively new technique, which combines ultrashort echo time (0.006 ms) with arterial spin labelling (ASL). The ASL technique uses magnetically labelled blood as endogenous contrast, and the final angiographic image is generated by subtraction of pre- from post-labelled images, achieving background suppression. ZTE has minimal magnetic susceptibility artefact and the ASL technique improves the detection of low-flow signal.

Several studies have reported the usefulness of silent MRA for the characterisation of cerebrovascular diseases (atherosclerotic steno-occlusions, moyamoya disease, and arteriovenous malformations [AVMs])[3] and follow-up of treated aneurysms.[4-6] It has also recently been reported as being useful for dural AVFs and indirect CCFs.[7,8] In our experience, it is helpful for identification and follow-up of different kinds of cerebrovascular malformations, as it facilitates depiction of 'arterialised' veins/venous sinuses. Here we present a pictorial essay of our experience, illustrating the applicability of ZTE MRA in our clinical practice.

## Study Population

The relevant MRA scans were retrospectively retrieved from 1 January 2017 to 31 July 2022 using keyword search of radiology reports in the Radiology Information System, a system widely used by every radiology department in Hong Kong. All patients with ZTE MRA acquired for the evaluation or follow-up of vascular malformations with positive imaging findings were included. Patients with cerebrovascular abnormalities other than AVM and AVF were excluded. The corresponding MRI images and DSA studies were also reviewed.

## Zero Echo Time Magnetic Resonance Imaging Protocol

MRI images were acquired using either a 1.5T (Ingenia; Philips, Best, the Netherlands) or a 3T scanner (SIGNA Architect; General Electric Healthcare, Milwaukee [WI], United States) with 20- and 32-channel head coils, respectively. The ZTE MRA can only be acquired in the 3T scanner. MRA scan parameters are listed in the Table.

DSA was performed using a biplane angiography system (Allura Xper FD 20/20; Phillips, Amsterdam, the Netherlands, and ARTIS icono biplane; Siemens, Erlangen, Germany), under local anaesthesia and using femoral arterial access.

## Case 1

A 59-year-old woman who presented with a left-sided third cranial nerve palsy was diagnosed with a left-sided direct-type CCF and a left supraclinoid ICA saccular aneurysm on DSA. Both were treated simultaneously with placement of a flow diverter in the segment of vessel from the cavernous ICA to the middle cerebral artery, with additional transvenous coil packing in the left cavernous sinus. She was noted to have residual CCF on follow-up DSA. On MRI, TOF MRA image (Figure 1a) showed coil-related magnetic susceptibility artefacts in the left cavernous sinus, which obscured the signal around the left ICA. ZTE MRA (Figure 1b and 1c) more clearly depicted abnormal extra-stent signal in the left cavernous sinus, corresponding to the residual CCF, and abnormal flow signal in the left pterygoid plexus, which correlated with the venous drainage on DSA (Figure 1d).

## Case 2

A 55-year-old woman presented with left 6th and

**Table.** Relative comparison of common cerebral magnetic resonance angiography techniques.

| | Need for IV contrast | Scan time | Spatial resolution | Temporal resolution | AVF/AVM visualisation |
|---|---|---|---|---|---|
| TOF MRA | - | ++ | ++++ | - | ++ |
| ZTE MRA | - | ++++ (longest) | + | - | +++ |
| Phase contrast MRA | - | +++ | +++ | - | + |
| CE-MRA | + | + (shortest) | ++ | ++++ | +++ |

Abbreviations: AVF = arteriovenous fistula; AVM = arteriovenous malformation; CE-MRA = contrast-enhanced magnetic resonance angiography; IV = intravenous; MRA = magnetic resonance angiography; TOF = time-of-flight; ZTE = zero echo time.

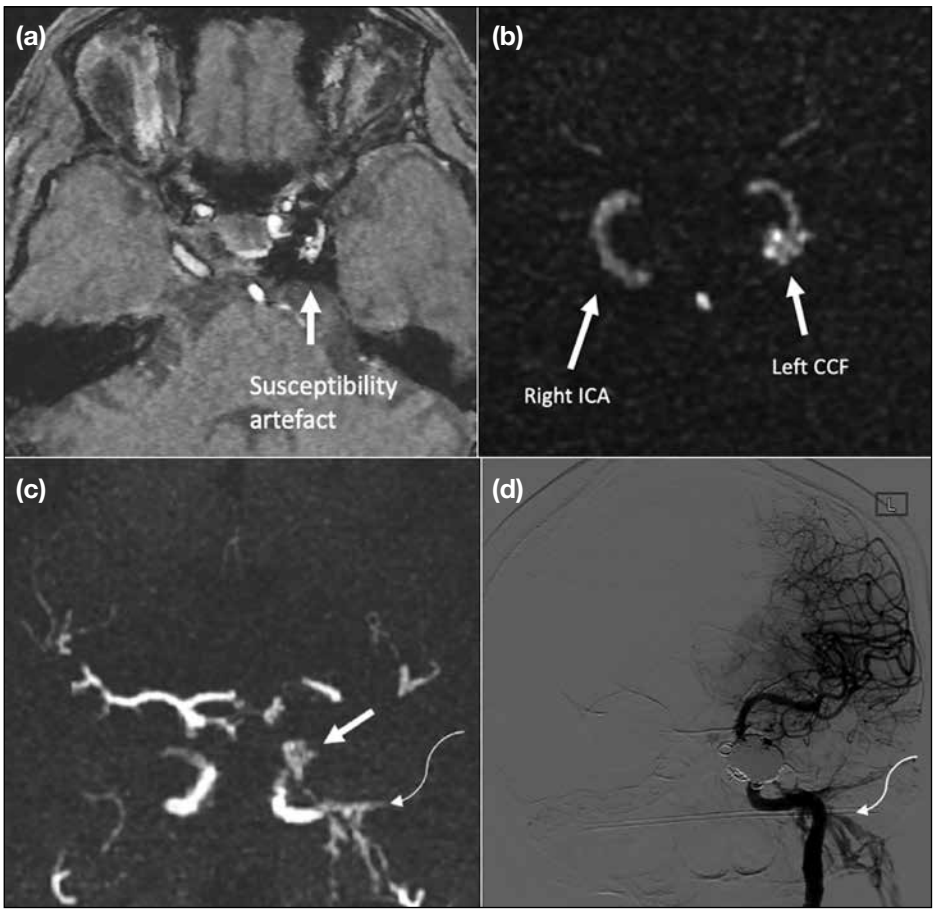


**Figure 1.** Case 1. Time-of-flight magnetic resonance angiography (MRA) image (a) showing susceptibility artefacts around the flow diverter (arrow). Zero echo time (ZTE) MRA image (b) clearly showing abnormal extra-stent flow signals in the left cavernous sinus, confirmed to be residual left direct carotid cavernous fistula (CCF) on digital subtraction angiography (DSA). A coronal reformat of maximum intensity projection ZTE MRA (c) shows the residual left CCF (straight arrow) and drainage into the left pterygoid plexus (curved arrow). Corresponding DSA image (d) also shows the drainage into the left pterygoid plexus (curved arrow).
Abbreviation: ICA = internal carotid artery.

12th cranial nerve palsies. TOF MRA demonstrates heterogeneous flow signal within an abnormally dilated left condylar confluence (Figure 2a) and subtle flow signal around the left vertebral artery (Figure 2b). ZTE MRA more clearly depicts abnormal arterialised flow within the left condylar confluence (Figure 2d) and pronounced asymmetry in the left vertebral artery region, secondary to arterialised flow signal in the venous plexus surrounding the left vertebral artery (Figure 2e). ZTE MRA additionally showed abnormal signal in the left cavernous sinus and superior ophthalmic vein, which was suspected to be concomitant CCF (Figure 2f), with a differential diagnosis of retrograde flow from the condylar dural AVF. The abnormality in the left superior ophthalmic vein is not visible on TOF images (Figure 2c). DSA confirmed both the left condylar confluence dural AVF (Figure 2h) and concurrent left CCF (Figure 2g).

## Case 3

A 62-year-old man presented with dizziness. DSA revealed a dural AVF over the right occipital region, with arterial feeders from the right external carotid artery and the right vertebral artery, and venous drainage into the right sigmoid sinus with retrograde flow to the right transverse sinus. Transvenous embolisation was subsequently performed with complete occlusion of the dural AVF angiographically. Follow-up MRA (Figure 3a and 3b) showed evidence of recurrence of the dural AVF. Both TOF and ZTE MRA showed hypertrophied feeding arteries in the right occipital region and flow signal within the right sigmoid sinus suggestive of arteriovenous shunting. ZTE MRA shows additional retrograde flow signal in the left transverse sinus. A second DSA (Figure 3c) confirmed the recurrent dural AVF and a second transvenous embolisation procedure was performed.

## Case 4

A 69-year-old man presented with acute haemorrhage in the left temporooccipital region. DSA showed evidence of dural AVF in the left occipital region, with an arterial feeder from the left occipital artery, and venous drainage into the left sigmoid sinus, left inferior petrosal sinus, and left internal jugular vein. The patient

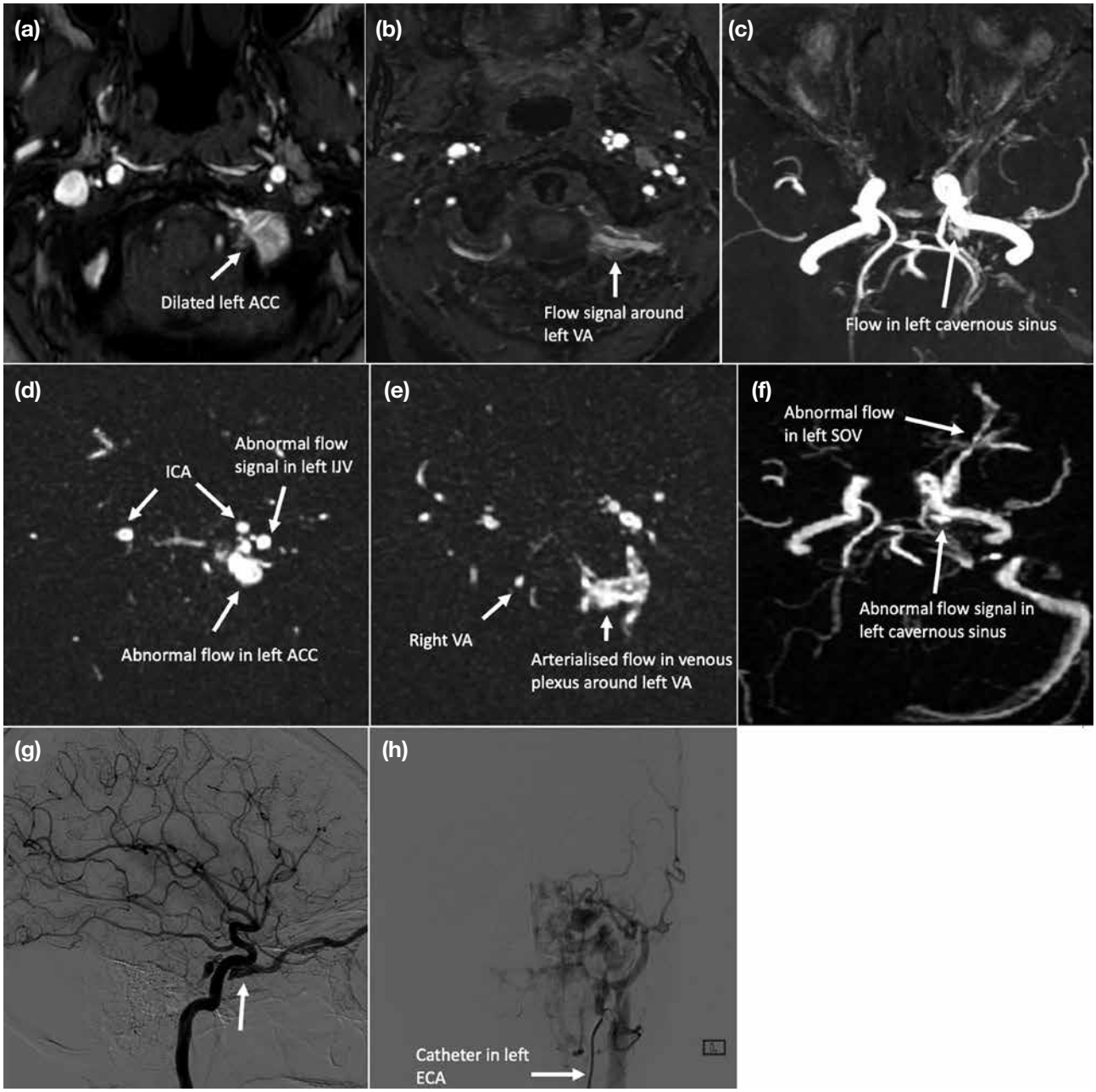


**Figure 2.** Case 2. Time-of-flight magnetic resonance angiography (MRA) [a-c] demonstrates an abnormally dilated left condylar confluence with heterogeneous flow signal (a) [arrow] and subtle flow signal around the left vertebral artery (b) [arrow]. Zero echo time (ZTE) MRA (d-f) clearly showing abnormal arterialised flow within the left condylar confluence (d) and in the venous plexus surrounding the left vertebral artery (e). Additional abnormal signal in the left cavernous sinus and superior ophthalmic vein, which are more clearly shown on ZTE MRA (f), raises suspicion of concomitant carotid cavernous fistula (CCF) or retrograde flow from the condylar dural arteriovenous fistula (AVF). Lateral digital subtraction angiography (DSA) image (g) on left internal carotid artery injection confirms the concomitant left CCF with drainage into the superior ophthalmic vein (arrow). Frontal DSA image (h) on left external carotid artery injection showing the left condylar confluence dural AVF.

Abbreviations: ACC = anterior condylar confluence; ECA = external carotid artery; ICA = internal carotid artery; IJV = internal jugular vein; SOV = superior ophthalmic vein; VA = vertebral artery.

declined embolisation and elected to undergo imaging surveillance. TOF MRA showed subtle abnormal flow signal in the left sigmoid sinus (Figure 4a and 4b) which was unmistakable on the ZTE MRA (Figure 4c and 4d) and more convincing of arteriovenous shunting. Furthermore, ZTE MRA demonstrated venous drainage to the left inferior petrosal sinus (Figure 4d), which could not be appreciated on TOF MRA image.

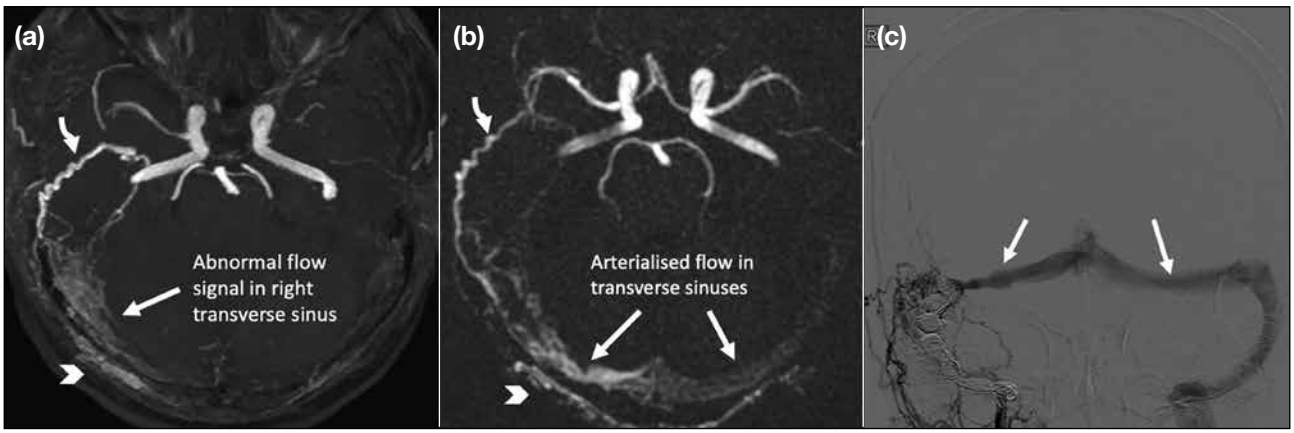


**Figure 3.** Case 3. Time-of-flight magnetic resonance angiography (MRA) [a] showing abnormal flow in the right transverse sinus (arrow), while zero echo time MRA (b) showing arterialised flow in both transverse sinuses (arrows). Note the arterial feeders from the right posterior auricular (curved arrows in [a] and [b]) and occipital arteries (arrowheads in [a] and [b]). Anteroposterior digital subtraction angiography image (c) after right external carotid artery injection confirms the dural arteriovenous fistula, with drainage into both transverse sinuses (arrows).

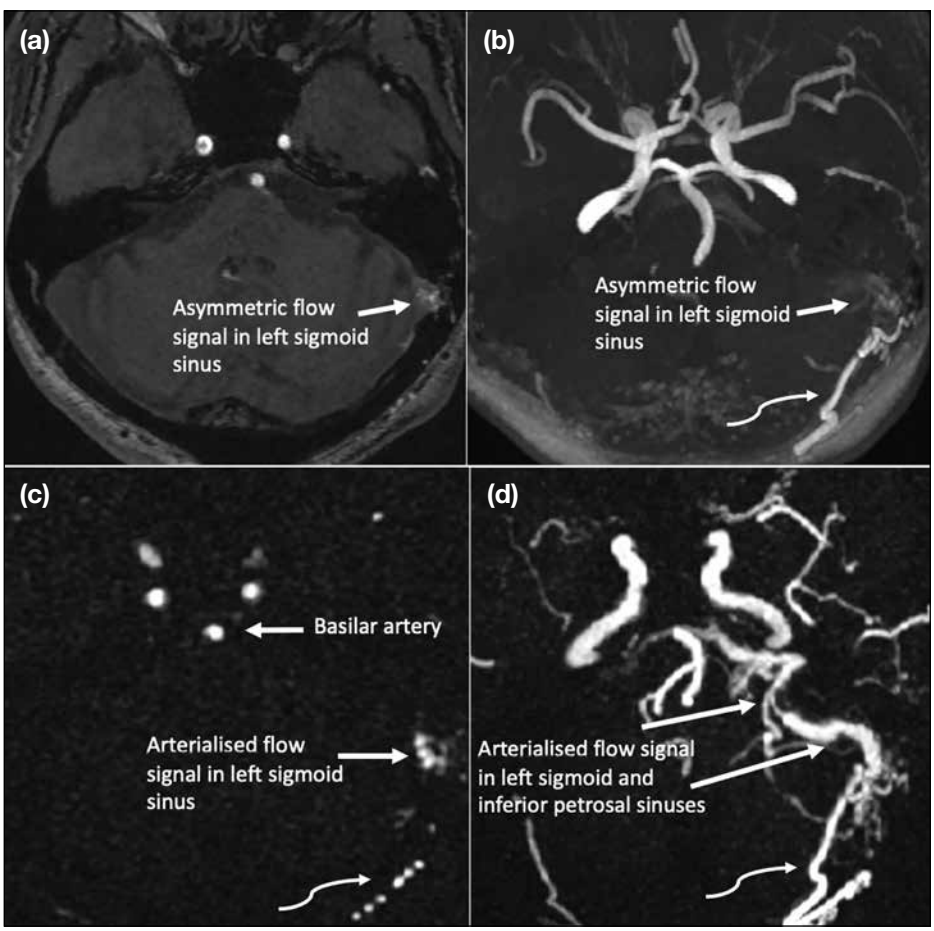


**Figure 4.** Case 4. Time-of-flight magnetic resonance angiography (MRA) [a, b] showing subtle abnormal flow signal in the left sigmoid sinus (arrows), which was unmistakable on zero echo time (ZTE) MRA (c, d) and more convincing of arteriovenous shunting. The ZTE MRA maximum intensity projection image (d) additionally depicts drainage into the left inferior petrosal sinus. Note the dilated left occipital arterial feeder (curved arrows in [b] to [d]).

## Case 5

A 27-year-old woman presented with left occipital lobe haematoma. Investigation with MRA (Figure 5) showed prominent vasculatures and possible nidus at the left occipital region, suspicious of an underlying AVM. TOF MRA showed a prominent vessel in the region which was more conspicuous in the ZTE MRA, owing to background signal suppression of the technique.

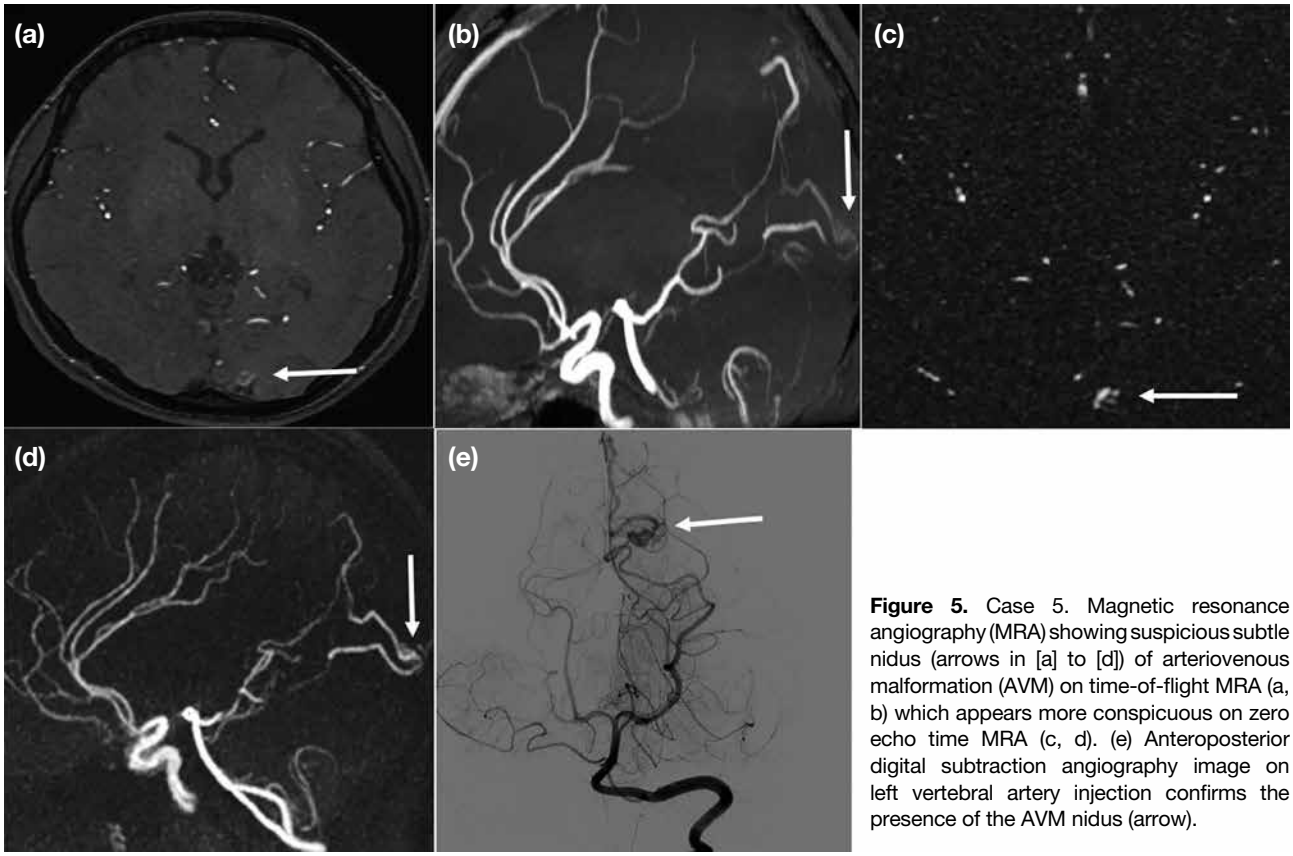


**Figure 5.** Case 5. Magnetic resonance angiography (MRA) showing suspicious subtle nidus (arrows in [a] to [d]) of arteriovenous malformation (AVM) on time-of-flight MRA (a, b) which appears more conspicuous on zero echo time MRA (c, d). (e) Anteroposterior digital subtraction angiography image on left vertebral artery injection confirms the presence of the AVM nidus (arrow).

Subsequent DSA (Figure 5e) confirmed a small left occipital AVM, with arterial feeder from left posterior cerebral artery and early venous drainage into superior sagittal sinus. The patient was treated with transarterial embolisation.

### Case 6

A 53-year-old woman presented with headache. DSA showed an AVM over the left parieto-occipital region, with multiple arterial feeders from the left anterior cerebral artery, middle cerebral artery, and posterior cerebral artery and early venous drainage into the superior sagittal and transverse sinuses. Two-stage treatment was performed with embolisation of the left PCA and subsequent radiosurgery. A small residual nidus was noted on follow-up DSA. Further imaging surveillance was performed with MRA, in which TOF MRA showed subtle flow signal in the left parieto-occipital region (Figure 6a), likely corresponding to the residual nidus. The abnormality was more clearly manifested on ZTE MRA (Figure 6b).

## DISCUSSION

We demonstrated the utility of ZTE MRA in the initial and follow-up evaluation of patients with cerebrovascular malformations. In particular, ZTE MRA allowed for a more confident diagnosis and better characterisation of CCFs, dural AVFs, and AVMs. The imaging was not constrained by artifacts from prior embolisation or stenting. While most arteriovenous shunts could be depicted on TOF MRA, occasionally, the abnormal flow signals may be subtle, and ZTE MRA provided additional strong supporting evidence to proceed to DSA for final confirmation.

TOF MRA relies on the in-flow enhancement effect for detection of signal and is dependent on the alignment of vessels relative to the scan plane. If the direction of flowing blood is parallel to the scan plane, the spins are exposed to repetitive excitation pulses and the flow signal may be saturated and lost.[9] It is also prone to magnetic susceptibility artefacts and may demonstrate artefactual flow signal in normal venous structures.

In ZTE MRA, the ZTE nature minimises the sensitivity to magnetic field heterogeneity and the phase dispersion of the labelled blood flow signal, hence decreasing magnetic susceptibility artefacts.[10] The ASL technique

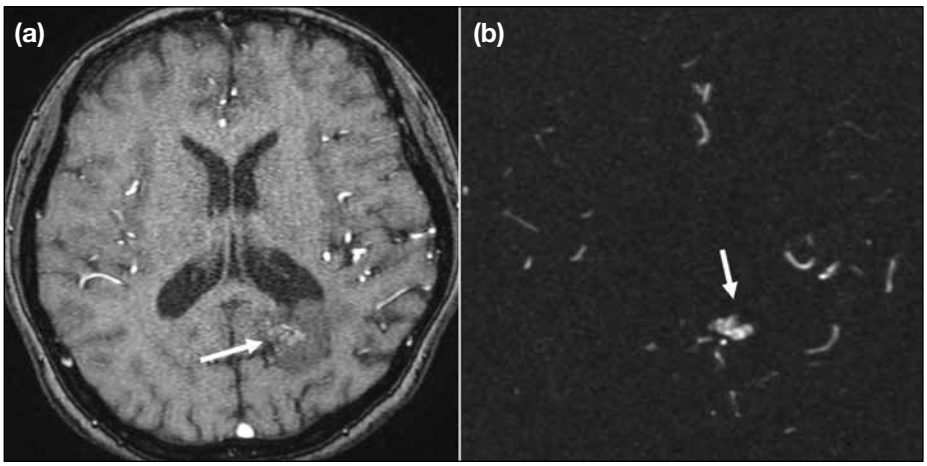


**Figure 6.** Case 6. Time-of-flight magnetic resonance angiography (MRA) showing subtle flow signal in the left parieto-occipital region (a) which is clearly manifested on zero echo time MRA (b), suggestive of residual arteriovenous malformation nidus (arrows).

uses the water molecules within arterial blood as an endogenous tracer. Hence, it is less influenced by the blood flow state and is not affected by the blood flow direction. The ultrashort echo time acquisition is a defining feature of ZTE MRA that differentiates it from other ASL-based MRA methodologies.

In normal circumstances, venous structures are not expected to show a signal in ZTE MRA because only the protons in the arteries are magnetically labelled. Hence, the signal detected in these vascular regions would suggest underlying arteriovenous shunting. This, too, allows for easier image interpretation.

The background suppression achieved with ZTE MRA also increases the sensitivity of detecting abnormal flow against a dark background. In this sequence, ASL is used as a preparation pulse. A control image is first obtained before the labelling pulse and the labelled image is acquired subsequently. Subtraction of the unlabelled from the labelled images generates the angiographic images and achieves background suppression.[11] Our experience highlights such advantage, with abnormal flow signals being more conspicuous on ZTE than TOF MRA, allowing for their easy detection and straightforward interpretation. Furthermore, the ZTE pulse sequence minimises gradient switching, resulting in a quieter scan, which could potentially improve patients' comfort during the exmination.[12]

ZTE MRA is not without disadvantages, however. First, it requires longer imaging time (~6 mins vs. ~3 mins for TOF) and thus is theoretically more susceptible to motion artefact. However, from our experience, most patients were able to tolerate the prolonged acquisition. Second, it has slightly lower spatial resolution due to greater slice thickness and larger pixel size. Further, the low background signal may lead to reduced anatomical information as background structures are not well delineated. In addition, ZTE MRA does not allow vessel selectivity or time-resolved acquisition as in other ASL-based MRA techniques, which could enhance shunt characterisation; however, it still provides a robust screening method prior to reference standard DSA. Finally, ZTE MRA is limited by scanner and hardware availability.

## CONCLUSION

ZTE MRA is a useful adjunct to TOF MRA and has good concordance with DSA, potentially obviating the need for CE-MRA. ZTE MRA allows for easier recognition of abnormal vascular shunts, increasing confidence in making the diagnosis as well as improving the characterisation of cerebrovascular malformations.

## REFERENCES

1. Morelli, JN, Gerdes CM, Schmitt P, Ai T, Saettele MR, Runge VM, et al. Technical considerations in MR angiography: an image-based guide. J Magn Reson Imaging. 2013;37:1326-41.
2. Watanabe K, Kakeda S, Watanabe R, Ohnari N, Korogi Y. Normal flow signal of the pterygoid plexus on 3T MRA in patients without DAVF of the cavernous sinus. AJNR Am J Neuroradiol. 2013;34:1232-6.
3. Shang S, Ye J, Dou W, Luo X, Qu J, Zhu Q, et al. Validation of zero TE-MRA in the characterization of cerebrovascular diseases: a feasibility study. AJNR Am J Neuroradiol. 2019;40:1484-90.
4. Shang S, Ye J, Luo X, Qu J, Zhen Y, Wu J. Follow-up assessment of coiled intracranial aneurysms using ZTE MRA as compared

with TOF MRA: a preliminary image quality study. Eur Radiol. 2017;27:4271-80.
5. Takano N, Suzuki M, Irie R, Yamamoto M, Teranishi K, Yatomi K, et al. Non–contrast-enhanced silent scan MR angiography of intracranial anterior circulation aneurysms treated with a low-profile visualized intraluminal support device. AJNR Am J Neuroradiol. 2017;38:1610-6.
6. Oishi H, Fujii T, Suzuki M, Takano N, Teranishi K, Yatomi K, et al. Usefulness of silent MR angiography for intracranial aneurysms treated with a flow-diverter device. AJNR Am J Neuroradiol. 2019;40:808-14.
7. Balasubramanian AP, Kannath SK, Rajan JE, Singh G, Kesavadas C, Thomas B. Utility of silent magnetic resonance angiography in the evaluation and characterisation of intracranial dural arteriovenous fistula. Clin Radiol. 2021;76:712.e1-8.
8. Kandasamy S, Kannath SK, Enakshy Rajana J, Kesavadas C, Thomas B. Non-invasive angiographic analysis of dural carotid cavernous fistula using time-of-flight MR angiography and silent MR angiography: a comparative study. Acta Radiol. 2023;64:1290-7.
9. Azuma M, Hirai T, Shigematsu Y, Kitajima M, Kai Y, Yano S, et al. Evaluation of intracranial dural arteriovenous fistulas: comparison of unenhanced 3T 3D time-of-flight MR angiography with digital subtraction angiography. Magn Reson Med Sci. 2015;14:285-93.
10. Ryu KH, Baek HJ, Moon JI, Choi BH, Park SE, Ha JY, et al. Usefulness of noncontrast-enhanced silent magnetic resonance angiography (MRA) for treated intracranial aneurysm follow-up in comparison with time-of-flight MRA. Neurosurgery. 2020;87:220-8.
11. Irie R, Suzuki M, Yamamoto M, Takano N, Suga Y, Hori M, et al. Assessing blood flow in an intracranial stent: a feasibility study of MR angiography using a silent scan after stent-assisted coil embolization for anterior circulation aneurysms. AJNR Am J Neuroradiol. 2015;36:967-70.
12. Ljungberg E, Damestani NL, Wood TC, Lythgoe DJ, Zelaya F, Williams SC, et al. Silent zero TE MR neuroimaging: current state-of-the-art and future directions. Prog Nucl Magn Reson Spectrosc. 2021;123:73-93.

Hong Kong J Radiol. 2024;27(2):e125-34. Published 13 Jun 2024 | https://doi.org/10.12809/hkjr2317714

PICTORIAL ESSAY

# Radiologic-Pathologic Review of Non-Epithelial Malignancies and Metastases in the Breast: A Pictorial Essay

**RYS Mak[1], AHC Wong[1], CKM Mo[1], KH Chin[1], JSC Wong[2], AYT Lai[1], WWC Wong[1]**

*[1]Department of Radiology, Pamela Youde Nethersole Eastern Hospital, Hong Kong SAR, China*
*[2]Department of Nuclear Medicine, Pamela Youde Nethersole Eastern Hospital, Hong Kong SAR, China*

## INTRODUCTION

Most malignant tumours in the breast are primary epithelial malignancies. Non-epithelial malignancies and metastases from other organs or tissues are rare. Many such malignancies have variable and non-specific radiological features and may resemble epithelial breast carcinomas or even benign breast lesions. Nevertheless, familiarity with their common imaging appearance is crucial for facilitating timely diagnosis and determining radiopathological concordance. This pictorial essay reviews the radiological appearance of important non-epithelial malignancies and metastases in the breast with histopathological correlation.

## METASTASES TO THE BREAST

Metastases to the breasts from non-mammary primary tumours account for 0.5% to 2.0% of all breast malignancies.[1] The most common sources are melanoma; non-Hodgkin lymphoma; sarcoma; and carcinoma of the lung, stomach, ovaries, and kidney.[1] Clinically, metastases to the breast are generally not associated with chest wall fixation, *peau d'orange* appearance, Paget's disease of bone, skin retraction, nipple retraction, or discharge.[2] The lesions tend to be superficially located in the upper outer quadrant.[3]

The most common mammographic manifestations of metastases to the breast are one or more circumscribed upper outer quadrant masses (Figure 1) without spiculation or calcifications.[4] Another reported manifestation is a diffuse pattern resembling inflammatory breast carcinoma in cases of lymphatic metastases, most commonly from contralateral breast cancer, gastric, and ovarian carcinoma.[2,5]

***Correspondence:*** *Dr RYS Mak, Department of Radiology, Pamela Youde Nethersole Eastern Hospital, Hong Kong SAR, China*
*Email: mys877@ha.org.hk*

Submitted: 25 March 2023; Accepted: 29 September 2023.

Contributors: RYSM, JSCW, AYTL and WWCW designed the study. RYSM, AHCW, CKMM, KHC and AYTL acquired the data. RYSM, AHCW, JSCW and AYTL drafted the manuscript. CKMM, KHC, AYTL and WWCW critically revised the manuscript for important intellectual content. All authors had full access to the data, contributed to the study, approved the final version for publication, and take responsibility for its accuracy and integrity.

Conflicts of Interest: All authors have disclosed no conflicts of interest.

Funding/Support: This study received no specific grant from any funding agency in the public, commercial, or not-for-profit sectors.

Data Availability: All data generated or analysed during the present study are available from the corresponding author on reasonable request.

Ethics Approval: The study was approved by the Hong Kong East Cluster Research Ethics Committee of Hospital Authority, Hong Kong (Ref No: HKECREC-2022-035). The requirement for patient consent was waived by the Committee due to the retrospective nature of the study.

Acknowledgement: The authors thank Dr KC Leung from the Department of Clinical Pathology of Pamela Youde Nethersole Eastern Hospital for critically revising the manuscript.

Declaration: Part of the manuscript was previously presented as a poster in the 30th Annual Scientific Meeting of the Hong Kong College of Radiologists (12-13 November 2022, virtual).

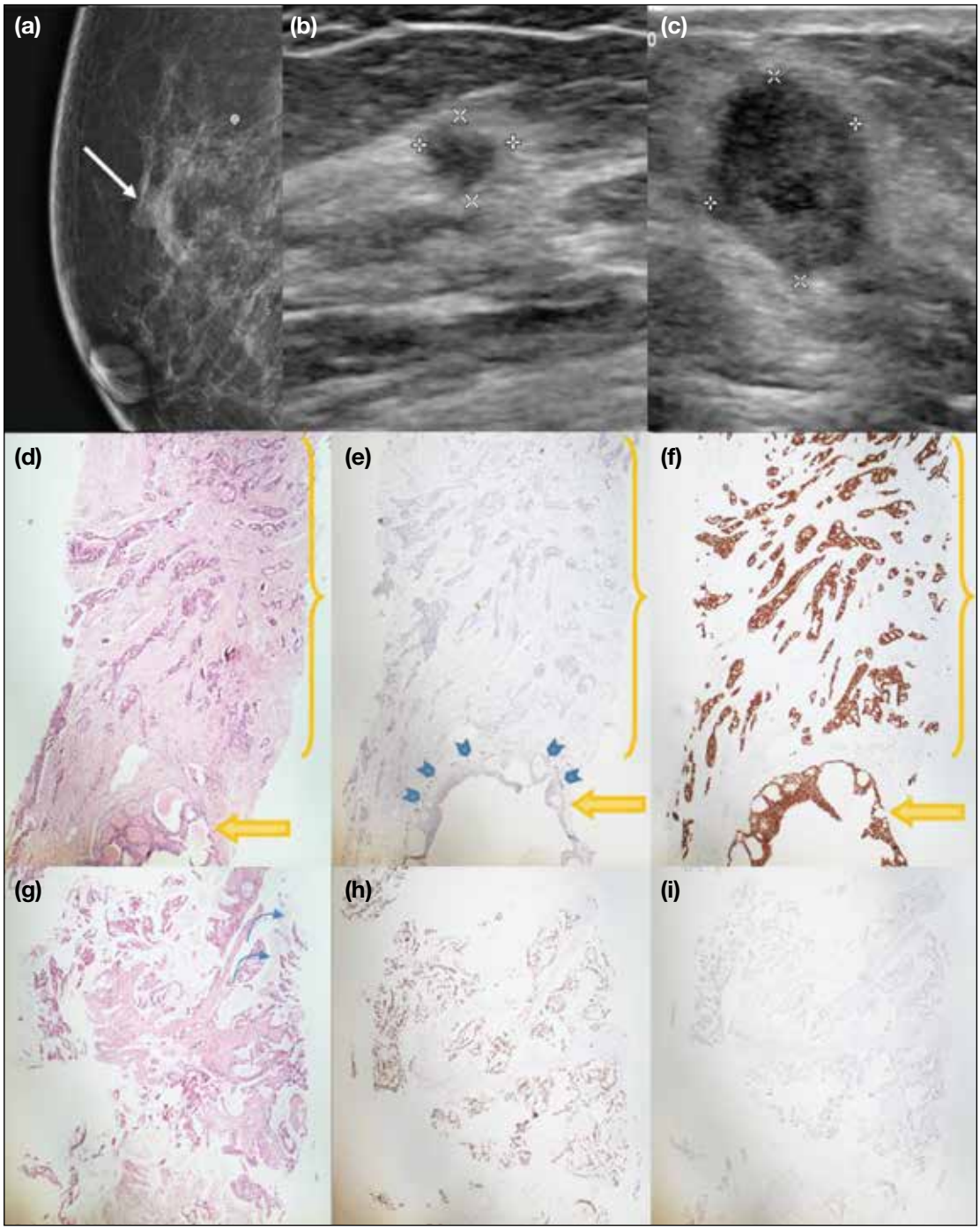


**Figure 1.** An 81-year-old woman with known carcinoma of the lung was found to have synchronous primary right breast invasive ductal carcinoma and a right axillary metastatic lesion from lung adenocarcinoma. (a) Mammogram showing an oval isodense mass in the upper outer quadrant of the right breast at anterior depth (arrow). (b) Ultrasound reveals a corresponding irregular hypoechoic mass in the upper outer quadrant of the right breast. (c) Another oval hypoechoic mass with non-parallel (taller-than-wide) orientation is seen in the right axillary subcutaneous region. (d-f) Low-power views (×4) of the right breast mass biopsy in haematoxylin and eosin (H&E) staining (d), p63 staining (e) and GATA binding protein 3 (GATA-3) staining (f) showing invasive ductal carcinoma (yellow brackets) featuring infiltrative nests and tubules. On immunohistochemistry (IHC), the tumour cells are diffusely positive for GATA-3, supportive of primary breast malignancy. A small component of ductal carcinoma in situ (yellow arrows) with preservation of the myoepithelial layer is highlighted by p63 staining (blue arrowheads in [e]). (g-i) Low-power views (×4) of the right axillary mass biopsy in H&E staining (g), thyroid transcription factor-1 (TTF-1) staining (h) and GATA-3 staining (i) showing fibroadipose tissue infiltrated by irregular glands, with some extracellular mucin pools in proximity (curved arrows in [g]). The morphology and IHC profile were similar to those of a specimen of prior lung carcinoma in the same patient (not shown). The tumour cells are diffusely positive for TTF-1 and negative for GATA-3. Overall findings are consistent with metastatic adenocarcinoma with mucinous features of a lung primary. Image courtesy of Dr KC Leung, Department of Clinical Pathology, Pamela Youde Nethersole Eastern Hospital, Hong Kong (d-i).

Sonographic findings are similarly non-specific; they can appear as solid masses that are circumscribed or ill-defined and hypo- or hyperechoic, with posterior shadowing or enhancement (Figure 1).[4,6]

Metastatic tumours can be recognised pathologically by their unusual histological patterns, lack of an in situ component, predominant periductal and/or perilobular distribution, and extensive lymphovascular involvement.[7] In addition, clinical history, comparison of the histology of mammary and extramammary tumours (if any), and use of immunohistochemical markers that are organ- or tumour-specific provide indispensable information for delineating the origin of the primary tumour (Figure 1).[7]

## SARCOMA

Breast sarcomas are a group of aggressive tumours of mesenchymal origin accounting for <1% of all breast malignancies.[8] They can be primary, or secondary to previous radiotherapy for breast or intrathoracic malignancies.[8] Primary sarcomas occur predominantly in women, with the highest incidence in patients aged between 45 and 50 years, except for angiosarcomas, which tend to occur in younger women with a reported mean age of <40 years.[9,10] The most common subtypes of breast sarcomas are angiosarcomas, fibrosarcomas, and undifferentiated pleomorphic sarcomas.[9] Angiosarcomas have a worse prognosis than other types of breast sarcomas (Figures 2 and 3).[11]

On mammography, the most common finding is a solitary, oval, high-density mass with either indistinct or circumscribed margins and no calcifications (Figure 3).[10] However, coarse osteoid calcifications may occasionally be found in breast sarcomas with osteosarcoma features.[11,12]

On ultrasound, breast sarcomas typically appear as oval masses with indistinct margins, hypoechoic or complex echotexture, posterior acoustic shadowing, and internal vascularity (Figure 3).[10] Diffuse abnormal mixed hyper-and hypoechogenicity without a discrete mass has been reported in up to 38% of patients with breast angiosarcoma.[13] Hypervascularity on colour Doppler imaging is a typical feature of angiosarcoma; up to 54% of masses are hyperechoic or mixed hyper- and hypoechoic, which may also reflect the vascular nature of angiosarcoma.[13]

On magnetic resonance imaging, breast sarcoma typically appears as an oval irregular mass that is hypointense on T1-weighted images and hyperintense on T2-weighted images, with heterogeneous initial rapid enhancement, and washout curves (i.e., a relatively rapid uptake with reduction in enhancement towards the latter part of the study) or plateau curves (i.e., initial uptake followed by the plateau phase towards the latter part of the study) on dynamic imaging.[10]

## LYMPHOMA

Breast lymphoma is a haematological neoplasm that originates in the lymphoid tissue of the breast and may be primary or secondary. Together, they

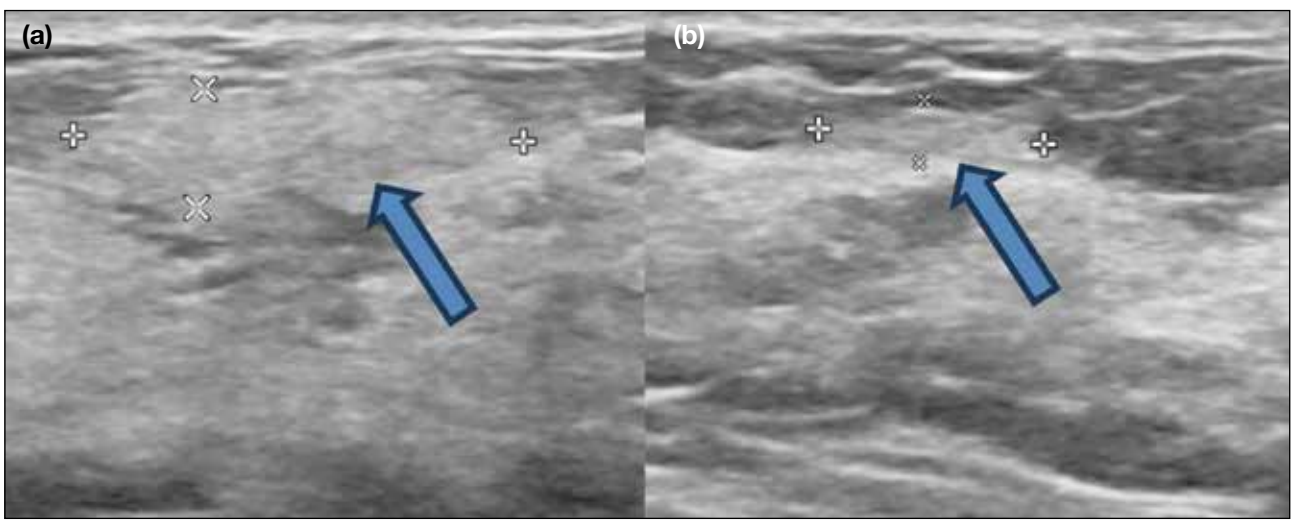


**Figure 2.** A 43-year-old woman first presented with lumpiness in the upper outer quadrant of the right breast. No suspicious mass or microcalcifications were seen on initial bilateral mammograms. Two oval, parallel echogenic lesions (arrows) with indistinct border were detected on ultrasound at the site indicated by the patient. Histopathology showed adipose tissue only. After 1 year, she returned with a rapidly enlarging mass in the upper outer quadrant of the right breast; the findings are shown in Figure 3.

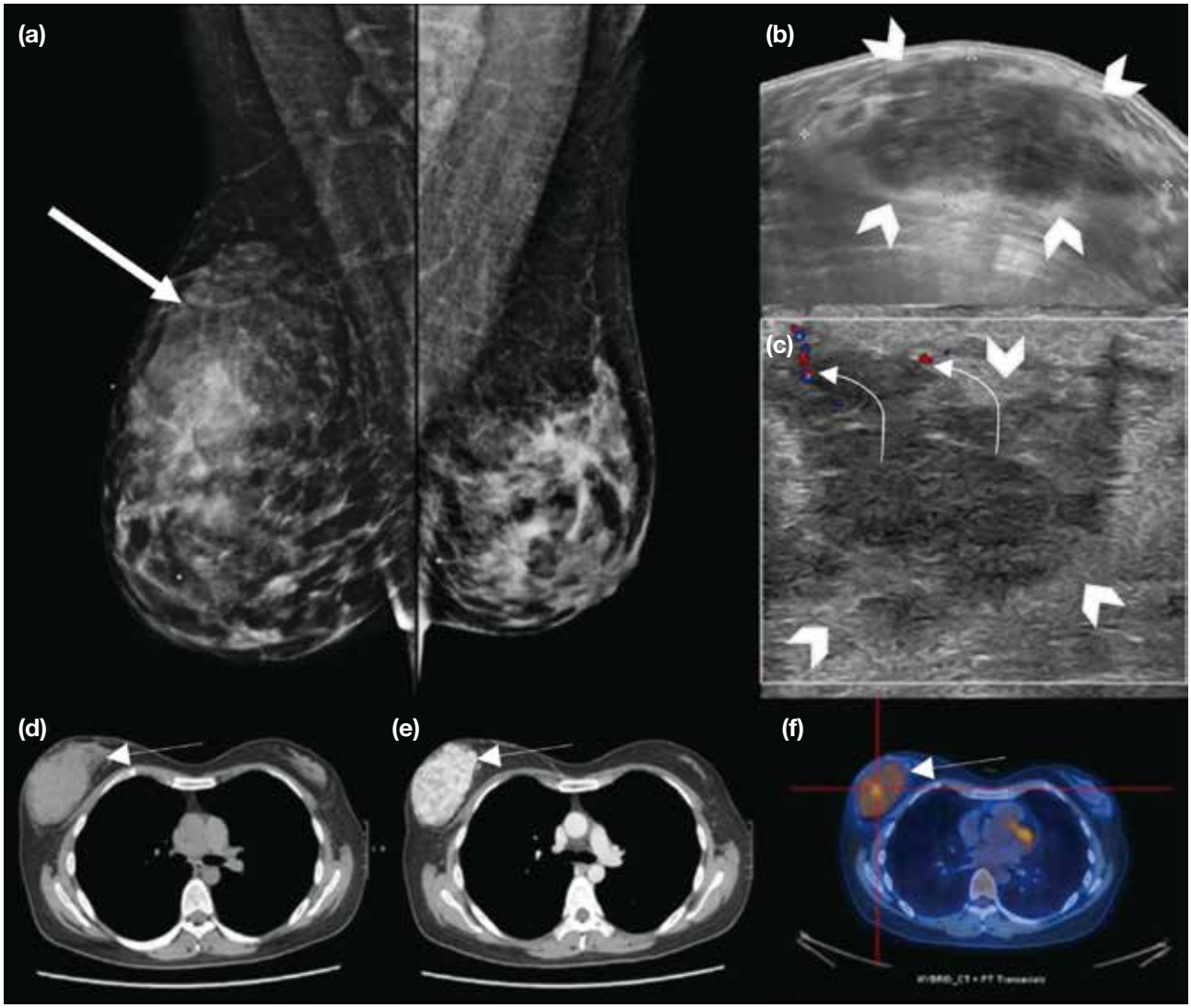


**Figure 3.** The same patient described in Figure 2 returned complaining of a rapidly enlarging right breast mass at 1 year after initial assessment. (a) The current bilateral mammograms in mediolateral oblique view shows a new iso- to hyperdense mass with obscured border occupying most of the upper outer quadrant of the right breast (thick arrow). (b, c) A large irregular heterogeneous mass (arrowheads) is seen in the upper outer quadrant of the right breast on ultrasound. Its periphery is mainly hyperechoic and blends in with the normal breast tissue. Minimal peripheral vascularity is noted (curved arrows in [c]). Staging contrast-enhanced computed tomography (d, e) and $^{18}$F-fluorodeoxyglucose positron emission tomography/computed tomography (f) show a corresponding avidly enhancing hypermetabolic right breast mass (thin arrows) with no distant metastases. The histopathological diagnosis was angiosarcoma.

represent approximately 0.04% to 0.7% of all breast malignancies.[14] Primary breast lymphoma accounts for 0.85% to 2.2% of all extranodal malignant lymphomas, while secondary breast lymphoma is the most common malignancy with secondary involvement of the breast.[15,16] Breast lymphoma most commonly presents as a painless, enlarging, palpable mass.[15] Multiple masses are found in <10% of patients and bilateral involvement is found in approximately 10% of patients, although these findings are more commonly identified in secondary breast lymphoma cases.[15]

On mammography, breast lymphoma manifests as a solitary, non-calcified, oval or lobulated mass. It may have circumscribed or indistinct margins (Figure 4). Infiltrative patterns such as global asymmetry and trabecula and skin thickening are uncommon findings.[12] Skin thickening and lymphedema are reported in only up to 8% of patients (Figure 5).[17] Calcifications, architectural distortion, and spiculations are rare.[12]

Sonographic features of breast lymphoma are non-specific, appearing as an oval or irregular mass of hyper-,

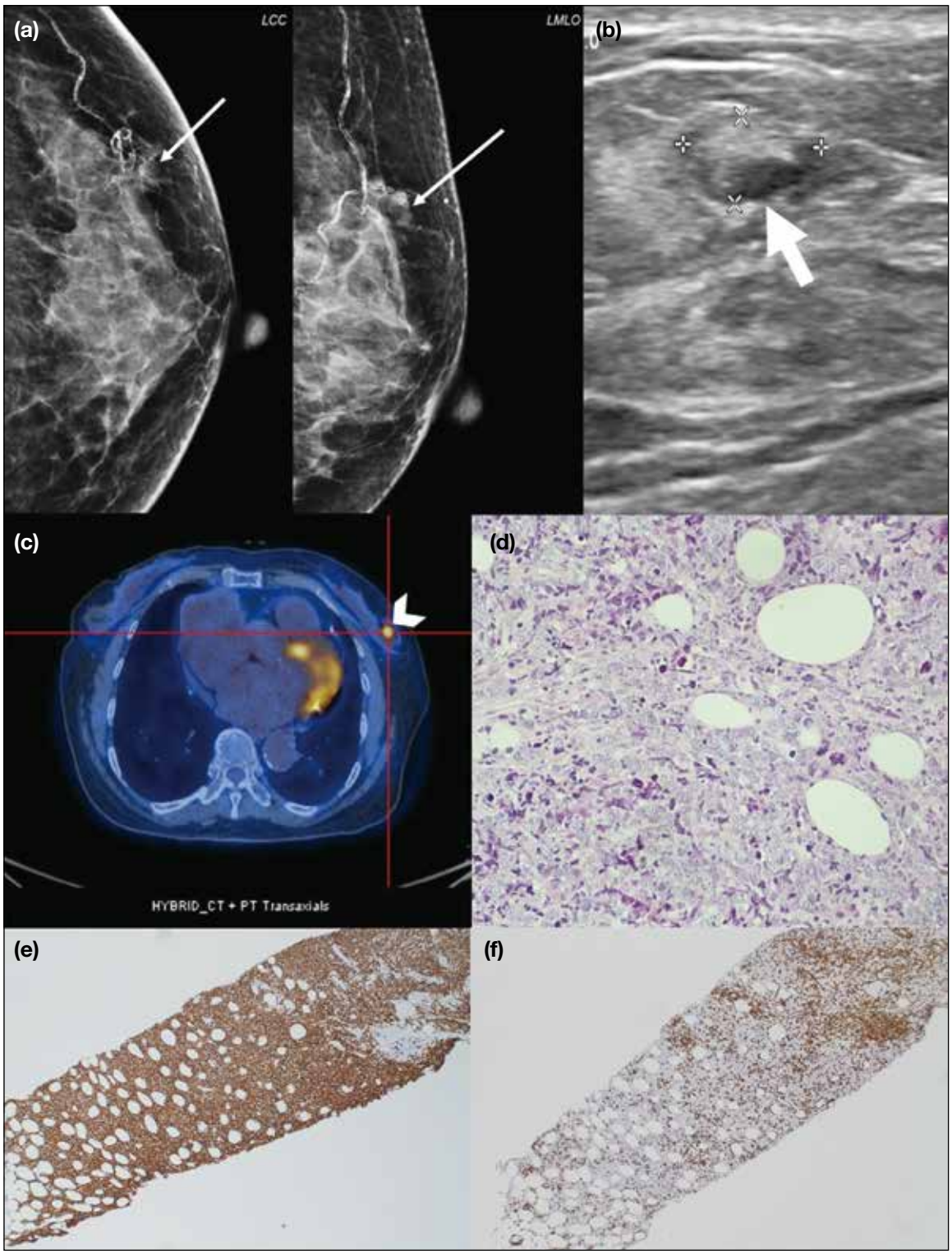


**Figure 4.** Primary diffuse large B-cell lymphoma presenting as a palpable left breast lump in an 88-year-old woman. (a) Cropped magnified views of left mammogram focusing on the upper outer quadrant showing an oval, circumscribed, equal density mass (thin arrows). (b) A corresponding oval circumscribed, mixed echogenicity mass is seen in the left breast at 1 o'clock position on ultrasound (thick arrow). (c) The left breast mass is hypermetabolic on $^{18}$F-fluorodeoxyglucose positron emission tomography/computed tomography with no extramammary hypermetabolic foci (arrowhead). (d) High-power view (×400) of the breast mass biopsy with haematoxylin and eosin stain showing fibroadipose tissue infiltrated by sheets of medium- to large-sized neoplastic lymphoid cells. They possess irregular nuclear outlines, occasional nucleoli, and frequent apoptotic figures. On immunostaining (×40), the neoplastic lymphoid cells are diffusely positive for the B-cell marker CD20 (e) and negative for the T-cell marker CD3 (which highlights T lymphocytes in the background) [f]. Image courtesy of Dr Tiffany HT Chan and Dr HL Li, Department of Clinical Pathology, Pamela Youde Nethersole Eastern Hospital, Hong Kong (d-f).

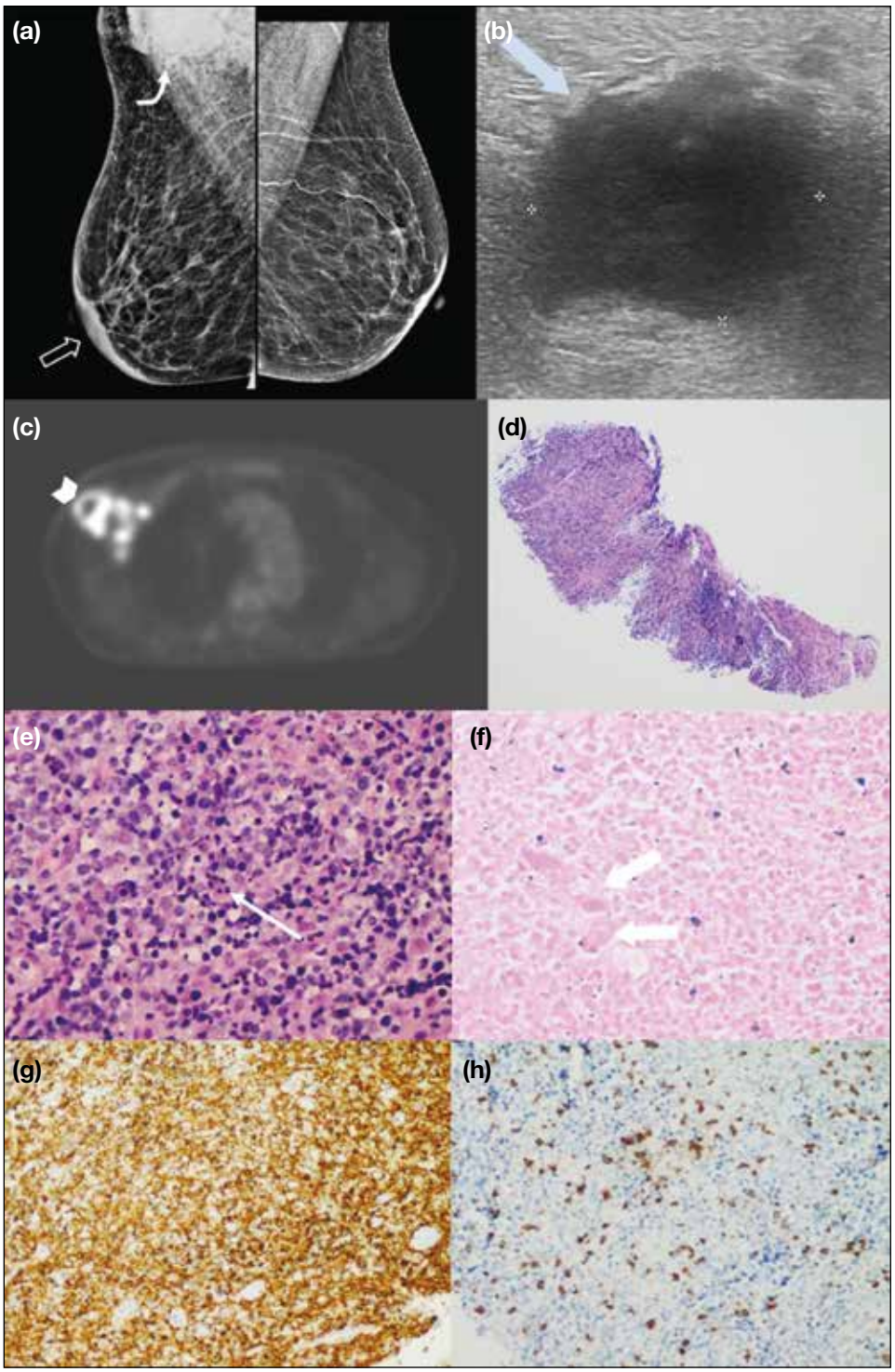


**Figure 5.** A 74-year-old woman presented with a right axillary mass. (a) Diffuse skin thickening and oedema (open arrow) of the right breast and axillary region were seen on bilateral mammograms in mediolateral oblique view. An enlarged right axillary lymph node (curved arrow) was also noted. (b) Ultrasound of the right axilla confirms the presence of enlarged irregular hypoechoic lymph nodes with loss of fatty hila (blue arrow). (c) The right axillary mass (arrowhead) demonstrates hypermetabolism on $^{18}$F-fluorodeoxyglucose positron emission tomography/computed tomography, with multiple other sites of nodal involvement. (d) Histology sections with haematoxylin and eosin (H&E) stain in low-power view (×40) reveals the viable areas of the tumour as hypercellular. (e) High-power view (H&E staining, ×400) of the viable area showing sheets of medium- to large-sized neoplastic lymphoid cells with mitotic and apoptotic figures (thin arrow). (f) High-power view (H&E staining, ×400) of the necrotic area showing ghost outlines of neoplastic cells (thick arrows). On immunostaining (×200), the neoplastic lymphoid cells are diffusely positive for CD20 (g) and negative for CD3 (h). Overall features are consistent with diffuse large B-cell lymphoma. Image courtesy of Dr CK Cheung and Dr F Hioe, Department of Clinical Pathology, Pamela Youde Nethersole Eastern Hospital, Hong Kong (d-h).

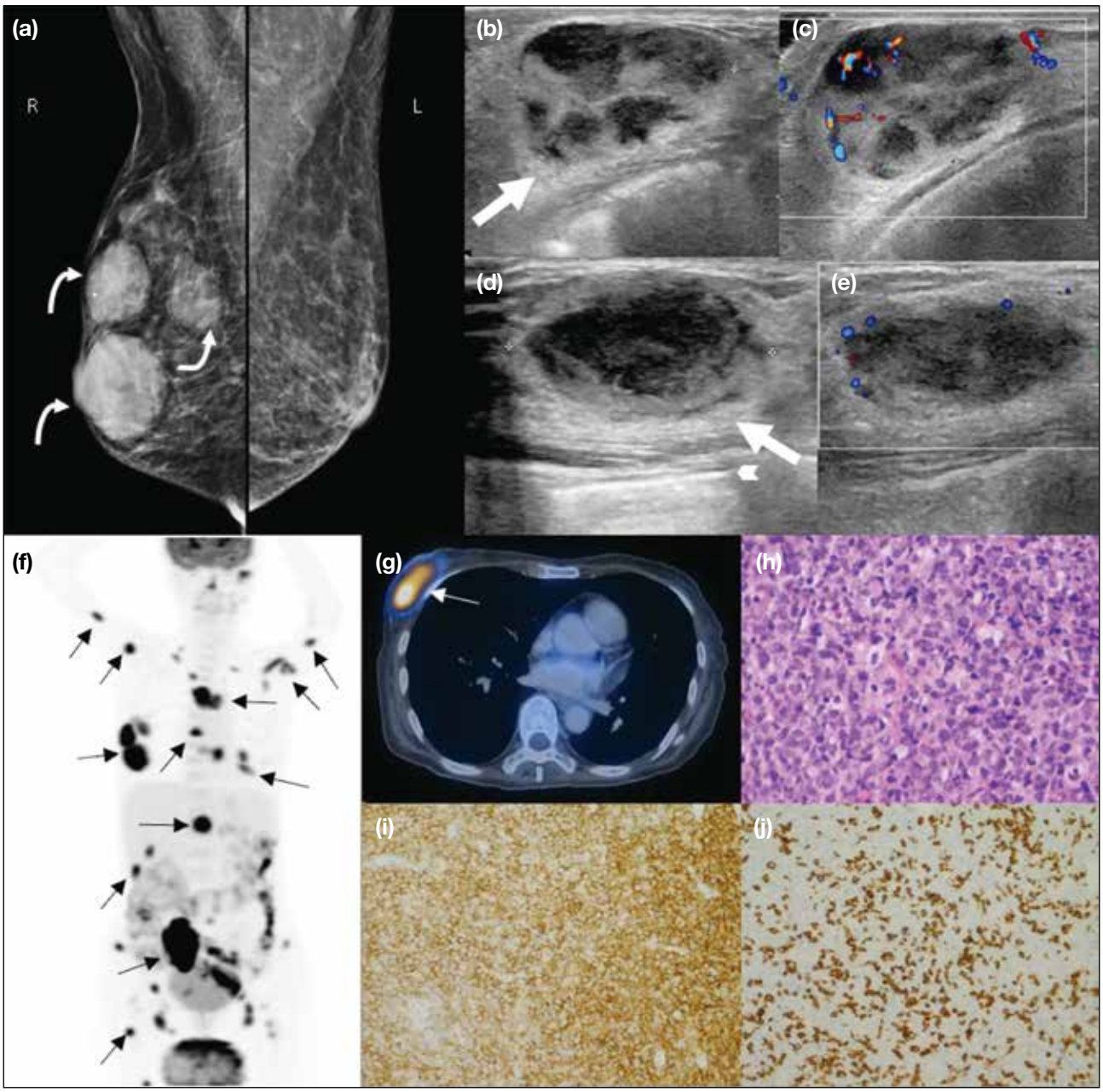


**Figure 6.** A 67-year-old woman with known history of stage IV follicular lymphoma with total metabolic response after chemotherapy presented with multiple new right breast lumps. (a) Bilateral mammograms showed three equal-density oval and circumscribed masses in the right breast without associated microcalcifications (curved arrows). (b-e) Multiple oval and circumscribed heterogeneous hypoechoic lesions were seen in the right breast, some with echogenic rims (thick arrows in [b] and [d]) and posterior enhancement (arrowhead in [d]). Internal vascularity is also visible in some of these lesions. (b, c) The first mass. Vascularity of this mass using Doppler ultrasound is shown in (c). (d) The second mass. The third mass with vascularity using Doppler ultrasound is shown in (e). (f, g) $^{18}$F-fluorodeoxyglucose positron emission tomography/computed tomography images demonstrating extensive hypermetabolic disease involving the right breast (g) and multiple organs and systems (f) [black and white thin arrows]. (h) High-power view (×400) of the breast masses biopsy with haematoxylin and eosin stain showing diffuse sheets of neoplastic lymphoid infiltrate comprising medium- to large-sized cells with irregular nuclear membranes, hyperchromatic nuclei, and occasional nucleoli. Mitotic figures and apoptotic bodies are noted. On immunostaining (×200), the neoplastic lymphoid cells were diffusely positive for CD20 (i) and negative for CD3 (j). Overall features are consistent with diffuse large B-cell lymphoma. Image courtesy of Dr Elaine Lee, Department of Diagnostic Radiology, The University of Hong Kong (f, g); Dr CK Cheung and Dr MW Ma, Department of Clinical Pathology, Pamela Youde Nethersole Eastern Hospital, Hong Kong (h-j).

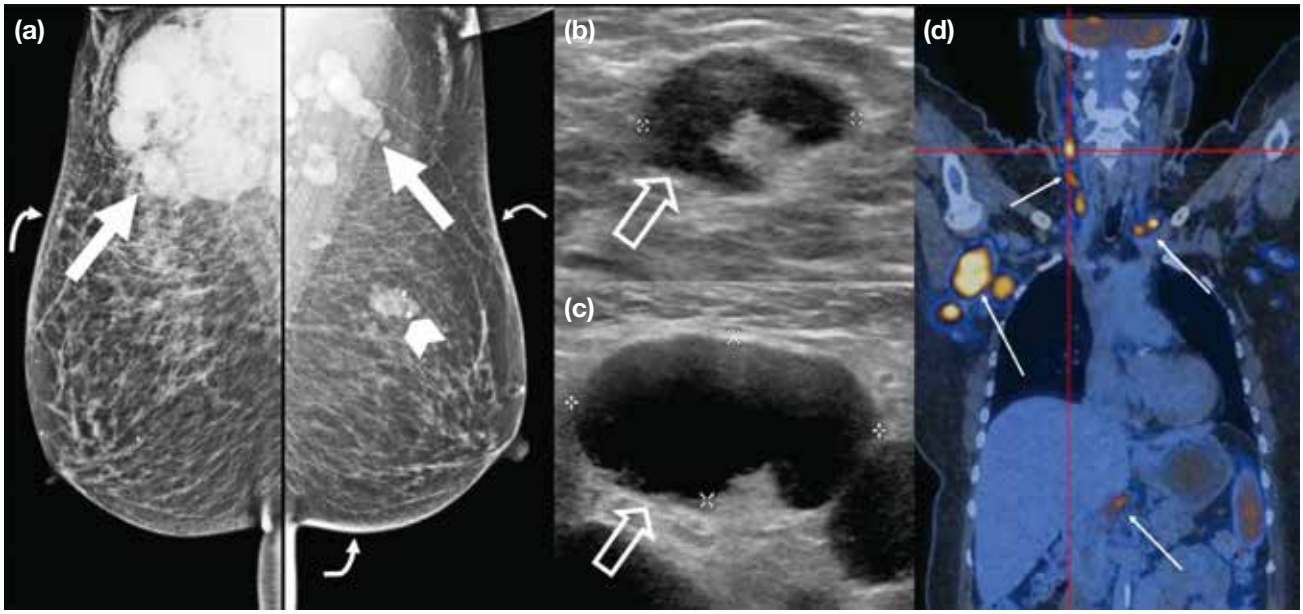


**Figure 7.** A 64-year-old woman presented with a right axillary mass. (a) Multiple bilateral enlarged axillary lymph nodes (thick arrows) and mild bilateral skin thickening (curved arrows) over both breasts are seen on bilateral mammograms. The mass with popcorn calcification in the left breast upper portion central depth (arrowhead) was a biopsy-proven fibroadenoma. (b, c) Ultrasound confirms the presence of multiple bilateral enlarged axillary lymph nodes with cortical thickening and loss of fatty hila (open arrows). (d) $^{18}$F-fluorodeoxyglucose positron emission tomography/computed tomography showed multiple hypermetabolic lymphadenopathies above and below the diaphragm (thin arrows), including both axillae. Histopathology of the right axillary lymph node confirmed classical Hodgkin lymphoma.

hypo-, or mixed echogenicity, with circumscribed to indistinct margins (Figure 4).[12,15] Posterior acoustic enhancement, echogenic rims, and onion-peel–like rims are common findings (Figure 6).[14] Masses typically appear hypervascular on Doppler ultrasound.[12,17] Axillary lymphadenopathy has been reported in up to 32% of patients (Figures 5 and 7).[17]

The overall preponderance of breast lymphomas are diffuse large B-cell lymphomas,[18,19] which typically show $^{18}$F-fluorodeoxyglucose ($^{18}$F-FDG) avidity on $^{18}$F-FDG positron emission tomography/computed tomography ($^{18}$F-FDG PET/CT).[20] $^{18}$F-FDG PET/CT is recommended for staging and response assessment of $^{18}$F-FDG–avid lymphomas[21]; its role in the management of breast lymphoma has also been suggested.[22]

No specific imaging features can reliably distinguish between primary and secondary breast lymphoma. In patients with known extramammary lymphoma, multiple masses or an inflammatory-like appearance such as trabecular and skin thickening without a mass are more likely to suggest secondary breast lymphoma.[15,17]

## PLASMACYTOMA

Plasmacytomas are tumours characterised by neoplastic monoclonal plasma cells in the bone or soft tissue (extramedullary). Extramedullary breast plasmacytomas are extremely rare and most commonly occur as a secondary event in patients with known multiple myeloma.[23] Clinically, breast plasmacytomas present as palpable lumps.

A retrospective study involving 53 cases of breast plasmacytoma examined its radiological features.[23] On mammography, they had a non-specific appearance, with dense, round, or oval masses with well- or ill-defined margins (Figure 8[24]), or as diffuse infiltration. On ultrasound, they can appear hypoechoic with well-defined margins but, less commonly, may display mixed hypo- to hyperechogenicity with indistinct margins and posterior acoustic enhancement or shadowing (Figure 8). No differentiating radiological features were found for primary and secondary breast plasmacytoma. Given the non-specific radiological features, the diagnosis of breast plasmacytoma relies on clinical suspicion when there is a history of multiple myeloma, and confirmation through histopathology.[23]

There are only a few reports on the magnetic resonance imaging features of breast plasmacytoma. Variable T1 and T2 signal intensities have been reported, including

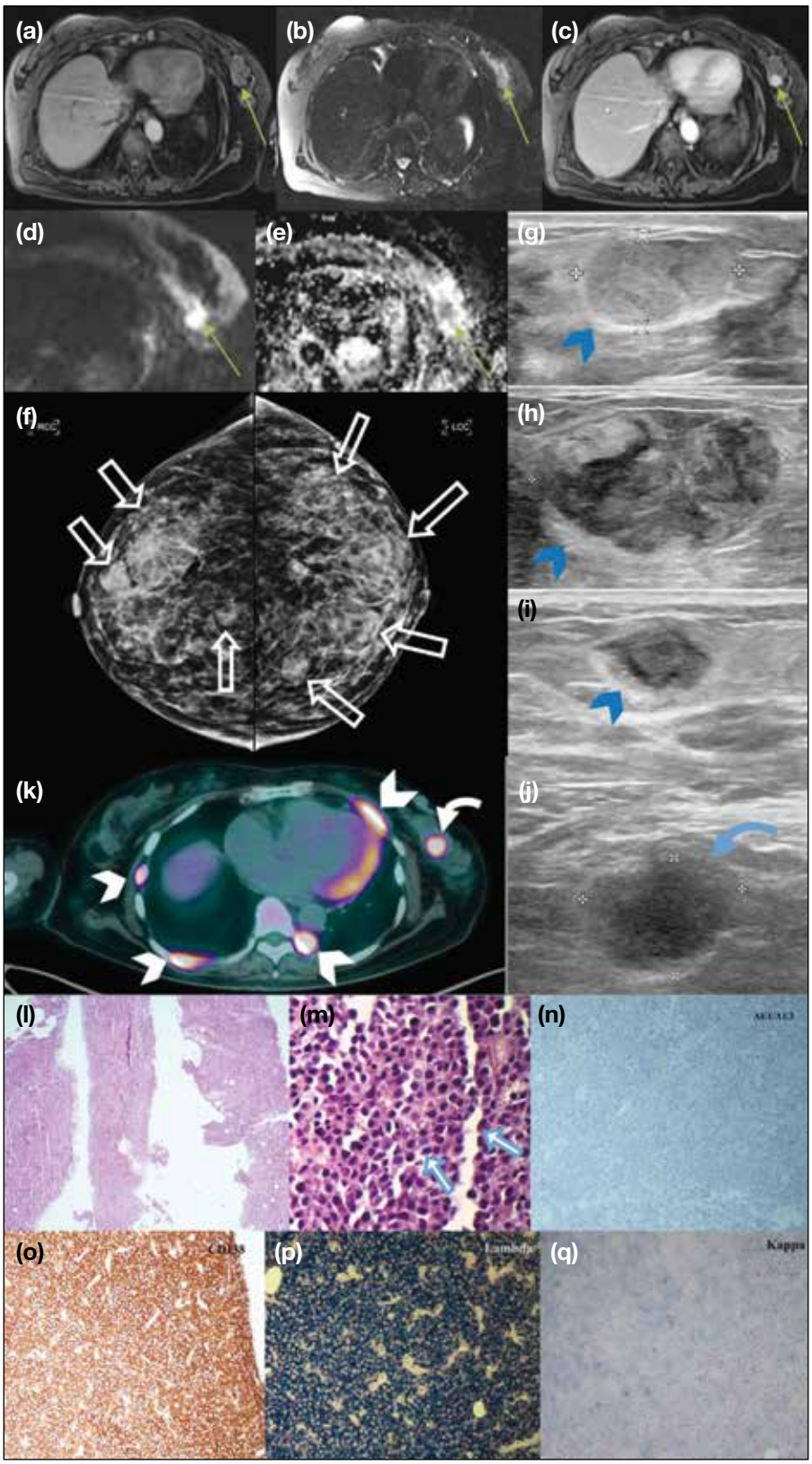


**Figure 8.** A 59-year-old woman with a known history of multiple myeloma was incidentally found to have a left breast lesion (thin arrows in [a] to [e]) in a contrast-enhanced magnetic resonance imaging study of the liver. The nodule is (a) isointense on the pre-contrast T1-weighted axial image, (b) hyperintense on the T2-weighted fat-saturated axial image, and (c) contrast-enhanced on the post-contrast T1-weighted axial image. Cropped images focusing on the lesion in the (d) diffusion-weighted imaging and (e) apparent diffusion coefficient sequences demonstrate restricted diffusion. (f) Further evaluation with bilateral mammography showing multiple equal- to high-density oval and irregular masses with circumscribed to ill-defined margins (white open arrows). (g-i) Ultrasound of both breasts showing multiple oval circumscribed masses corresponding to the mammographically detected lesions (blue arrowheads). The masses are of variable echogenicity, ranging from hyperechoic, mixed heterogeneous to hypoechoic. (j) A suspicious irregular hypoechoic left axillary lymph node with loss of fatty hilum is also seen (blue curved arrow). (k) Dual-tracer $^{18}$F-fluorodeoxyglucose/$^{11}$C-acetate positron emission tomography/computed tomography showing hypermetabolism in the bilateral breast masses (white curved arrow); left axillary lymph nodes; and multiple other lesions in the liver, abdominal cavity, subcutaneous tissue, and skeleton (white arrowheads), suggestive of multiple myeloma with extraosseous involvement. (l) Histology sections with haematoxylin and eosin stain in low-power view (×40) showing sheets of tumour cells. (m) High-power view (×400) showing tumour cells possessing eosinophilic cytoplasm with perinuclear hof (blue and white arrows) and hyperchromatic nuclei. Immunohistochemically (×200), the tumour cells are negative for epithelial marker AE1/AE3 (pancytokeratin) [n] and positive for plasma cell marker CD138 (o). In situ hybridisation (×200) for lambda (p) and kappa (q) showing lambda light chain restriction. Overall features are consistent with plasmacytoma. Reproduced and adapted with permission from the Hong Kong Academy of Medicine (a-f, k, n, and o)[24]; image courtesy of Dr TS Wong and Dr KC Leung, Department of Clinical Pathology, Pamela Youde Nethersole Eastern Hospital, Hong Kong (l-q).

low-to-isointense signal on T1-weighted images and intermediate-to-high signal on T2-weighted images (Figure 8[24]).[25,27] Restricted diffusion and homogenous enhancement with delayed washout kinetics have also been noted (Figure 8[24]).[25-27]

A limited number of studies have reported on $^{18}$F-FDG PET/CT findings in breast plasmacytoma.[26-29] Majority of these cases showed $^{18}$F-FDG avidity,[26,27,29] although low-grade uptake has also been reported.[28] Nevertheless, $^{18}$F-FDG PET/CT is increasingly being recognised as a valuable tool for the diagnosis and management of patients with plasma cell disorders, such as multiple myeloma and solitary plasmacytoma.[30] Several tracers other than $^{18}$F-FDG for PET/CT have also been investigated in patients with multiple myeloma.[30]

## CONCLUSION

Although non-epithelial malignancies of the breast show features different from those of epithelial breast carcinoma, in general their radiological appearance is generally variable and non-specific. Radiologists must interpret the imaging findings in conjunction with the clinical context. Biopsy remains the mainstay of diagnosis and should be considered in suspected cases.

## REFERENCES


1. Feder JM, de Paredes ES, Hogge JP, Wilken JJ. Unusual breast lesions: radiologic-pathologic correlation. Radiographics. 1999;19 Spec No:S11-26.
2. Lee SH, Park JM, Kook SH, Han BK, Moon WK. Metastatic tumors to the breast: mammographic and ultrasonographic findings. J Ultrasound Med. 2000;19:257-62.
3. Toombs BD, Kalisher L. Metastatic disease to the breast: clinical, pathologic, and radiographic features. AJR Am J Roentgenol. 1977;129:673-6.
4. Bartella L, Kaye J, Perry NM, Malhotra A, Evans D, Ryan D, et al. Metastases to the breast revisited: radiological-histopathological correlation. Clin Radiol. 2003;58:524-31.
5. Krishnan EU, Phillips AK, Randell A, Taylor B, Garg SK. Bilateral metastatic inflammatory carcinoma in the breast from primary ovarian cancer. Obstet Gynecol. 1980;55(3 Suppl):94S-96S.
6. Vergier B, Trojani M, de Mascarel I, Coindre JM, Le Treut A. Metastases to the breast: differential diagnosis from primary breast carcinoma. J Surg Oncol. 1991;48:112-6.
7. WHO Classification of Tumours Editorial Board. WHO Classification of Breast Tumours: WHO Classification of Tumours, 5th Edition. World Health Organization; 2019. pp 261-5.
8. Lim SZ, Ong KW, Tan BK, Selvarajan S, Tan PH. Sarcoma of the breast: an update on a rare entity. J Clin Pathol. 2016;69:373-81.
9. Bousquet G, Confavreux C, Magné N, de Lara CT, Poortmans P, Senkus E, et al. Outcome and prognostic factors in breast sarcoma: a multicenter study from the rare cancer network. Radiother Oncol. 2007;85:355-61.
10. Matsumoto RA, Hsieh SJ, Chala LF, de Mello GG, de Barros N. Sarcomas of the breast: findings on mammography, ultrasound, and magnetic resonance imaging. Radiol Bras. 2018;51:401-6.
11. Smith TB, Gilcrease MZ, Santiago L, Hunt KK, Yang WT. Imaging features of primary breast sarcoma. AJR Am J Roentgenol. 2012;198:W386-93.
12. Berg WA, Leung JW. Diagnostic Imaging: Breast (3rd Edition). Philadelphia: Elsevier Health Sciences; 2019. pp 730-5.
13. Yang WT, Hennessy BT, Dryden MJ, Valero V, Hunt KK, Krishnamurthy S. Mammary angiosarcomas: imaging findings in 24 patients. Radiology. 2007;242:725-34.
14. Shim E, Song SE, Seo BK, Kim YS, Son GS. Lymphoma affecting the breast: a pictorial review of multimodal imaging findings. J Breast Cancer. 2013;16:254-65.
15. Raj SD, Shurafa M, Shah Z, Raj KM, Fishman MD, Dialani VM. Primary and secondary breast lymphoma: clinical, pathologic, and multimodality imaging review. Radiographics. 2019;39:610-25.
16. Surov A, Holzhausen HJ, Wienke A, Schmidt J, Thomssen C, Arnold D, et al. Primary and secondary breast lymphoma: prevalence, clinical signs and radiological features. Br J Radiol. 2012;85:e195-205.
17. Yang WT, Lane DL, Le-Petross HT, Abruzzo LV, Macapinlac HA. Breast lymphoma: imaging findings of 32 tumors in 27 patients. Radiology. 2007;245:692-702.
18. Au W, Chan AC, Chow LW, Liang R. Lymphoma of the breast in Hong Kong Chinese. Hematol Oncol. 1997;15:33-8.
19. Picasso R, Tagliafico A, Calabrese M, Martinoli C, Pistoia F, Rossi A, et al. Primary and secondary breast lymphoma: focus on epidemiology and imaging features. Pathol Oncol Res. 2020;26:1483-8.
20. Weiler-Sagie M, Bushelev O, Epelbaum R, Dann EJ, Haim N, Avivi I, et al. $^{18}$F-FDG avidity in lymphoma readdressed: a study of 766 patients. J Nucl Med. 2010;51:25-30.
21. Cheson BD, Fisher RI, Barrington SF, Cavalli F, Schwartz LH, Zucca E, et al. Recommendations for initial evaluation, staging, and response assessment of Hodgkin and non-Hodgkin lymphoma: the Lugano classification. J Clin Oncol. 2014;32:3059-68.
22. Santra A, Kumar R, Reddy R, Halanaik D, Kumar R, Bal CS, et al. FDG PET-CT in the management of primary breast lymphoma. Clin Nucl Med. 2009;34:848-53.
23. Surov A, Holzhausen HJ, Ruschke K, Arnold D, Spielmann RP. Breast plasmacytoma. Acta Radiol 2010;51:498-504.
24. Mo CK, Lai AY, Lo SS, Wong TS, Wong WW. Bilateral breast multiple myeloma: a case report. Hong Kong Med J. 2022;28:488-90.
25. Neuhaus T, Hess T. Bilateral extramedullary plasmacytoma of the breast. Breast J. 2014;20:315-8.
26. Park YM. Imaging findings of plasmacytoma of both breasts as a preceding manifestation of multiple myeloma. Case Rep Med. 2016;2016:6595610.
27. Vong S, Navarro SM, Darrow M, Aminololama-Shakeri S. Extramedullary plasmacytoma of the breast in a patient with multiple myeloma. J Radiol Case Rep. 2020;14:14-23.
28. Ginat DT, Puri S. FDG PET/CT manifestations of hematopoietic malignancies of the breast. Acad Radiol. 2010;17:1026-30.
29. Rachh S, Puj K, Parikh A. $^{18}$F-FDG PET/CT in the evaluation of solitary extramedullary plasmacytoma: a case series. Asia Ocean J Nucl Med Biol. 2021;9:56-61.
30. Cavo M, Terpos E, Nanni C, Moreau P, Lentzsch S, Zweegman S, et al. Role of $^{18}$F-FDG PET/CT in the diagnosis and management of multiple myeloma and other plasma cell disorders: a consensus statement by the International Myeloma Working Group. Lancet Oncol. 2017;18:e206-17.

# CATEGORIES OF PAPERS

*Hong Kong Journal of Radiology* publishes various categories of articles. Each category serves a distinct purpose and is judged by different criteria.

## EDITORIAL

Commissioned article presenting the author's opinion on a topical subject or an article published in the current issue. Unsolicited Editorials are not accepted.

*Format:* An abstract is not required. The text is limited to 1000 words, with a maximum of 1 table or figure, and up to 10 references.

## REVIEW ARTICLE

Systematic reviews or meta-analyses of recent developments in a specific topic. Scoping reviews of the literature that identify area(s) for future research will also be considered. No new information is described, and no subjective opinion or personal experiences are expressed.

*Format:* A structured abstract of ≤250 words; headings should include: Introduction, Methods, Results, Conclusion. The text is limited to 5000 words, with a maximum of 20 tables and figures (total), and up to 60 references.

## ORIGINAL ARTICLE

Provides new information based on original research. Includes prospective studies with in-depth statistical analysis, unique retrospective observations of a disease or disorder, and studies of novel applications of an interventional procedure or treatment method.

*Format:* A structured abstract of ≤250 words; headings should include: Introduction, Methods, Results, Conclusion. The text is limited to 3500 words, with a maximum of 20 tables and figures (total), and up to 50 references.

## PERSPECTIVE

Narrative review articles discussing recent developments in a specific topic. No new information is described; may include subjective opinion or personal experiences.

*Format:* An unstructured abstract of ≤250 words. The text is limited to 2500 words, with a maximum of 20 tables and figures (total), and up to 60 references.

## PICTORIAL ESSAY

Teaching exercise with message in the figures and legends. Emphasis is on quality of the illustrations and clinical relevance of the message.

*Format:* An abstract is not required. The text is limited to 2500 words, with a maximum of 20 tables and figures (total), and up to 15 references.

## CASE REPORT

Brief discussion of a case with unique features not previously described. Additional cases (case series) may be added to augment the discussion. The discussion should be succinct and focus on a specific message.

*Format:* An abstract is not required. The text is limited to 1500 words, with a maximum of 8 tables and figures (total), and up to 15 references.

## BRIEF COMMUNICATION

This includes post-meeting commentary, update on new imaging or therapeutic advances, brief description of a specific technique or procedure or new equipment. Teaching exercise aimed at describing a certain radiological or radiotherapeutic technique for trainees and practising radiologists is also welcome.

*Format:* An abstract is not required. The text is limited to 1500 words, with a maximum of 8 tables and figures (total), and up to 15 references.

## LETTER TO THE EDITOR

Short letter on any matter of interest to journal readers, including comments on an article that has previously appeared in the journal. The authors of the article commented on would be invited to reply.

*Format:* An abstract is not required. The text is limited to 500 words, with up to 5 references. Figures and tables are permitted only exceptionally.

# INFORMATION FOR AUTHORS

## Aims and Scope

*Hong Kong Journal of Radiology* is the official peer-reviewed academic journal of the Hong Kong College of Radiologists. It is a multidisciplinary journal covering research work pertaining to the science and practice of the component specialties of the College. The journal publishes various categories of papers, including Reviews, Original Articles, Perspectives, Pictorial Essays, Case Reports, Brief Communications, and Letters to the Editor. Manuscripts will be subject to rigorous peer review. *HKJR* adheres to the Recommendations for the Conduct, Reporting, Editing, and Publication of Scholarly Work in Medical Journals of the International Committee of Medical Journal Editors (ICMJE; www.icmje.org), and the Core Practices of the Committee on Publication Ethics (COPE; publicationethics.org/).

## Journal Policies

**Reporting Guidelines:** *HKJR* recommends the use of reporting guidelines in the preparation of manuscripts, such as those advocated by the EQUATOR Network (eg, CONSORT for randomised trials).

**Funding:** Any sponsor(s) of the research involved, along with grant number(s) should be provided.

**Conflicts of interest:** All authors must provide a statement reporting any conflicts of interest. Where none exist, please state 'The authors have no conflicts of interest to declare.'

**Ethics:** All studies must be conducted in accordance with the Declaration of Helsinki. For studies involving humans, a statement must be included in the manuscript that provides the name of the review board and approval number (or waiver). A statement on patient/guardian consent must also be included. For studies involving animals, appropriate ethics approval is required, and this should be stated in the manuscript.

**Submission:** Manuscripts should be submitted online via HKAMedTrack (www.hkamedtrack.org/hkjr). Manuscripts must be unpublished works that are not under consideration by another publication.

**Copyright:** On acceptance of an article by the journal, the corresponding author will be asked to transfer copyright of the article to the College.

**Editing:** Accepted manuscripts will be copyedited according to journal style. Authors are responsible for all statements made in their work, including changes made by the copy editor.

**Proofs and Reprints:** The corresponding author will receive page proofs, which should be proofread and returned promptly. Corrections are limited to printer's errors — no substantial author's changes will be made without charge. Quotes for extra copies of reprints are available at the Editorial Office.

## Manuscript Preparation

In general, manuscripts should be prepared following the 'IMRaD' structure as recommended by the ICMJE. Please provide a **blinded** manuscript and separate title page in Word format (.doc or .docx). Manuscripts must be written in English. For accepted manuscripts, an abstract in Traditional Chinese will also be required.

**Authors:** Provide the full name, qualifications (maximum of two), and affiliation (where the study was conducted) for all authors. The authors' names in Chinese characters, if available, should also be provided. **The corresponding author**, on behalf of the authors, is responsible for all contact with the journal. Provide the full name, postal address, telephone and fax numbers, and email address of the corresponding author.

**Title:** Concisely convey the main topic of the study. Avoid obvious terms such as "a study of" or "novel". If appropriate, please include the study design in the title (eg, 'randomised controlled trial', 'systematic review', 'case report'). An abbreviated title of <45 characters is also required.

**Abstract:** For article types requiring an abstract, this should provide a complete summary of the article, including the aims/purpose, main methods, key results, and conclusions. Abbreviations and clinical or technical jargon should be avoided. Please refer to the Categories of Papers for details.

**Key Words:** A maximum of five relevant index terms should be provided, selected from the Medical Subject Headings (MeSH; www.ncbi.nlm.nih.gov/mesh).

**Tables:** Submit tables on separate pages in as simple a format as possible. They should be numbered and concisely titled. Abbreviations should be defined in footnotes.

**Figures:** Restricted to the minimum necessary to support the textual material. Illustrations should be submitted as separate files (.jpg format, ≥350-dpi resolution). All figures should be numbered with a legend to indicate the anatomical area and pathological condition shown. All symbols and abbreviations should be defined in the legend. Please ensure that legends and illustrations correspond.

**References:** Should be numbered in the order in which they are first cited in the text. Each reference citation should be in superscript Arabic numerals after full-stops and commas. In the reference list, include the complete title, and names and initials of all authors.

**Acknowledgement(s):** Any individuals who contributed substantially to the study but does not qualify for inclusion as an author should be acknowledged. Written permission from acknowledged individuals is required.

Please refer to the *HKJR* website for further guidance:
http://www.hkjr.org/page/information-authors

# The Hong Kong Society of Diagnostic Radiologists Trust Fund

## Hong Kong Society of Diagnostic Radiologists Research Grant

The Hong Kong Society of Diagnostic Radiologists (HKSDR) was founded in 1977 to promote interflow of professional knowledge in diagnostic radiology and to foster close contact among doctors working in the field of diagnostic radiology. The HKSDR Trust Fund was established in 1985.

Taking into account the rapid progress in imaging technology and thus the need to promote research to advance our knowledge and to serve our patients better, the Trust Fund offers three awards of up to HK$17,000 each and is open to application.

The application should be made by the principal investigator of the research project related to the scientific or clinical aspects of diagnostic radiology to be conducted in Hong Kong. The principal investigator should be a trainee/specialist in the field of diagnostic radiology. He/she has to be a registered medical practitioner in Hong Kong.

Application and enquiry can be directed to:

Dr. Lam Chiu Ying Flora, Hon Secretary of Trust Fund Working Group
c/o Ms. HY Ng, Department of Diagnostic & Interventional Radiology
Kwong Wah Hospital
25 Waterloo Road, Yaumatei, Kowloon, Hong Kong.
Tel: (852) 3517 5189